MEASUREMENT OF PERNITRIC ACID, HYDROGEN CHLORIDE, AND SULFUR DIOXIDE DURING THE INTERCONTINENTAL CHEMICAL TRANSPORTATION EXPERIMENT CAMPAIGN

A Dissertation
Presented to
The Academic Faculty

by

Sae Wung Kim

In Partial Fulfillment
of the Requirements for the Degree
Doctor of Philosophy in the
School of Earth and Atmospheric Sciences

Georgia Institute of Technology
December 2007

MEASUREMENT OF PERNITRIC ACID, HYDROGEN CHLORIDE, AND SULFUR DIOXIDE DURING THE INTERCONTINENTAL CHEMICAL TRANSPORTATION EXPERIMENT CAMPAIGN

Approved by:

Dr. L. Gregory Huey, Advisor
School of Earth and Atmospheric Sciences
Georgia Institute of Technology

Dr. Rodney J Weber
School of Earth and Atmospheric Sciences
Georgia Institute of Technology

Dr. Gao Chen
Chemistry and Dynamics Branch
NASA Langley Research Center

Dr. Paul H. Wine
School of Chemistry and Biochemistry
Georgia Institute of Technology

Dr. Irina N. Sokolik
School of Earth and Atmospheric Sciences
Georgia Institute of Technology

Date Approved: November, 5, 2007

To my dad, Jongsoo Kim (1946 – 2006)

ACKNOWLEDGEMENTS

First of all, I would like to express sincere appreciation to my advisor, Greg Huey. His insightful guidance made possible this work. His office was always open and he welcomed any discussion even though he was always very busy. I have learned the way of thinking as a scientist from numerous discussions with him. Especially, I would like to thank to him for showing great patience and generosity for cultural and language differences.

I also would like to thank other Georgia Tech CIMS group members: Bob Stickel, Dave Tanner, Steve Sjostedt, Anne Case-Hanks, Jeff Peischl, Oscar Vargas, and Jin Liao. During two intensive INTEX field campaigns, Bob was in the field with me and taught me a great lesson to be a good field scientist. He also enjoyed bringing me to local attractions and nice restaurants and introducing me to fine wines during field campaigns.

The science team of the INTEX project should be a coauthor of this study. The comprehensive dataset from various research teams facilitates seamless data analyses for this study. The ground crew of the NASA DC-8 was dedicated to making science possible in any circumstance. I also want to thank my thesis committee members: Gao Chen, Irina Sokilik, Rodney Weber, and Paul Wine (alphabetical order) for being very accommodating and supportive throughout my time here.

Last but not least, I would like to thank my family in Korea and only family here in the U.S., my wife Youngjin.

TABLE OF CONTENTS

LIST OF TABLES

LIST OF FIGURES

SUMMARY

This study presents airborne measurements (0 km < z < 12 km) of HO_2NO_2, HCl and SO_2 using chemical ionization mass spectrometry (CIMS) during the Intercontinental Chemical Transport Experiment (INTEX) field campaign, an intensive study to characterize the chemical composition of the troposphere in the eastern United States, Mexico City, and the North Pacific which is the outflow region of Asia.

The first direct in situ measurements of HO_2NO_2 were made in the free troposphere over the eastern U.S. during summer 2004. The highest mean mixing ratio of 76 pptv (median = 77 pptv, σ= 39 pptv) was observed in the altitude range of 8-9 km. Highly constrained steady state calculations of HO_2NO_2 using measured HO_x levels are poorly correlated with observed HO_2NO_2 in the upper troposphere (8 km < z < 12 km; the median ratio of $[HO_2NO_2]_{SS\text{-}MEA}/[HO_2NO_2]_{MEA}$ = 2.9). However, steady state HO_2NO_2 using model-derived HO_x shows reasonable agreement with measurements in the free troposphere ($[HO_2NO_2]_{SS\text{-}MEA}/[HO_2NO_2]_{MEA}$ = 1.3). These results indicate that observed HO_2 and HO_2NO_2 are in poor agreement in the upper troposphere but that HO_2NO_2 levels are consistent with current photochemical theory.

The vertical distribution of HCl was measured over the north Pacific during May 2006 from the marine boundary layer (MBL) up to lower stratosphere. Recent stratospheric influence in the upper troposphere (8 km < z < 12 km) was efficiently identified from enhanced HCl (up to ~100 pptv) relative to very low background levels (< 2pptv). In the remote MBL, the acidification of seasalt aerosols by HNO_3 appeared to be the major source of HCl, with level consistently over 20 pptv (up to 400 pptv). Although

HCl was generally under detection limit (< 2pptv) in the mid troposphere (4 km < z < 8 km), a case study suggests that HCl may be produced in this altitude range by the dechlorination of Cl-containing dust aerosols.

The distribution of SO_2 was measured in the outflow region of the eastern U.S. and Asia; two major anthropogenic SO_2 source regions. This study presents vertical and horizontal distributions of SO_2 and relevant gas phase and aerosol parameters to characterize SO_2 transport in the troposphere. SO_2 in the boundary layer was efficiently transported to the upper troposphere by deep convection and frontal uplift processes. High SO_2 in convective plume in the upper troposphere were strongly correlated with ultrafine aerosols (diameter less that< 0.01 μm).Conversely, SO_2 from frontal uplift shows a strong correlation with non-volatile aerosols (0.01 μm to 7 μm). Comparisons of SO_2 products from global 3-D chemical transportation models (GEOS-CHEM and MOZART) with observations suggest that sulfur sources are relatively well described but that the oxidation mechanism needs refinement.

CHAPTER 1

INTRODUCTION

1.1 Overview

Airborne measurements have provided much of our knowledge about the vertical and horizontal distributions and chemistry of trace gases and aerosol in the atmosphere. The spatial scale of airborne studies depends on the performance of the airborne platform. The NASA DC-8 research aircraft, the platform used in this study, has a very large spatial coverage (1000 ft – 42,000 ft of the altitude coverage, up to 12 hours of duration, 5,400 miles range). Moreover, the large scientific payload (30,000 lbs) allows it to accommodate a large suite of instruments that can address a range of issues such as: probing the chemical evolution of emissions over large spatial extents, satellite sensor validation, and validation of global and regional chemical transport models.

Since the Pacific Exploratory Missions beginning in 1991, new findings from airborne field campaigns using the NASA DC-8 have illustrated that atmospheric chemistry in remote regions is much more complex than expected due to anthropogenic influences. Representative findings of anthropogenic perturbations in upper tropospheric HO_x -NO_x chemistry [Jaglé et al., 2001] and SO_2 enhancements in the free troposphere [Thornton et al., 1999] are presented in the next sections.

Another useful tool to probe atmospheric chemistry on the global scale is the satellite borne sensor. For these applications, raw data, mostly radiation measurements in a given spectral region are converted into final products such as mixing ratios by inverse techniques. Therefore, retrieval algorithms require at least a reasonable *a priori*, derived

from in situ measurements mostly by airborne measurements. Airborne data are also essential for the validation of retrieval algorithms. Heald et al. [2003] detail how in situ airborne measurements, satellite measurements and global chemical transport models can be integrated to study global problems.

Since trace gases and aerosol measurements from any platform have spatial and temporal limitations, scientists have developed three dimensional chemical transport models (CTMs) to probe global scale phenomena in atmospheric chemistry. Airborne measurements and CTMs have proven to be complementary. Observations have been utilized for validations of CTMs, and predictions of CTMs have been used as the basis for flight planning during airborne campaigns. Moreover, the most recent global climate model to assess global climate change adapts a chemistry module for more precise assessments [IPCC, 2007]. Hence, validations of CTMs using airborne measurements are also vital for more precise estimates of global climate change.

1.2 Outline

This work presents airborne measurements of HO_2NO_2, HCl and SO_2 by chemical ionization mass spectrometry (CIMS) during the Intercontinental Chemistry Transportation Experiment field campaign (INTEX). The INTEX field campaign consisted of two separate phases using the NASA DC-8 aircraft platform equipped with a comprehensive suite of measurements of both gases and aerosol. INTEX-NA-the first phase of the INTEX study, conducted in July and August of 2004, focused on polluted outflow from the eastern U.S [Singh et al., 2007].

The second phase of the study, INTEX-B, was conducted in March and May 2006. During the early portion of the study (March, 2006), the NASA DC-8 was deployed in Houston to sample the far and near field polluted outflow from Mexico City as part of the Megacity Initiative: Local and Global Research Observations (MILAGRO). In the later portion of the study (April – May, 2006), polluted Asian outflow was sampled from aircraft deployments in Honolulu, HI and Anchorage, AK. DC-8 deployments during the field campaign are summarized in Table 1.1. In addition, flight tracks for the entire INTEX mission are shown in the Figure 1.1. Additional description of the field campaigns, measured parameters, and major findings is presented in the first section of Chapter II.

The first part of this thesis focuses on the first direct measurements of pernitric acid, HO_2NO_2, in the upper troposphere. HO_2NO_2 is an important reservoir for both HO_x and NO_x in low temperature environments such as in the upper troposphere or at high latitudes. This study focuses on the INTEX-NA data for the analysis of HO_2NO_2 because the campaign was conducted during the summer season, when photochemical activity is at a maximum. In addition, relatively fresh, NO_x rich, plumes from intense deep convection during the field campaign give a unique environment to test upper tropospheric photochemistry in a high NO_x environment when HO_2NO_2 mixing ratios are likely to be maximum [Bertram et al., 2007]. The HO_2NO_2 data is analyzed using both simple steady state and time dependent photochemical models. Radiative transfer calculations are also performed to estimate the overtone photolysis rate of HO_2NO_2, which is probably the most uncertain loss pathway for this species.

Table 1.1 A summary of the INTEX field campaign and measured species by the CIMS instrument during the field campaign

Campaigns	Deployment Sites	# of Science Flights	Periods	Measured Species by CIMS
INTEX-NA	Mascoutha, IL Pease, NH	18	7/1 – 8/14, 2004	HO_2NO_2, and SO_2
INTEX-B Phase I	Houston, TX	7	3/1 – 3/21, 2..6	HO_2NO_2 and SO_2
INTEX-B Phase II	Honolulu, HI Anchorage, AK	10	4/17 – 5/15, 2..6	HO_2NO_2, SO_2 , and HCl

*HCl was only measured during the Anchorage, AK deployment.

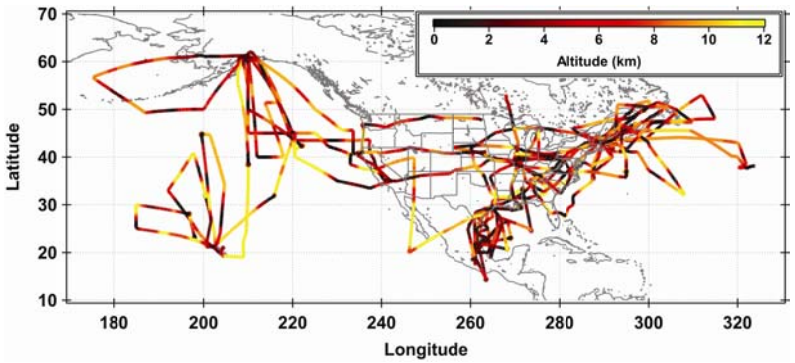

Figure 1.1 The flight tracks during the whole INTEX field campaign with color coded altitude.

During the Anchorage deployment of INTEX-B, HCl was measured by CIMS (Table 1.1). HCl in the atmosphere is thought to have two distinct primary sources. One is a product of stratospheric chlorine chemistry initiated by the photolysis of chlorofluorocarbons (CFCs), and the other is acidification of seasalt aerosols by HNO_3 or H_2SO_4 in the marine boundary layer (MBL). Although, many ground based and a limited numbers of airborne measurements of HCl have been performed, the first comprehensive airborne measurements from the marine boundary layer up to the lower stratosphere are reported in this study.

The general features of the vertical distribution of HCl are discussed and compared with previous measurements. In addition, the transport of stratospheric ozone into the troposphere is assessed using HCl as a tracer. Finally, the average Cl radical number density is estimated for the remote MBL. The Cl radical is a stronger oxidant for some important tropospheric VOCs such as Ethane, Propane, and DMS than OH. Because of the technical difficulties in measurement of Cl atom, many studies have tried to estimate Cl atom number density in the MBL using observations of hydrocarbons [Singh et al., 1996a, 1996b; Wingenter et al., 1996; Rudolph et al., 1996, 1997; Jobson et al., 1998; Wingenter et al., 1999]. However, HCl is produced from the reaction of Cl with most VOCs and can serve a more direct proxy for chlorine oxidation.

SO_2 is an important precursor of sulfate aerosols. Despite the importance of understanding of global distributions of SO_2, measurements have not been routinely performed due to technical difficulties in detecting trace levels of SO_2 in the free troposphere [Brasseur et al., 1999]. In this study we use a CIMS instrument with a high sampling frequency and a low detection limit, to measure SO_2 distributions in the outflow

of the eastern U.S. and Asia, two major global SO_2 source regions, and Mexico City, the most populated megacity in the North America.

This study presents tropospheric distributions of measured SO_2 and sulfate ratio ($[SO_4^{2-}]/([SO_2]+[SO_4^{2-}])$), which is a good indicator for the degree of sulfur oxidation. In addition, the characteristics of the distribution of SO_2 in the upper troposphere such as the origins of high SO_2 plumes and specific uplift processes from the boundary layer are investigated. Since 3-D models are important tools to evaluate global climate change, the measured SO_2 is compared to predictions from two global CTMs (GEOS-CHEM and MOZART). Finally, SO_2 distributions in the lower stratosphere and the MBL, where carbonyl sulfide and dimethyl sulfide (DMS), respectively are thought to be the major SO_2 sources are presented.

In the next sections, a brief review of tropospheric chemistry relevant to the species measured in this work is presented. In the next chapter, integrated on the NASA DC-8 aircraft and calculation schemes for the data analysis are presented.

1.3 Background

1.3.1 HO_x-NO_x Chemistry in the Troposphere

Levy [1971] proposed a radical chain reaction of HO_x, O_3, CO, and methane (Figure 1.2) as being central to tropospheric chemistry. Chameides and Walker [1973] and Crutzen [1973] proposed that the coupling of HO_x and NO_x chemistry could be the origin of tropospheric ozone. Before this time tropospheric ozone had been assumed to only be transported from the troposphere. (Figure 1.3)

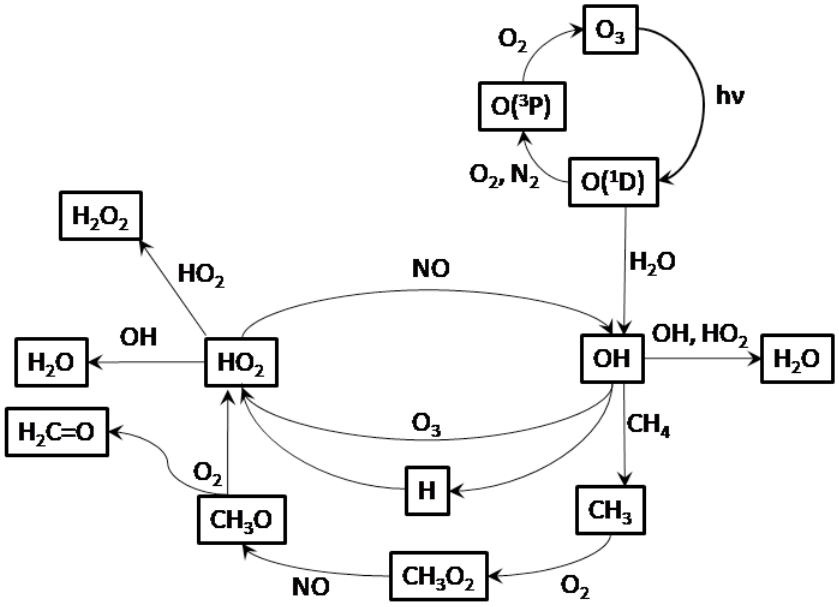

Figure 1.2 The schematic diagram of tropospheric HO_x reactions proposed by Levi [1971].

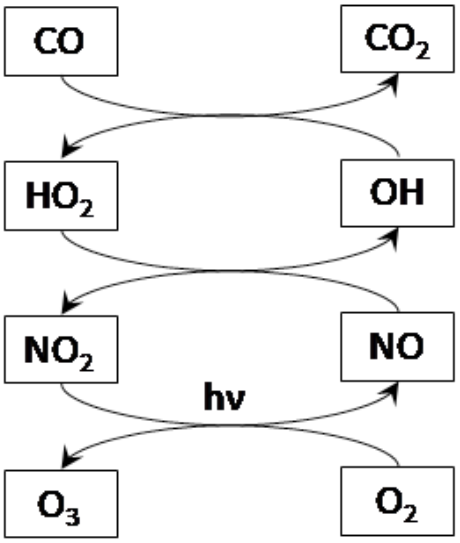

Figure 1.3 The schematic of tropospheric ozone production from HO_x-NO_x reactions proposed by Chaemeides and Walker, [1973] and Crutzen [1973].

In the past three decades, numerous intensive studies to understand HO_x-NO_x chemistry have been conducted. These results have been thoroughly summarized in the following papers. Thompson [1995] summarized both observations and model predictions of the OH radical. Bradshaw et al. [2000] summarized observations of the distribution of NO_x in the remote free troposphere from NASA airborne missions. Jaeglé [2001] summarized HO_x radical chemistry in the upper troposphere. In addition, Crutzen and Lelieveld [2001] reviewed human impacts on atmospheric chemistry, especially perturbations of the oxidation power of the atmosphere by anthropogenic activity.

In this section, HO_x-NO_x chemistry in the upper troposphere is reviewed, as this is the region of the atmosphere where HO_2NO_2 is thought to be most important. Aircraft measurements of HO_x have been conducted since 1996 [Folkins et al., 1997; Wennberg et al., 1998; Brune et al., 1998, 1999]. These studies suggested that in the upper troposphere, other sources of HO_x in addition to water vapor are necessary to reconcile the underestimation of HOx observations by photochemical models [Jaeglé et al., 2001 and references therein]. The enhanced radical source leads to higher ozone production rates than previously expected. Therefore, several studies have reevaluated the radiative forcing of upper tropospheric ozone, an important greenhouse gas because of the low temperature environment of upper troposphere [Wang and Sze, 1980; Lacis et al., 1990; Bernsten et al., 1997; Shindell et al., 2003].

Many studies have focused on investigating the importance of various HO_x sources and the physical processes by which they are transported to the upper troposphere. Deep convection has been established as an important mechanism for transporting HO_x precursors from the planetary boundary layer to the upper troposphere

[Dickerson et al., 1987; Thornton et al., 1997; Wang and Prinn, 2000]. In addition the importance of oxygenated volatile organic compounds, such as acetone and aldehydes, and peroxides as radical sources in the dry upper troposphere have been established in the last decade [Chatfield and Crutzen, 1984; Singh et al., 1995; Arnold et al., 1997; Prather and Jacob, 1997; Jaeglé et al., 1997; Cohan et al., 1999; Müller and Brasseur, 1999].

Many airborne studies have observed acetone mixing ratios in the range of 0.2 – 3 ppbv throughout the troposphere [Singh, et al., 1994, 1995, 2000, 2001; Arnold et al., 1997; Wohlfrom et al., 1999]. The major sources of acetone are terrestrial vegetation and atmospheric oxidation of organic precursors such as isoalkanes [Jacob et al., 2002]. The lifetime of acetone in the troposphere is of the order of a month due to oxidation by OH and photolysis [Gierczak et al., 1998]. Photolysis becomes the major loss pathway in the free troposphere at altitudes above 3 km due to the decrease of the OH rate constant with temperature [Gierczak et al., 1998]. The photolysis of acetone produces radicals, which can be converted into stable species such as PAN, acetic acid, and peracetic acids as described in the following reactions [Singh et al., 1995];

$$CH_3COCH_3 + h\nu + (2O_2) \rightarrow CH_3COO_2 + CH_3O_2 \qquad \text{R 1.1}$$

$$CH_3COO_2 + NO_2 \rightarrow CH_3CO(O_2)NO_2 \text{ (PAN)} \qquad \text{R 1.2}$$

$$CH_3COO_2 + HO_2 \rightarrow CH_3COOH + O_3 \text{ (67\%)} \qquad \text{R 1.3.1}$$

$$\rightarrow CH_3COO_2H + O_2 \text{ (33\%)} \qquad \text{R 1.3.2}$$

$$CH3COO_2 + NO + (O_2) \rightarrow CH_3O_2 + CO_2 + NO_2 \qquad \text{R 1.4}$$

$$CH_3O_2 + NO \rightarrow CH_3O + NO_2 \qquad \text{R 1.5}$$

$$CH_2O + O_2 \rightarrow CH_2O + HO_2 \qquad \text{R 1.6}$$

$$CH_2O + hv \rightarrow CO + H_2 \ (\sim 50\%) \qquad \text{R 1.7.1}$$

$$\rightarrow H + CHO + (2O_2) \qquad \text{R 1.7.2}$$

$$\rightarrow 2HO_2 + CO \ (\sim 30\%) \qquad \text{R 1.7.3}$$

$$CH_2O + OH \rightarrow CHO + H_2O \ (\sim 20\%) \qquad \text{R 1.8}$$

In the upper troposphere, the other important sources of HO_x are peroxides (H_2O_2 and CH_3OOH). Both H_2O_2 and CH_3OOH are products of radical chemistry as illustrated in R 1.9 and R1.10;

$$HO_2 + HO_2 \rightarrow H_2O_2 + O_2 \qquad \text{R 1.9}$$

$$CH_3O_2 + HO_2 \rightarrow CH_3OOH + O_2 \qquad \text{R 1.10}$$

The main sink of peroxides in the atmosphere is photolysis with a lifetime of a few days

$$H_2O_2 + hv \rightarrow 2OH \qquad \text{R 1.11}$$

$$CH_3OOH + hv \rightarrow OH + HO_2 + CH_2O \qquad \text{R 1.12}$$

Although H_2O_2 is a fairly soluble species with a Henry's Law constant of 8×10^4M atm^{-1} compared with CH_3OOH (3×10^4 M atm^{-1}) [O'Sullivan et al., 1996], both species are detected at high levels in deep convection plumes [Cohan et al., 1999].

In the upper troposphere, the major aldehyde species that serve as HO_x sources, are formaldehyde (HCHO) and acetaldehyde (CH_3CHO). Unexpected high levels of those aldehyde species in the background free troposphere of tropical ocean regions were

reported by Singh et al. [2001] with mixing ratio level of 70 – 300 pptv for formaldehyde and 60 – 100 pptv for acetaldehyde. However, it should be noted that acetaldehyde measurements in the remote free troposphere are considered to be technically very difficult and do not have wide acceptance in the atmospheric chemistry community [Finalyson-Pitts and Pitts, 2000]. VOC oxidation is considered to be the main source of aldehyde species in the atmosphere [Seinfeld and Pandis 1997] but comparisons of observations with the GEOS-CHEM model results over the tropical pacific troposphere indicate a significant underestimation by the model [Singh et al., 2001]. The major sinks of aldehydes in the upper troposphere compounds are photolysis and reaction with OH. Further reactions of H atoms (R 1.13) and CH_3 radicals (R 1.17) produce HO_2 radicals in the atmosphere.

<Formaldehyde>

Photolysis

$$HCHO + hv \rightarrow H + HCO \qquad \text{R 1.13}$$

$$\rightarrow H_2 + CO \qquad \text{R 1.14}$$

OH oxidation

$$HCHO + OH \rightarrow HCO + H_2O \qquad \text{R 1.15}$$

<Acetaldehyde>

Photolysis

$$CH_3CHO + hv \rightarrow CH_4 + CO \qquad \text{R 1.16}$$

$$\rightarrow CH_3 + HCO \qquad \text{R 1.17}$$

OH oxidation

$$CH_3CHO + OH \rightarrow CH_3CO + H_2O \qquad \text{R 1.18}$$

With the findings described above a more complete understanding of HO_x-NO_x chemistry in the upper troposphere has been obtained as diagrammed in Figure 1.4. Photochemical calculations using the updated scheme have demonstrated better agreements with measured HO_x results for several studies [Mckeen et al., 1997; Folkins et al., 1997; Wennberg et al., 1998; Brune et al., 1998]. However, a number of studies have still reported higher HO_x levels in the upper troposphere than can be explained with known HO_x sources especially close to sunrise and sunset [Brune et al., 1999; Wennberg et al., 1999; Jaeglé et al., 1999; Faloona et al., 2000]. These studies have commonly indicated that a lack of understanding of HO_2NO_2 chemistry or mixing ratios, unmeasured in the UT previous to this work, may be the reason for the model/measurement disagreements. In particular, several studies have demonstrated that observed HO_x levels are much larger at high NO_x levels than predicted by photochemical theory [Faloona et al., 2000]. Olson et al. [2006] illustrated that the discrepancies can be moderated by eliminating temporal inhomogeneity and including comprehensive HO_x sources from measurements. However, Ren et al. [2007] reported an observed-to-predicted HO_2 ratio of 2.5 in the upper troposphere during INTEX-NA, the most recent NASA airborne field campaign in high NO_x conditions. This indicates a fundamental lack of understanding of ozone production rates at high NO_x levels that are commonly encountered in the UT [Bertram et al., 2007] due to convective activity. The measurements of pernitric acid in this work are particularly important for providing insight into this issue as it is the most important reservoir of HO_x and NO_x in the UT for these conditions (Figure 1.4).

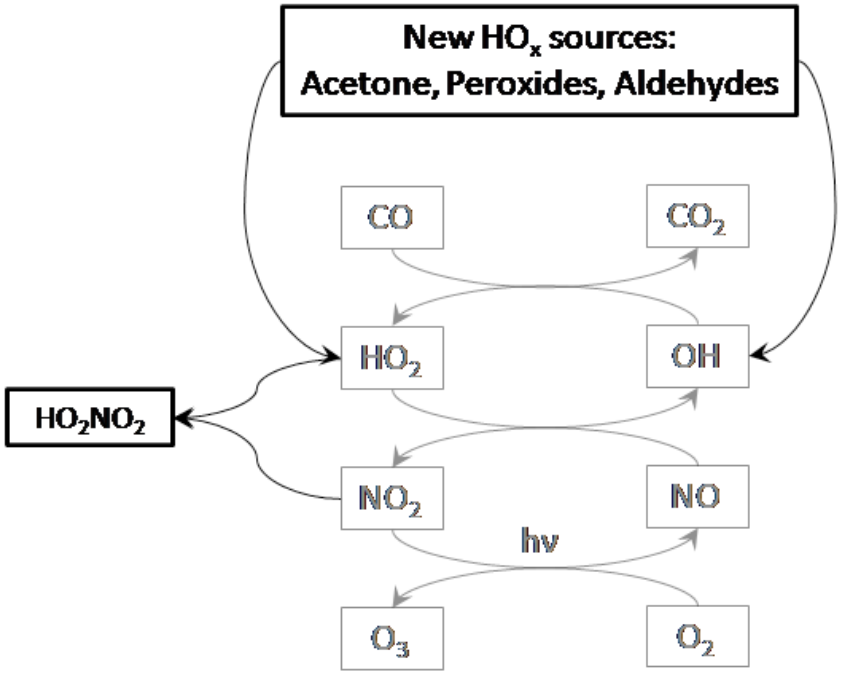

Figure 1.4 The updated HO_x-NO_x cycle in the upper troposphere since Levy [1971] from several studies of several airborne field campaigns in the mid 1990s. The grey reaction cycle represents one proposed by Crutzen [1974].

1.3.2. HCl in the Troposphere and the Lower Stratosphere

A diagram of the global HCl budget is shown in Figure 1.5. Various chemical and physical processes determine the fate of HCl including the dechlorination of seasalt aerosols which is thought to be the biggest HCl source in the troposphere, deposition to ocean and land surfaces, and the dissolution into cloud droplets. Due to the high solubility of HCl, removal processes are much faster than oxidation by OH. For example, the overall lifetime of HCl in the marine boundary layer (MBL) is estimated to be of the order of one day. Therefore, HCl produced in the MBL is not expected to be efficiently transported to other regions of the atmosphere.

One interesting aspect of chlorine chemistry in the MBL is that it may contribute to ozone production in the polluted MBL, where the level of NO_x and VOCs are relatively high. In these environments, dechlorination reactions of seasalt aerosols with NO_2 and N_2O_5 may produce significant amounts of compounds such as ClNO, $ClNO_2$, and Cl_2 [Behnke et al., 1997; Schweitzer et al., 1998; Finlayson-Pitts, 2003; Rossi et al., 2003]. These compounds can photolyze rapidly to produce Cl radicals. The Cl radicals can efficiently oxidize many VOCs to produce HCl and peroxy radicals, precursors of ozone. These processes have been reported by Spicer et al. [1998] and Finley and Saltzman [2006]. Finley and Saltzman [2006] estimated that 5-6 ppb of O_3, monitored in the research site (Irvine ,California, USA) was produced by Cl radical oxidation processes. However, in both of these studies HCl was not measured which would have confirmed the presence of high levels of Cl atoms leading to ozone production.

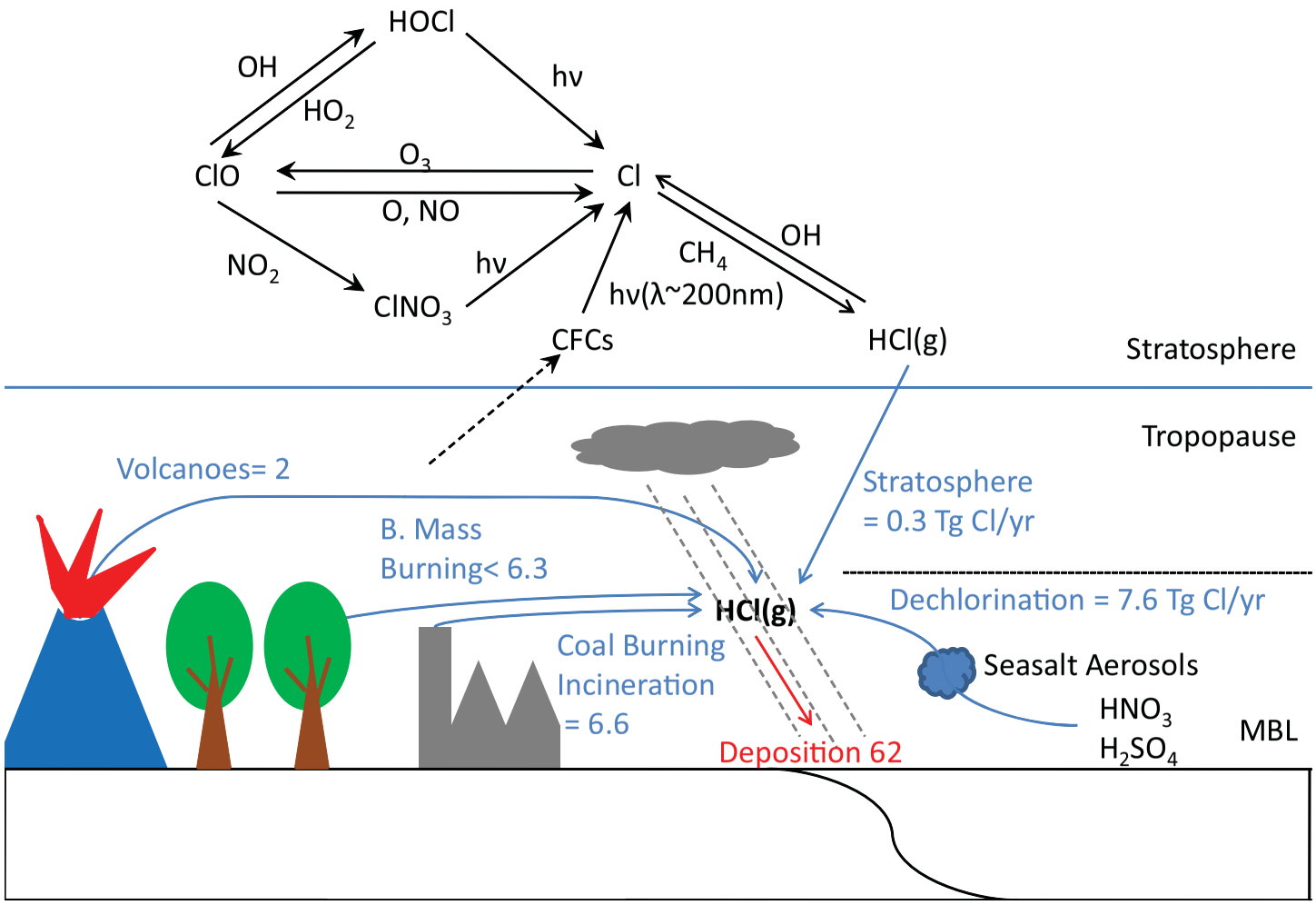

Figure 1.5 The schematic diagram of global tropospheric budget of HCl (in Tg Cl) and the stratospheric radical reaction cycle of Cl [Molina and Rowland, 1974]. Note for the huge deficit of sources to compensate the deposition term.

Anthropogenic sources such as incineration and coal combustion processes are also important sources of HCl (Figure 1.5). Coal contains a chlorine impurity of the order of 5-2000 ppmm. During the combustion process, most of the chlorine is converted in to gas phase HCl [Sun et al., 2000]. Indeed, Alpine (Coldu Dome, 4250 m ASL, French Alps) ice core analysis suggests that coal burning and incineration processes have increased background HCl [Legrand et al., 2002]. Biomass burning is also a significant source in the troposphere. Trebs et al. [2004] reported a large diurnal variation of HCl ranging from undetectable to a few hundred pptv in the Amazon basin where active biomass burning was taking place. This implies that HCl may be a direct emission from biomass burning [Andreae et al., 1996] or that dechlorination processes driven by photochemically produced HNO_3 may be a source of HCl [Trebs et al., 2004]. The diurnal variation pattern of Cl containing aerosols in biomass burning plumes was found to be consistent with the production of HCl by a dechlorination process [Trebs et al., 2005].

Although the contribution of stratospheric HCl to the tropospheric budget is relatively low (Figure 1.5), stratospheric Cl chemistry has been extensively studied due to its role in stratospheric ozone depletion. For a review of stratospheric chlorine chemistry see Molina [1996] and Solomon [1999]. The major source of chlorine in the stratosphere is the photolyis of chlorofluorocarbons (CFCs). These compounds are very stable in the troposphere but degrade in the stratosphere due to the presence of shorter wavelength radiation. The resultant Cl radicals take part in a series of reactions that destroy O_3. The terminal stratospheric chlorine cycle is effectively terminated by the reaction of the Cl radical with CH_4 to produce HCl, which has a relatively long lifetime (~30 days at 20 km,

Webster et al., 1994). There are limited measurements of HCl in the stratosphere and UT [Marcy et al., 2004; Lelieveld et al., 1999]. Recent observations by Marcy et al. [2004] indicate that HCl is an excellent tracer to evaluate transport from the stratosphere to the troposphere. However, the analysis of stratospheric ozone transport performed by Marcy et al. [2004] is dependent upon background free tropospheric levels of HCl being very low. This assumption is consistent with their observations but is in contrast to previous measurements of HCl in the free troposphere. Consequently, the HCl measurements performed over a wide range of altitudes provide an opportunity to resolve this issue.

A comprehensive review of HCl observations in the troposphere has been performed by Keene et al., [1999]. In this work a budget analysis of HCl was performed based on observed concentrations and identified sources. It was found that a significant unidentified source of HCl (twice the known source) was needed to explain observed levels. Keene et al [1999] suggested that the source due to dechlorination of sea salt aerosol might be severely underestimated and this could account for the missing source of chlorine. The observations in this thesis allow a test of this hypothesis.

1.3.3 Tropospheric SO_2

Sulfur dioxide is the dominant sulfur species emitted to the atmosphere with a large fraction of this coming form anthropogenic activity such as coal burning (Table 1.2). SO_2 (S(IV)) is oxidized by both gas phase and aqueous mechanisms in the atmosphere [Barresheim et al., 1995; Brasseur et al., 1999]. The dominant product of SO_2 oxidation is sulfate (S(VI)) which exists primarily in aerosols or cloud drops in the

atmosphere [Seinfeld and Pandis, 1997]. Therefore, aerosol formation and growth processes are highly coupled to sulfur emissions and oxidation.

Table 1.2 Estimates of global sulfur emissions (Tg S/yr) [Berresheim et al, 1995]

Source	H_2S	DMS	CS_2	OCS	SO_2	SO_4	Total[†]
Fossile Fuel Combustion+Industry	Total reduced S : 2.2				70	22	71-77 (Mid 80) (68/6)
Biomass burning	< 0.01?	-	<0.01?	0.0075	2.8	0.1	2.2-3.0 (1.4/1.1)
Oceans	< 0.3	15-25	0.08	0.08	-	40-320	15-25 (8.4/11.6)
Wetlands	0.006 -1.1	0.003-0.68	0.0003-0.06	-	-	-	0.01-2 (0.8/0.2)
Plants + Soils	0.17-0.53	0.05-0.16	0.02-0.05	-	-	2-4	0.25-0.7 (0.3/0.2)
Volcanoes	0.5-1.5	-	-	0.01	7-8	2-4	9.3-11.8 (7.6/3.0)
Antropogenic							73-80
Natural							25-40
Total							98-120

[†]Numbers in parentheses are flux from Northern Hemisphere/Southern Hemisphere

Dimethyl sulfide (DMS), emitted by phytoplankton in the ocean surface [Andrae 1990] is believed to be the major source of SO_2 in the remote MBL from oxidation by OH during the day and NO_3 during the night. Due to complexities of the reaction mechanism, DMS oxidation in the atmosphere is not well defined. Lab and field studies of DMS oxidation processes are well summarized in Ubanski and Wine [1999], Ravishankara et al. [1997] and Hewitt et al. [1997]. Recently, laboratory studies have investigated oxidation reactions of by products of DMS oxidation such as DMSO [Urbanski et al., 1998] and CH_3SO_2 [Kukui et al., 2000]. In addition, chamber studies to simulate natural conditions have been conducted to probe DMS oxidation processes [Sorensen et al., 1996; Barnes et al., 1996; Patroescu et al., 1999; Falbe-Hansen et al., 2000]. However, due to inconsistencies of experimental conditions among the studies, the results from chamber studies have shown a wide range of the SO_2 yield from DMS. For these reasons, modeling studies have been compared with comprehensive field measurements of DMS, SO_2, and OH to deduce the "best-estimated" yield of SO_2 from DMS oxidation. Chen et al. [2000] reported 0.65 ± 0.15 for a conversion efficiency for SO_2 from DMS using a ground measurement dataset from Christmas Island. Davis et al. [1999] also reported 0.72 ± 0.22 of the conversion efficiency using an airborne measurement dataset over the MBL near Christmas Island. In this study, a comprehensive measurement dataset and MOZART model results over the remote North Pacific are compared to examine DMS contributions for SO_2 distributions in the remote MBL.

Carbonyl sulfide (OCS) is another reduced form of sulfur that is important in the atmosphere. The major sources of OCS to the troposphere are oxidation of CS_2, oceanic and anthropogenic emissions [Seinfeld and Pandis, 1997; Blake et al., 2004]. OCS is

chemically stable in the troposphere (the chemical lifetime is ~35 years mainly due to photolysis and the overall lifetime is ~5 years mostly due to vegetation uptake) with an average mixing ratio of ~500 pptv [Chin and Davis, 1995]. However, in the stratosphere shorter wavelength ultraviolet radiation can photolyze OCS leading to the formation of SO_2 (~10 year chemical lifetime; Chin and Davis [1995]). This process was suggested as the major source of stratospheric SO_2 by Crutzen [1976]. The origin of stratospheric SO_2 had been investigated since Junge et al., [1961] reported stratospheric sulfate aerosols. However, Chin and Davis [1995] performed calculations using a 1-D model that indicated that other significant sources of sulfur are needed in addition to OCS photolysis to explain the sulfate aerosols in the stratosphere. This finding was confirmed by a recent analysis using 3-D chemical transport model [Pitari et al., 2002; Timmreck, 2001], which indicated that only 43% of global stratospheric sulfate aerosols can be explained by the OCS photolysis. Instead, injections of SO_2 into the stratosphere from deep convection in the region of the intertropical convergence zone (ITCZ) are needed to support the stratospheric sulfate burden [Kjellstrom, 1998; Pitari et al., 2002; Timmreck, 2001]. However, the analysis of the stratospheric dataset by Singh et al. [1997] during Pacific Exploratory Mission (PEM)-West reported a correspondence between the decrease of the OCS mixing ratio (30 pptv) with an increase in the SO_2 mixing ratio. They concluded that OCS was the major source of SO_2 in the stratosphere air. The observations of SO_2 in the lower stratosphere in this work allow the investigation of the relationship between stratospheric OCS and SO_2.

Due to its climatic importance, sulfur chemistry is included in general circulation models (GCM) that are used to predict climate scenarios. However, as summarized in the

report of the Intergovernmental Panel on Climate Change (IPCC) there is little correlation between predictions by different models of sulfur emissions, lifetime and production efficiency of sulfate. Those differences cause significant uncertainties in estimations of radiative forcing from sulfate aerosols [IPCC, 2007]. Some global modeling studies of sulfate aerosols have been conducted to validate their SO_2 model products with airborne measurements. The comparisons have shown that global CTMs reasonably capture the convection features and boundary layer mixing ratio of SO_2 [Chin et al., 1996; Chin et al., 2000; Park et al., 2005]. However, some studies also suggested that model treatments of cloud-SO_2 interactions are needed for further investigations [Tu et al., 2003; Tu et al., 2004; Park et al, 2004].

1.4 References

Andrae, M. O.: Ocean-atmospehere interactions in the global biogeochemical sulfur cycle, Marine Chemistry, 30, 1-29, 1990.

Andrae, M. O., Atlas, E., Harris, G. W., Helas, G., de Kock, A., Koppmann, R., Maenhaut, W., Mano, S., Pollock, W. H., Rudolph, J., Scharffe, D., Schebeske, G., and Welling, M.: Methyl halide emissions from savanna fires in southern Africa, Journal of Geophysical Research, 101, 23603-23613, 1996.

Arnold, F., Burger, V., Droste-Fanke, B., Grimm, F., Krieger, A., Schneider, J., and Stilp, T.: Acetone in the upper troposphere and lower stratosphere impact on trace gases and aerosols, Geophysical Research Letters, 24, 3017-3020, 1997.

Barnes, I., Becker, K. H., and Patroescu, I.: FTIR product study of oh initiated oxidation of dimethyl sulfide: Observation of carbonyl sulfide and dimethyl sulphoxide, Atmospheric Environment, 30, 1805-1714, 1996.

Behnke, W., George, C., Scheer, V., and Zetzsch, C.: Production and decay of $clno_2$ from the reaction of gaseous N_2O_5 with NACL solution: Bulk and aerosol experiments, Journal of Geophysical Research, 102, 3795-3804, 1997.

Berntsen, T. K., Iasksen, I. S. A., Myhre, G., Fuglestvedt, J. S., Stordal, F., Alsvik Larsen, T., Freckleton, R. S., and Shine, K. P.: Effects of anthropogenic emissions on tropospheric ozone and its radiative forcing, Journal of Geophysical Research, 102, 28101-28126, 1997.

Berresheim, H., Wine, P. H., and Davis, D. D.: Sulfur in the atmosphere, in: Composition, chemistry, and climate of the atmosphere, edited by: Singh, H. B., Wiley, New York, 1995.

Bertram, T. H., Perring, A. E., Wooldridge, P. J., Crounse, J. D., Kwan, A. J., Wennnberg, P. O., Scheuer, E., Dibb, J., Avery, M., Sachse, G., Vay, S., Crawford, J. H., McNaughton, C. S., Clarke, A., Pickering, K. E., Fuelberg, H., Huey, G., Blake, D. R., Singh, H. B., Hall, S. R., Shetter, R. E., Fried, A., Heikes, B. G., and Cohen, R. C.: Direct measurements of the convective recycling of the upper troposphere, Science, 315, 816 - 820, 2007.

Blake, N. J., Streets, D. G., Woo, J.-H., Simpson, I. J., Green, J., Meinardi, S., Kita, K., Atlas, E., Fuelberg, H. E., Sachse, G., Avery, M. A., Vay, S. A., Talbot, R. W., Dibb, J. E., Bandy, A. R., Thornton, D. C., Rowland, F. S., and Blake, D. R.: Carbonyl sulfide and carbon disulfide: Large-scale distributions over the western pacific and emissions from Asia during TRACE-P, Journal of Geophysical Research, 109, doi:10.1029/2003JD004259, 2004.

Bradshaw, J., DAvis, D., Grodzinsky, G., Smyth, S., Newell, R., Sandholm, S., and Liu, S.: Observed distribution of nitrogen oxides in the remote free troposphere from the NASA global tropospheric experiment programs, Reveiws of Geophysics, 38, 61-116, 2000.

Brasseur, G., Orlando, J. J., and Tyndall, G. S.: Atmospheric chemistry and global change, 1st ed., Topics in environmental chemistry, edited by: Birks, J. W., Oxford University Press, New York, 1999.

Brune, W. H., Tan, D., Faloona, I. C., Weinheimer, A. J., Campos, T. L., Ridley, B. A., Vay, S. A., Collins, J. E., Sachse, G. W., Jaeglé, L., and Jacob, D. J.: Airborne in situ OH and HO_2 observations in the cloud free troposphere and lower stratosphere during success, Geophysical Research Letters, 25, 1701-1704, 1998.

Brune, W. H., Tan, D., Faloona, I. F., Jaglé, L., Jacob, D. J., Heikes, B. G., Snow, J., Kondo, Y., Shetter, R., Sachse, G. W., Anderson, B., Gregory, G. L., Vay, S., Singh, H. B., Davis, D. D., Crawford, J. H., and Blake, D. R.: OH and HO_2 chemistry in the north atlantic free troposphere, Geophysical Research Letters, 26, 3077-3080, 1999.

Chameides, W. L., and Walker, J. C. G.: A photochemical theory of tropospheric ozone, Journal of Geophysical Research, 78, 8751-8759, 1973.

Chatfield, R. B., and Crutzen, P. J.: Sulfur dioxide in remote oceanic air: Cloud transport of reactive precursors, Journal of Geophysical Research, 89, 7111-7132, 1984.

Chen, G., Davis, D. D., Kasibhatla, P., Bandy, A. R., Thornton, D. C., Huebert, B. J., Clarke, A. D., and Blomquist, B. W.: A study of DMS oxidation in the tropics: Comparison of Christmas Island field observations of DMS, SO_2, and DMSO with model simulation, Journal of Atmospheric Chemistry, 37, 137-160, 2000.

Chen, W.-T., Liao, H., and Seinfeld, J. H.: Future climate impacts of direct radiative forcing of anthropogenic aerosols, tropospheric ozone, and long lived greenhouse gases, Journal of Geophysical Research, 112, doi:10.1029/2006JD008051, 2007.

Chin, M., and Davis, D.: A reanalysis of carbonyl sulfide as a source of stratospheric background sulfur aerosols, Journal of Geophysical Research, 100, 8993-9005, 1995.

Chin, M., Jacob, D. J., Gardner, G. M., Foreman-Fowler, M. S., Spiro, P. A., and Savoie, D. L.: A global three-dimensional model of tropospheric sulfate, Journal of Geophysical Research, 101, 18667-18690, 1996.

Chin, M., Rood, R. B., Lin, S.-J., Muller, J.-F., and Thompson, A. M.: Atmospheric sulfur cycle simulated in the global model gocart: Model descripion and global properties, Journal of Geophysical Research, 105, 24671-24687, 2000.

Cohan, D. S., Schultz, M. G., Jacob, D. J., Heikes, B. G., and Blake, D. R.: Convective injection and photochemical decay of peroxides in the tropical upper troposphere: Methyl iodide as a tracer of marine convection Journal of Geophysical Research, 104, 5717-5724, 1999.

Crutzen, P. J.: Ozone production rates in an oxygen-hydrogen-nitrogen oxide atmosphere, Pure and Applied Geopysics, 96, 320-327, 1973.

Crutzen, P. J.: The possible importance of ocs for the sulfate layer of the stratosphere, Geophysical Research Letters, 3, 73-76, 1976.

Crutzen, P. J., and Lelieveld, J.: Human impacts on atmospheric chemistry, Annual Review of Earth and Planetary Science, 2001.

Davis, D., Chen, G., Bandy, A., Thornton, D., Eisele, F., Mauldin, L., Tanner, D., Lenschow, D., Fuelberg, H., Huebert, B., Heath, J., Clarke, A., and Blake, D.: Dimethyl sulfide oxidation in the equatorial pacific: Comparison of model simulations with field observations for DMS, SO_2, H_2SO_4 (g), MSA(g), MS, and NSS, Journal of Geophysical Research, 104, 5765-5784, 1999.

Dickerson, R. R., Huffman, G. J., Luke, W. T., Nunnermacker, L. J., Pickering, K. E., Lesie, A. C. D., Lindsey, C. G., Slinn, W. G. N., Kelly, T. J., Daum, P. H., Delany, A. C., Greenberg, J. P., Zimmerman, P. R., Boatman, J. F., Ray, J. D., and Stedman, D. H.: Thunderstorms: An important mechanism in the transport of air pollutants, Science, 235, 460-465, 1987.

Falbe-Hansen, F., Sorensen, S., Jensen, N., Pedersen, T., and Hjorth, J.: Atmospheric gas-phase reactions of dimethylsulphoxide and dimethylsulphone with OH and NO_3 radicals, cl atmos, and ozone, Atmospheric Environment, 34, 1543-1551, 2000.

Faloona, I. C., Tan, D., Brune, W. H., Jaeglé, L., Jacob, D. J., Kondo, Y., Koike, M., Chatfield, R., Pueschel, R., Ferry, G., Sachse, G., Vay, S., Anderson, B., Hannon, J., and Fuelberg, H.: Obseravtions of hox and its relationship with NO_x in the upper troposphere during SONEX, Journal of Geophysical Research, 105, 3771-3783, 2000.

Finlayson-Pitts, B. J.: The tropospheric of sea salt; a molecular-level view of the chemistry of NaCl and NaBr, Chemistry Review, 103, 4801-4822, 2003.

Finlayson-Pitts, B. J., and Pitts, J. N.: Chemistry of the upper and lower atmopshere-theory, experiments, and applications, 1st ed., Academic Press, New York, 2000.

Finley, B., and Saltzman, E.: Measurement of Cl_2 in coastal urban air, Geophysical Research Letters, 33, L11809,doi:11810.11029/12006GL025799, 2006.

Folkins, I., Wennnberg, P. O., Hanisco, T. F., Andersen, J. G., and Salawitch, R. J.: OH, HO_2, and no in two biomass burning plumes: Sources of hox and implications for ozone production, Geophysical Research Letters, 24, 3185-3188, 1997.

Gierczak, T., Burkholder, J. B., Bauerle, S., and Ravishankara: Photochemistry of acetone under tropospheric conditions, Chemical Physics, 231, 229-244, 1998.

Heald, C. L., Jacob, D. J., Fiore, A. M., Emmons, L. K., Gille, J. C., Deeter, M. N., Warner, J., Edwards, D. P., Crawford, J. H., Hamlin, A. J., Sachse, G. W., Browell, E. V., Avery, M. A., Vay, S. A., Westberg, D. J., Blake, D. R., Singh, H. B., Sandholm, S. T., Talbot, R. W., and Fuelberg, H. E.: Asian outflow and trans-pacific transport of carbon monoxide and ozone pollution: An integrated satellite, aircraft, and model perspective, Journal of Geophysical Research, 108,

4804,doi:4810.1029/2003JD003507, 2003.

Hewitt, C. N., Davison, B., Cox, R. A., Toumi, R., Ayres, G. P., and Ravishankara, A. R.: Field measurements of dimethyl sulfide and its oxidation products in the atmosphere, Philosophical Transactions: Biological Sciences, 352, 183-189, 1997.

IPCC: Climate change 2007: The physical science basis, Cambridge University Press, Cambridge, UK and New York, US, 2007.

Jaeglé, L., Jacob, D. J., Brune, W. H., and Wennnberg, P. O.: Chemistry of HO_x radicals in the upper troposphere, Atmospheric Environment, 35, 469-489, 2001.

Jaeglé, L., Jacob, D. J., Wennnberg, P. O., Spivakovsky, C. M., Hanisco, T. F., Lanzendorf, E. J., Hintsa, E. J., Fahey, D. W., Keim, E. R., Proffitt, M. H., Atlas, E. L., Flocke, F., Schauffler, S., McElroy, C. T., Midwinter, C., Pfister, L., and Wilson, J. C.: Observed OH and HO_2 in the upper troposphere suggest a major source from convective injection of peroxides, Geophysical Research Letters, 1997.

Jaeglé, L., Jacob, D. J., Brune, W. H., Faloona, I. C., Tan, D., Kondo, Y., Sachse, G. W., Anderson, B., Gregory, G. L., Vay, S., Singh, H. B., Blake, D. R., and Shetter, R.: Ozone production in the upper troposphere and the influence of aircraft during sonex: Approaching NO_x-saturated conditions, Geophysical Research Letters, 26, 3081-3084, 1999.

Jobson, B. T., Parrish, D., Goldan, P., Kuster, W., Feshenfeld, F. C., Blake, D. R., Blake, N. J., and Niki, H.: Spatial and temporal variability of nonmethane hydrocarbon mixing ratios and their relation to photochemical lifetime, Journal of Geophysical Research, 103, 13557-13567, 1998.

Junge, C. E., Chagnon, C. W., and Manson, J. E.: A world-wide stratospheric aerosol layer, Science, 133, 1478-1479, 1961.

Keene, W. C., Aslam, M., Khalil, K., Erickson, D. J., McCulloch, A., Graedel, T. E., Lobert, J. M., Aucott, M. L., Gong, S. L., Harper, D. B., Kleiman, G., Midgley, P., Moore, R. M., Seuzaret, C., Sturges, W. T., Benkovitz, C. M., Koropalov, V., Barrie, L. A., and Li, Y. F.: Composite global emissions of reactive chlorine from anthropogenic and natural resorces; reactive chlorine emissions inventory, Journal of Geophysical Research, 104, 8429-8440, 1999.

Kjellstrom, E.: A three-dimensional global model study of carbonyl sulfide in the troposphere and the lower stratosphere, Journal of Atmospheric Chemistry, 29, 151-177, 1998.

Kukui, A., Bossoutrot, V., Laverdet, G., and Le Bras, G.: Mechanism of the reaction of CH_3SO_2 with NO_2 in relation to atmopsheric oxidation of dimethyl sulfide: Experimental and theoretical study, Journal of Physical Chemistry, 104, 935-946, 2000.

Lacis, A. A., Wuebbles, D. J., and Logan, J. A.: Radiative forcing of climate by changes

in the vertical distribution of ozone, Journal of Geophysical Research, 95, 9971-9981, 1990.

Legrand, M., Preunkert, S., Wagenbach, D., and Fischer, H.: Seasonaly resolved alpine and greenland ice core records of anthropogenic HCl emissions over the 20th century, Journal of Geophysical Research, 107, 4139,4110.1029/2001JD001165, 2002.

Levy II, H.: Normal atmosphere: Large radical and formaldehyde concentration predicted, Science, 173, 141-143, 1973.

Marcy, T. P., Fahey, D. W., Gao, R. S., Popp, P. J., Richard, E. C., Thompson, T. L., Rossenlof, K. H., Ray, E. A., Salawitch, R. J., Atherton, C. S., Bergmann, D. J., Ridley, B. A., Weinheimer, A. J., Loewenstein, M., Weinstock, E. M., and Mahoney, M. J.: Quantifying stratospheric ozone in the upper troposphere with in situ measurements of HCl, Science, 304, 261-265, 2004.

McKeen, S. A., Gierczak, T., Burkholder, J. B., Wennnberg, P. O., Hanisco, T. F., Keim, E. R., Gao, R.-S., Liu, S. C., Ravishankara, A. R., and Fahey, D. W.: The photochemistry of acetone in the upper troposphere: A source of odd-hydrogen radicals, Geophysical Research Letters, 24, 3177-3180, 1997.

Molina, M. J.: Role of chlorine in stratospheric chemistry, Pure and Applied Chemistry, 68, 1749-1756, 1996.

Muller, J.-F., and Brasseur, G.: Sources of upper tropospheric HO_x: A three-dimensional study, Journal of Geophysical Research, 104, 1705-1715, 1999.

O'Sullivan, D. W., Lee, M., Noone, B. C., and Heikes, B. G.: Henry's law constant determinations for hydrogen peroxides, methylhydrogenperoxide, hydroxymethylhydroperoxide, ethylhydroperoxide, and peroxyacetic acid, Journal of Physical Chemistry, 100, 3241-3247, 1996.

Olson, J. R., Crawford, J. H., Chen, G., Brune, W. H., Faloona, I. C., Tan, D., Harder, H., and Martinez, M.: A reevaluation of airborne HO_x observations from nasa field campaigns, Journal of Geophysical Research, 111, doi:10.1029/2005JD006617, 2006.

Park, R. J., Jacob, D. J., Field, B. D., Yantosca, R. M., and Chin, M.: Natural and transboundary pollution influences on sulfate-nitrate-ammonium aerosols in the united sates: Impications for policy, Journal of Geophysical Research, 109, doi:10.1029/2003JD004473, 2004.

Park, R. J., Jacob, D. J., Palmer, P. I., Clarke, A. D., Weber, R. J., Zondlo, M. A., Eisele, F. L., Bandy, A. R., thornton, D. C., Sachse, G. W., and Bond, T. C.: Export efficiency of black carbon aerosol in continental outflow: Global implications, Journal of Geophysical Research, 110, doi:10.1029/2004JD005435, 2005.

Patroescu, I. V., Barnes, I., Becker, K. H., and Mihaloposlos, N.: Ft-IR product study of the oh-initiated oxidation of dms in the presence of nox, Atmospheric

Environment, 33, 25-35, 1999.

Pitari, G., Manicini, E., Rizi, V., and Shindell, D. T.: Impact of future climate and emission changes on stratospheric aerosols and ozone, Journal of Atmospheric Sciences, 59, 414-440, 2002.

Prather, M. J., and Jacob, D. J.: A persistent imbalance in HO_x and NO_x photochemistry of the upper troposphere driven by deep tropical convection, Geophysical Research Letters, 24, 3189-3192, 1997.

Ravishankara, A. R., Rudich, Y., Talukdar, R., Barone, S. B., Le Bras, G., Fish, D. J., Ayres, G. P., and Cox, R. A.: Oxidation of atmospheric reduced sulfur compounds: Perspective from laboratory studies, Philosophical Transactions: Biological Sciences, 352, 171-182, 1997.

Ren, X., Olson, J. R., Crawford, J. H., Brune, W. H., Mao, J., Long, R. B., Chen, G., Avery, M. A., Sachse, G. W., Barrick, J. D., Diskin, G. S., Huey, L. G., Fried, A., Cohen, R. C., Heikes, B., Wennnberg, P., Singh, H. B., Blake, D. R., and Shetter, R. E.: Hox observation and model comparison during INTEX-A 2004, Journal of Geophysical Research, Submitted, 2007.

Rossi, M. J.: Heterogeneous reactions on salts, Chemical Reviews, 103, 4823-4882, 2003.

Rudolph, J., Koppmann, R., and Plass-Dulmer, C.: The budget of ethane and tetrachloroethene: Is there evidence for an impact of reactions with chlorine atoms in the troposphere?, Atmospheric Environment, 30, 1887-1894, 1996.

Rudolph, J., Ramacher, B., Plass-Dulmer, C., Muller, K.-P., and Koppmann, R.: The indirect determination of chlorine atom concentration in the troposphere from changes in the patterns of non-methane hydrocarbons, Tellus, 49B, 592-601, 1997.

Schindell, D. T., Faluvegi, G., and Bell, N.: Preindustrial-to-present-day radiative forcing by tropospheric ozone from improved simulations with giss chemistry-climate gcm, Atmospheric Chemistry and Physics, 3, 1675-1702, 2003.

Schweitzer, F., Mirabel, P., and George, C.: Multiphase chemistry of N_2O_5, $ClNO_2$ and $BrNO_2$, Journal of Physical Chemistry A, 102, 3942-3952, 1998.

Seinfeld, J. H., and Pandis, S. N.: Atmospheric chemistry and physics-from air pollution to climate change, 1st ed., Wiley-Interscience Publication, New York, 1997.

Singh, H., Chen, Y., Staudt, A., Jacob, D., Blake, D., Heikes, B., and Snow, J.: Evidence from the pacific troposphere for large global sources of oxygenated organic compounds, Nature, 410, 1078-1081, 2001.

Singh, H., Chen, Y., Tabazadeh, A., Fukui, Y., Bey, I., Yantosca, R., Jacob, D., Arnold, F., Wohlfrom, K., Atlas, E., Flocke, F., Blake, D., Blake, N., Heikes, B., Snow, J., Talbot, R., Gregory, G., Sachse, G., Vay, S., and Kondo, Y.: Distribution and fate

of selected oxygenated organic species in the troposphere and lower stratosphere over the Atlantic, Journal of Geophysical Research, 105, 3795-3805, 2000.

Singh, H. B., Brune, W. H., Crawford, J., and Jacob, D.: Overview of the summer 2004 intercontinental chemical transport experiment-north America (INTEX-A), Journal of Geophysical Research, 111, doi:10.1029/2006JD007905, 2007.

Singh, H. B., Chen, Y., Gregory, G. L., Sachse, G. W., Talbot, R., Blake, D. R., Kondo, Y., Bradshaw, J. D., Heikes, B., and Thornton, D.: Trace chemical measurements from the northern midlatitude lowermost stratosphere in early spring: Distribution, correlaiton, and fate, Geophysical Research Letters, 24, 127-130, 1997.

Singh, H. B., Gregory, G. L., Anderson, B., Browell, E., Sachse, G. W., Davis, D. D., Crawford, J., Bradshaw, J. D., Talbot, R., Blake, D. R., Thornton, D., Newell, R., and Merrill, J.: Low ozone in the marine boundary layer of the tropical Pacific ocean;photochemical loss, chlorine atoms, and entrainment, Journal of Geophysical Research, 101, 1907-1914, 1996a.

Singh, H. B., Kanakidou, M., Crutzen, P. J., and Jacob, D. J.: High concentrations and photochemical fate of oxygenated hydrocarbons in the global troposphere, Nature, 378, 50-54, 1995.

Singh, H. B., O'Hara, D., Herlth, D., Sachse, G., Blake, D. R., Bradshaw, J. D., Kanakidou, M., and Crutzen, P. J.: Acetone in the atmosphere: Distribution, sources, and sinks, Journal of Geophysical Research, 99, 1821-1836, 1994.

Singh, H. B., Thakur, A. N., Chen, Y. E., and Kanakidou, M.: Tetrachloroethylene as an indicator of low cl atom concentrations in the troposphere, Geophysical Research Letters, 23, 1529-1532, 1996b.

Solomon, S.: Stratospheric ozone depletion: A review of concepts and history, Reviews of Geophysics, 37, 275-316, 1999.

Sorensen, S., Falbe-Hansen, H., Mangoni, M., Hjorth, J., and Jensen, N.: Observation of dmso and $CH_3S(O)OH$ from gas phase reaction between dms and oh, Journal of Atmospheric Chemistry, 24, 299-315, 1996.

Spicer, C. W., Chapman, E. G., Finlayson-Pitts, B. J., Plastridege, R. A., Hubbe, J. M., and Fast, J. D.: Unexpected high concentrations of molecular chlorine in coastal air, Nature, 394, 353-356, 1998.

Sun, J. Q., Crocker, C. R., and Lillemoen, C. M.: The effect of coal combustion flue gas components on low-level chlorine speciation using EPA method 26a, Journal of the Air and Waste Management Association, 50, 936-940, 2000.

Thompson, A. M.: Measuring and modling the tropospheric hydroxyl radical (OH), Journal of Atmospheric Sciences, 52, 3315-3327, 1995.

Thornton, D. C., Bandy, A. R., Bloomquist, B. W., Talbot, R. W., and Dibb, J. E.:

Transport of sulfur dioxide from the Asian Pacific Rim to the North Pacific troposphere, Journal of Geophysical Research, 102, 28489-28499, 1997.

Timmreck, C.: Three-dimensional simulation of stratospheric background Journal of Geophysical Research, 106, 28313-28332, 2001.

Trebs, I., Meixner, F. X., Otjes, R., Jongejan, P., and Andrae, M. O.: Real-time measurements of ammonia, acidic trace gases and water soluble inorganic aerosol species at a rural site in the Amazon basin, Atmospheric Chemistry and Physics, 4, 967-987, 2004.

Trebs, I., Metzger, S., Meixner, F. X., Helas, G., Hoffer, A., Rudich, Y., Falkovich, A. H., Moura, A. L., da Silva Jr., R. S., Artaxo, P., Slanina, J., and Andrae, M. O.: The NH_4-NO_3-Cl-SO_4^{2-}-H_2O aerosol system and its gas phase precursors at a pasture site in the Amazon basin: How relevant are mineral cations and soluble organic acids?, Journal of Geophysical Research, 110, doi:10.1029/2004JD005478, 2005.

Tu, F. H., Thornton, D. C., Bandy, A. R., Carmichael, G. R., Tang, Y., Thornhill, K. L., Sachse, G. W., and Blake, D. R.: Long-range transport of sulfur dioxide in the central pacific, Journal of Geophysical Research, 109, doi:10.1029/2003JD004309, 2004.

Tu, F. H., Thornton, D. C., Bandy, A. R., Kim, M.-S., Carmichael, G., Tang, Y., Thornhill, L., and Sachse, G.: Dynamics and transport of sulfur dioxide over the yellow sea during trace-p, Journal of Geophysical Research, 108, 8790, doi:8710.1029/2002JD003227, 2003.

Urbanski, S. P., Stickel, R. E., and Wine, P. H.: Mechanistic and kinetic study of the gas-phase reaction of hydroxyl radical with dimethyl sulfoxide, Journal of Physical Chemistry, 102, 10522-10529, 1998.

Urbanski, S. P., and Wine, P. H.: Chemistry of gas phase organic sulfur centered radicals, in: S-centered radicals, edited by: Alfassi, Z. B., John Willey, New York, 97-140, 1999.

Wang, C., and Prinn, R. G.: On the roles of deep convective clouds in troposphere chemistry, Journal of Geophysical Research, 105, 22,269-222,297, 2000.

Wang, W.-C., and Sze, N. D.: Coupled effects of atmospheric N_2O and O_3 on the earth's climate, Nature, 286, 589-590, 1980.

Wennnberg, P. O., Hanisco, T. F., Jaeglé, L., Jacob, D. J., Hintsa, E. J., Lanzendorf, E. J., Andersen, J. G., Gao, R.-S., Keim, E. R., Donnelly, S. G., Del Negro, L. A., Fahey, D. W., McKeen, A., Salawitch, R. J., Webster, C. R., May, R. D., Herman, R. L., Proffitt, M. H., Margitan, J. J., Atlas, E. L., Schauffler, S. M., Flocke, F., McElroy, C. T., and Bui, T. P.: Hydrogen radicals, nitrogen radicals, and the production of O3 in the upper troposphere, Science, 279, 49-53, 1998.

Wennnberg, P. O., Salawitch, R. J., Donaldson, D. J., Hanisco, T. F., Lanzendorf, E. J.,

Perkins, K. K., Lloyd, S. A., Vaida, V., Gao, R.-S., Hintsa, E. J., Cohen, R. C., Swartz, W. H., Kusterer, T. L., and Anderson, D. E.: Twilight observations suggest unknown sources of HO_x, Geophysical Research Letters, 26, 1373-1376, 1999.

Wingenter, O. W., Blake, D. R., Blake, N. J., Sive, C., Rowland, F. S., Atlas, E., and Flocke, F.: Tropospheric hydroxyl and atomic chlorine concentrations, and mixing timescales determined from hydrocarbon and halocarbon measurements mad over the southern ocean, Journal of Geophysical Research, 104, 21819-21818, 1999.

Wingenter, O. W., Kubo, M. K., Blake, N. J., Smith, J., T. W., Blake, D. R., and Rowland, F. S.: Hydrocarbon and halocarbon measurements as photochemical and dynamical indicators of atmospheric hydroxyl, atomic chlorine, and vertical mixing obtained during lagrangian flights, Journal of Geophysical Research, 101, 4331-4340, 1996.

Wohlfrom, K.-H., Hauler, T., Arnold, F., and Singh, H.: Acetone in the free troposphere and lower stratosphere: Aircraft based CIMS and GC measurements over the north Atlantic and a first comparison, Geophysical Research Letters, 26, 2849-2825, 1999.

Chapter 2

METHODS

2.1 Aircraft Payload

The NASA DC-8 research aircraft was used as the airborne platform for all of the measurements described in this thesis. The DC-8 was instrumented with a comprehensive suite of trace gas, aerosol, radiation, and meteorological measurements for the Intercontinental Chemical Transportation Experiment (INTEX) campaign. The mission was also supported by global 3D model products, satellite borne measurements, and ground based measurements to facilitate a comprehensive study of the transport of pollution. The DC-8 payload and model products for both INTEX-NA and INTEX-B are listed in Table 2.1. Observations and model products used in the analyses in this work are indicated in the table. All of the analyses in this work were performed with a one minute average merged dataset, processed by the NASA Tropospheric Chemistry Integrated Data Center (http://www-air.larc.nasa.gov/index.htm).

Table 2.1 Summary of DC-8 payload and global 3D models during the INTEX field campaign

Parameters	Method	Frequency	References	[a]NA	[b]B
[#]CO, CH_4	Diode laser spectrometer	1 sec	Sachse et al. [1987]	O	O
[#]O_3	Chemiluminescence	1 sec	Avery et al. [2001]	O	O
[#]H_2O (v)	Diode laser hygrometer	1 sec	Podolske et al. [2003]	O	O
CO_2	Non Dispersive IR Spectrometry	1 sec	Vay et al. [2003]	O	O
[#]H_2O_2, [#]CH_2O, [#]CH_3OOH	HPLC	~ min	Lee et al. [1995]	O	O
[#]OH, [#]HO_2	LIF	20 secs	Brune et al. [1995]	O	O
NO	Chemiluminescence	1 sec	Ryerson et al. [1999]	X	O
PANs, Oxygenated Hydrocarbons, HCN	GC-ECD, GC-PID	~ min	Singh et al. [2007]	O	O
HNO_3, H_2O_2, HNO_3, PAA	CIMS	few secs	Crounse et al.[2006]	O	X
[#]NO_2, ANs, PNs, HNO_3	Thermal Dissociaiton - LIF	few secs	Thornton et al. [2000]	O	O
[#]CH_2O	Tunable Diode Laser Spectrometry	few secs	Roller et al. [2006]	O	O
[#]NMHCs and [#]Halocarbons	Whole air sampling	~ min	Blake et al. [2003]	O	O
[#]HNO_3, [#]Fine aerosol sulfate	Mist Chamber	~ min	Dibb et al. [2003]	O	O
Bulk aerosol ionic composition (Cl^- NO_3^- etc)	Filter	~ min	Dibb et al. [2003]	O	O
Aerosol ionic composition	PILS-IC	~ min	Hennigan et al. [2006]	O	X
[#]Physical Aerosol Parameters (size distributions, counts, etc)	Wing Pod instruments	variable	Shinozuka et al. [2007]	O	O
[#]Photolysis frequencies	Scanning Actinic Flux Spectroradiometers	10 secs	Shetter and Müller. [1999]	O	O
Tropospheric O_3, aerosols, cloud profiles	LIDAR	-	Wulfmeyer et al. [2006]	O	O
Stratospheric O_3, aerosols, cloud, temperature profiles	Raman LIDAR	-	Burris et al. [1998]	X	O
Basic Met. Parameters (Temperature, Pressure etc)	Sensors in NASA-DC8	1 sec	-	O	O
[#]GEOS-CHEM	Global 3D Model		Bey et al. [2001]	O	O
[#]MOZART	Global 3D Model		Lamarque et al. [2005]	O	O
[#]NASA Langley Photochemical Model	Photochemical Box Model		Crawford et al.[1999]	O	O
RAQMS	Regional Model		Pierce et al. [2003]	X	O

[#] Parameters, used in this study. [a]Column indicates measured parameter during INTEX-NA, [b]Column indicates measured parameter during INTEX-B

2.2 Chemical Ionization Mass Spectrometer

The observations of HCl, HO_2NO_2, and SO_2 reported in this work were all conducted with a chemical ionization mass spectrometer (CIMS) using SF_6^- ion chemistry. A schematic diagram of the CIMS system is presented in Figure 2.1, which is very similar to that described by Slusher et al. [2004]. The CIMS system contains a quadruple mass-filter and a channeltron detector for the quantification of analyte ions from a flow-tube ion molecule reactor. This combination has been widely used in atmospheric chemistry field due to its high selectivity and sensitivity [Huey, 2007]. In addition to the basic components, a collisional dissociation chamber (CDC) and a RF octopole are attached to enhance the sensitivity and selectivity of the instrument. The CDC is a region of the high ion kinetic energy where water (and other weakly bound) cluster ions are dissociated [Tanner et al, 1997] as shown in following reaction.

$$X^-(H_2O) + M \rightarrow X^- + H_2O + M \qquad \text{R 2.1}$$

Water clusters of analyte ions have been demonstrated to be a significant problem with applying the CIMS technique to measuring HO_2NO_2 [Slusher et al., 2001]. For this reason, the installation of the CDC improves the performance of the technique at higher dew points. A RF octopole ion guide is also utilized in the CIMS between the exit of the flow-tube and the entrance to the quadruple chamber. A technical description of RF octopole and other ion beam focusing methods can be found in Röttgen et al [2006].

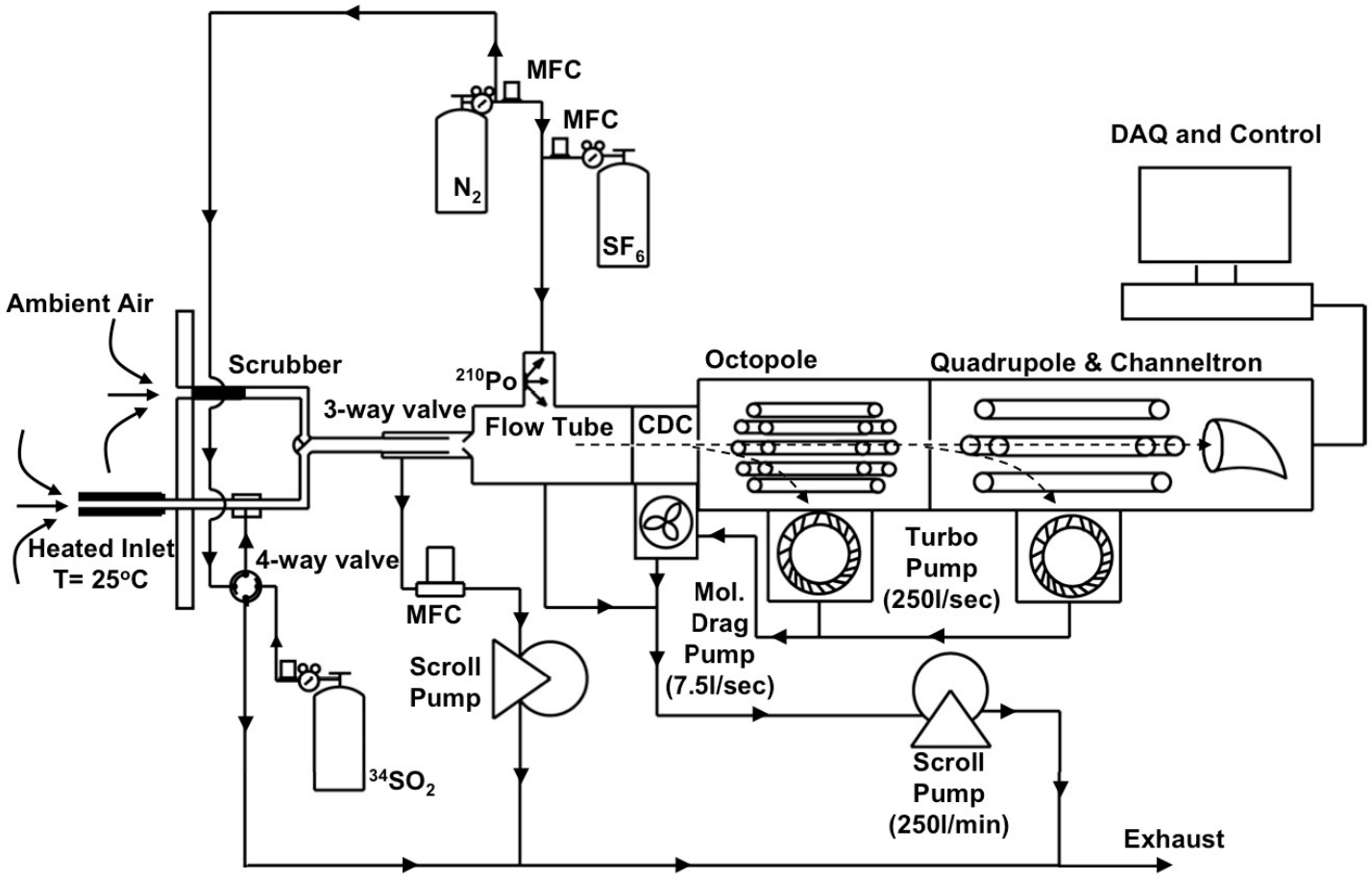

Figure 2.1 The schematic diagram of CIMS system, integrated on NASA DC-8 for the INTEX field campaign

Figure 2.1 also contains the schematic of the inlet system for sampling ambient air on the DC-8. The inlet tubing was fluorinated ethylene propylene (FEP, Teflon®) tubing (0.5″ O.D) maintained at a constant temperature of 298 K. The inlet tubing extended 40cm beyond the aircraft surface, in an elliptically shaped strut, to allow sampling outside of the airplane's boundary layer. A three-way valve at the upstream of the inlet switched between ambient and scrubbed air which was obtained by, passing ambient air through activated charcoal and nylon wool. This allowed automated measurement of the background signal of the CIMS on all channels. The total flow through the inlet (5.5-7.5 slpm) comprised the flow sampled by the CIMS (~2.5 slpm in the atmospheric pressure, altitude dependent) and an excess flow of 5slpm maintained by a mass flow controller (MKS M100B) and a small scroll pump (Air Squared: BN34-45BG-01LH). The excess inlet flow allowed for short residence times and minimal wall interactions at all altitudes. The total inlet flow was calculated by measuring the flow through the sampling orifice as a function of upstream pressure, which was continuously monitored with a capacitance manometer (MKS Type 722). Air was sampled into the flow tube (~50 sccm) through a 0.5 mm dia. orifice where it is selectively ionized by SF_6^-, synthesized in a ^{210}Po ion source (P-2041, NRD) and added to the flow tube in 2-4 slpm of UHP nitrogen (Scott-Marrin). The specific reactions between analytes gaseous species and SF_6^- are described in the next section.

A series of pumps were used to maintain the system components at appropriate pressures. The flow tube was maintained at a constant pressure of 12 - 13 torr with a scroll pump (Varian 300) and varying the ion source nitrogen flow as a function of

altitude. This was performed by feeding back the signal from the flow tube pressure sensor to the ion source mass flow controller. The CDC was maintained at ~0.5 torr by a molecular drag pump (Alcatel, MDP 5011). The pressures of the octopole, and quadrupole regions were maintained at ~ $2x10^{-3}$ torr, and ~ $5x10^{-5}$ torr, respectively by two turbodrag pumps (Varian Turbo-V300HT) which were backed by the flow tube scroll pump.

2.2.1 Ion Chemistry

Table 2.2 summarizes the reactions between SF_6^- ion and the analytes in this study (SO_2, HO_2NO_2, HCl, and NO_2) [Huey et al., 1995; Slusher et al., 2001]. Although NO_2 was not measured during the INTEX mission it was needed for post-field mission calibration of the HO_2NO_2 sensitivity. The highest yield ion product of SO_2 ($F_2SO_2^-$) and HCl (SF_5Cl^-) was monitored for their measurement. In the case of HO_2NO_2, however, NO_4^-(HF) was monitored to utilize its higher selectivity although it is a minor product (~25%).

The signal at $^{34}SF_6^-$ was also recorded to track the reagent ion level in the reaction chamber. In addition, to check for electrical noise the signal at 20 amu was also monitored as no ion signal is expected at this mass-to-charge ratio. The dwell times at each ion mass during the science flights are summarized in Table 2.3.

Table 2.2 SF_6^- ion chemistry used during the INTEX field campaign.

Reactant	Product	Yield (%)	k (10^{-9} cm^3 $molecule^{-1}$ s^{-1})	
[a]SO_2	$F_2SO_2^-$, SF_4	54	1.0 (±30%)	R2.2
	SF_5^-, FSO_2	26	1.0 (±30%)	R2.3
	FSO_2^-, SF_5	20		R2.4
[b]HO_2NO_2	SF_5^-	?	0.77 (±40%)	R2.5
	NO_4^-(HF)		0.29 (±40%)	R2.6
	NO_2^-(HF)		0.07 (±40%)	R2.7
	NO_3^-		0.03 (±40%)	R2.8
[a]HCl	SF_5Cl^-, products	44	1.5 (±30%)	R2.9
	SF_5^-, HF, Cl	33	0.42 (±30%)	R2.10
	Cl^-·HF, SF_5	23		R2.11
[a]NO_2	NO_2^-	100	0.14 (±30%)	R2.12

[a]Huey et al.,[1995], [b]Slusher et al.,[2001]

Table 2.3 Summary of dwell times for mass recorded during INTEX mission.

AMU	Dwell time (ms)	Analytes	Ion
20	50	N/A	
55	500	HCl	Cl^-HF
98	600	HO_2NO_2	NO_4^-(HF)
102	600	Ambient SO_2	$F_2{}^{32}SO_2^-$
104	600	Standard SO_2	$F_2{}^{34}SO_2^-$
162	600	HCl	SF_5Cl^-
148	50	N/A	SF_6^-

Potential interferences to the measurement of HCl in ambient air using SF_6^- ion chemistry were tested as this measurement was performed for the first time in this study. In general, ozone and water vapor can lead to significant interferences with SF_6^- ion chemistry [Slusher et al., 2001]. For this reason, laboratory tests were performed to evaluate the humidity and ozone dependence of the detection scheme. Water vapor was found to be a significant interference at even modest dew points (above -30 ^oC) to detection of HCl as $Cl^-\cdot HF$ (R 2.11). However, the dominant reaction channel of the HCl/SF_6^- reaction that produces SF_5Cl^- (R2.9) was found to be virtually immune to interference from both water and ozone. This was further tested in the field by taking mass spectra during flights in both the stratosphere (high ozone) and the marine boundary (high dew points). Two examples of spectra are shown in Figure 2.2. Both spectra, even though they are taken very rapidly demonstrate the natural isotope abundance of Cl (^{35}Cl:^{37}Cl = ~77.8:~ 24.2). These results indicate that HCl can be detected selectively with SF_6^- over a wide range of atmospheric conditions.

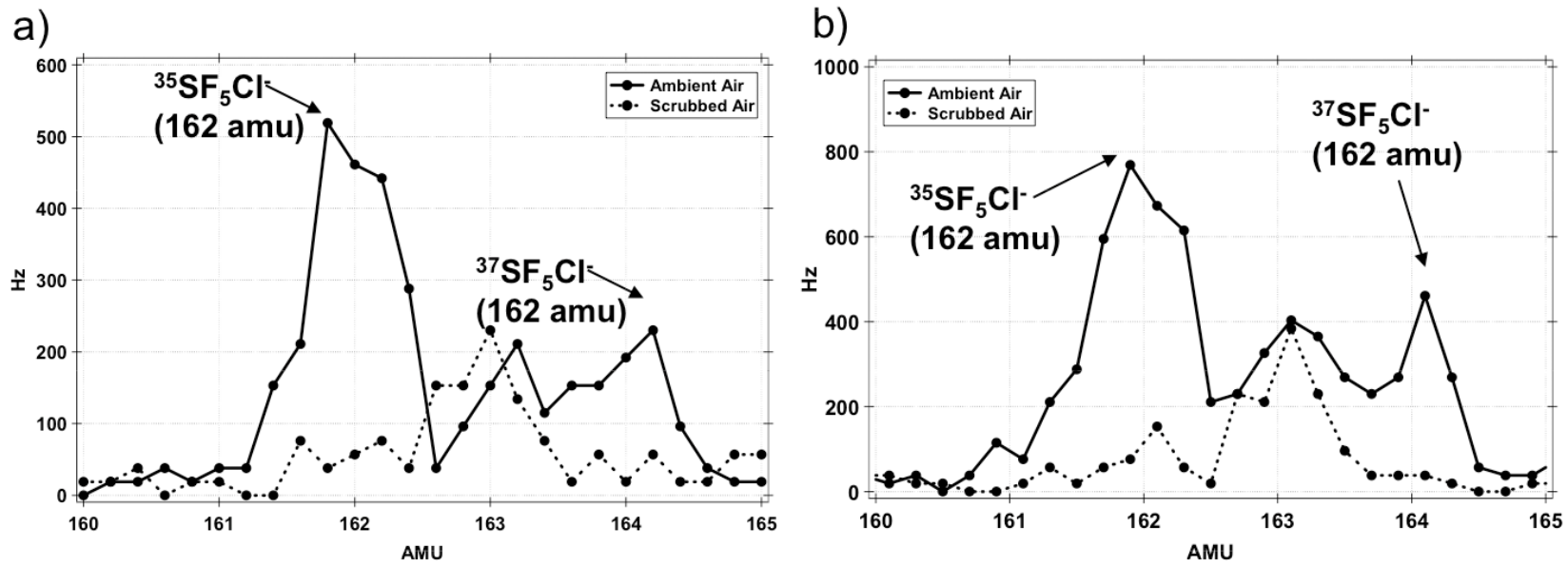

Figure 2.2 The mass spectrum, taken in the stratospheric sampling, representing high ozone matrix (a)) and the MBL sampling, representing high water vapor matrix.

2.2.2 Calibration

The sensitivity of SO_2 during the science flight was monitored periodically (every 2 minutes for a duration of 30 seconds) by performing a standard addition of a known amount of $^{34}SO_2$ to the inlet. The $^{34}SO_2$ calibration gas was mixed in the lab before each field campaign and its mixing ratio was determined by comparison with a $^{32}SO_2$ standard (Scott Marrin, INC. Riverside, CA (1.98 ppmv ± 5%)). The calibrated mixing ratio of the $^{34}SO_2$ standard was 850 ppbv ± 9.2% for INTEX-NA and 1670 ppbv ± 8.7% for INTEX-B. The isotopic purity of the $^{34}SO_2$ standard was high enough that it did not interfere with the measurement of ambient SO_2 (primarily $^{32}SO_2$) to any significant level (<2 pptv).

The sensitivities of the CIMS to HO_2NO_2 and HCl were not monitored in the field. Instead, the relative sensitivity to SO_2 was carefully examined by a post-mission lab calibration at various pressures and dew points that simulated the conditions encountered during the mission. This approach has several advantages as most of the factors that govern CIMS sensitivity (e.g. reaction time, reagent ion signal, number density of the flow reactor) are common to the SO_2, HO_2NO_2, and HCl detection schemes.

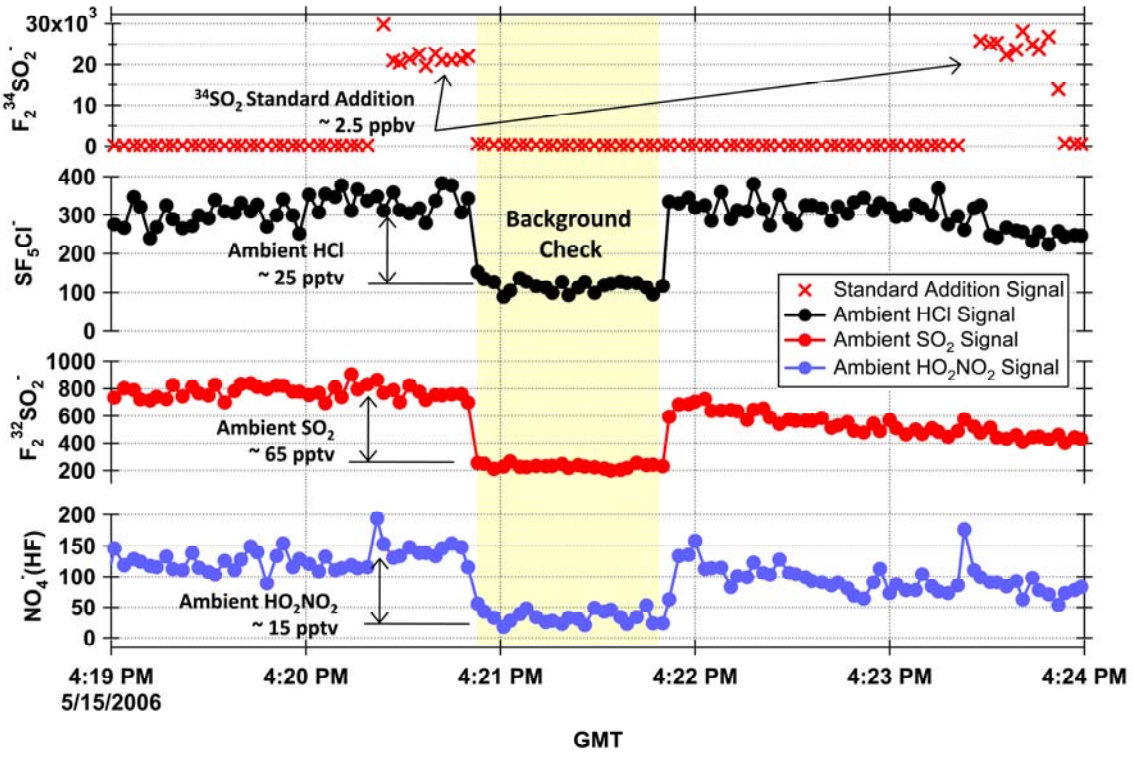

Figure 2.3 Typical temporal variations of analytes, standard additions, and background ion signal at an altitude of ~8 km during a science flight of the INTEX field campaign.

2.2.2.1 In Flight Calibration (SO_2)

Figure 2.3 shows temporal variations of ion signals ($F_2SO_2^-$, $F_2SO_2^-$, NO_4^-(HF), and SF_5Cl^-) during a typical science flight (at altitude of ~10 km) and includes ambient measurements, standard additions of $^{34}SO_2$, and a background signal measurement for each channel. The background signal was used to estimate the lower limit of detection (LLOD), estimated to be 2 pptv for a signal to noise ratio of one with the noise defined as 2σ of the background (30 seconds average). The overall uncertainty of 15% is defined by a combination of the accuracy of SO_2 standard (5%) and the statistical error at the 2σ level (1 second) of calibration signals (14%).

The analysis of calibration signals for the flight mission illustrate that the sensitivity of SO_2 has a negative correlation with the dew point of the ambient air because water vapors react with $F_2SO_2^-$ to produce SO_3^-. Therefore, a sudden change of dew point between standard additions especially in the boundary layer, where the dew point is relatively high and highly variable can increase the error in the SO_2 sensitivity. For this reason, dew point weighted interpolations were performed when a rapid change in dew point was encountered. For all other cases a linear interpolation with time was used to assess the SO_2 sensitivity. The typical sensitivity of SO_2 for the entire mission was more than 5 Hz/pptv in the free troposphere and 1 Hz/pptv in the planetary boundary layer.

2.2.2.2 Post Mission Calibration

2.2.2.2.1 HO_2NO_2

The sensitivity ratio of HO_2NO_2 to SO_2 was derived in two steps. First the sensitivity of HO_2NO_2 to NO_2 was obtained by thermally dissociating HO_2NO_2 in the inlet (T ~ 363 K) of the CIMS (R 2.2) to stochiometrically form NO_2 [Kenley et al., 1981; Slusher et al., 2001].

$$HO_2NO_2 + \text{Heat} \leftrightarrow HO_2 + NO_2 \qquad \text{R2.13, R2.-13}$$

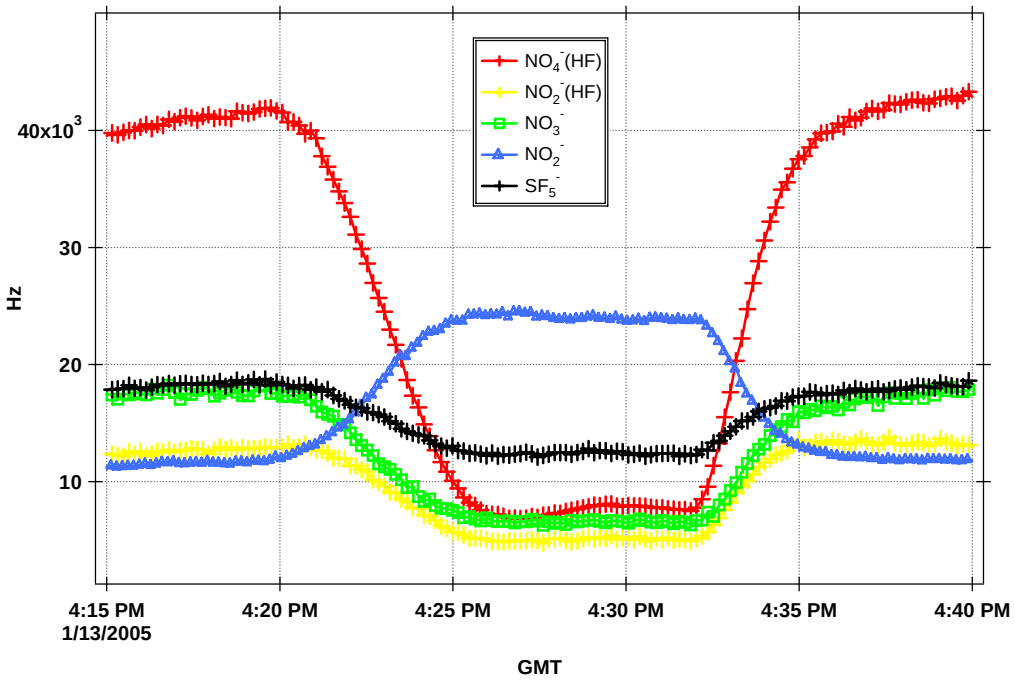

Figure 2.4 The temporal variation of ion products of HO_2NO_2 and NO_2 (see Table 2.2 and the text for the further detail of each ion species) during a heating cycle (368 K) of the inlet with 6.2 ppbv of HO_2NO_2 standard sample. The SF_5^- ion counts have been divided by 5.

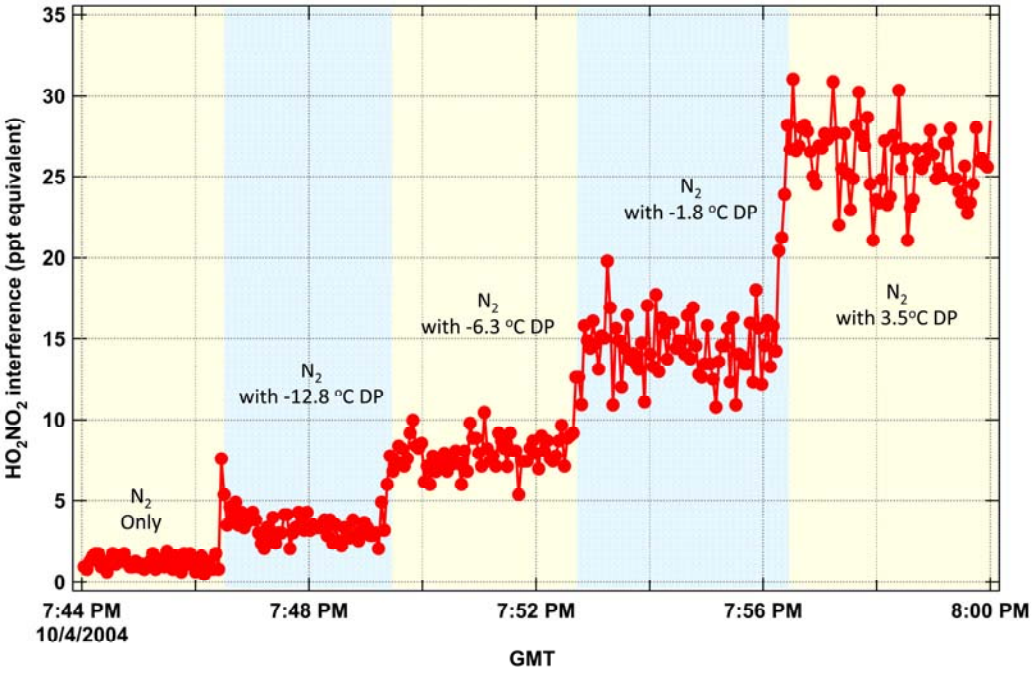

Figure 2.5 Signal from the the interference from water vapor at mass-to-charge ratio of the HO_2NO_2 product ion ($NO_4^-(HF)$). Ion signals on the y axis are given in mixing ratio equivalent of HO_2NO_2 for the experimental conditions.

Figure 2.4 presents temporal variations of all relevant ions during the heating cycle. After that, the sensitivity of NO_2 to SO_2 was measured by simultaneously adding known amounts of both these species to the inlet. Both the SO_2 and NO_2 were delivered from dilute standard mixtures (Scott Marrin, SO_2 247 ppbv ± 5 % and CO_2 350 ppmv in air, NO_2 99.2 ppmv ± 2 % in N_2) that had recently been re-analyzed. Both of these steps were carried out as a function of inlet pressure and dew point to replicate DC-8 flight conditions during INTEX-NA and INTEX-B. All of these tests were performed immediately after the each INTEX mission with the system in the identical configuration as on the aircraft.

The series of experiments assessed the sensitivity ratio of HO_2NO_2 relative to SO_2 as 0.74 (±13%) for the INTEX-NA and 0.67 (±13%) for the INTEX-B configuration. These ratios are consistent with the measured rate constants for the reactions of SF_6^- (Table 2.3). The ratio did not depend on the pressure and the dew point range encountered during the mission. The overall uncertainty for the HO_2NO_2 measurement is 24 %, defined by the combination of accuracy of SO_2 and NO_2 standard (5 % and 2 % respectively) and the statistical error at the 2 σ level (1 second) of calibration signals as 23.8 %. The LLOD for a 30 second average at the 2 σ level is estimated to be 2 pptv.

Water vapor is the most serious interference for detection of HO_2NO_2 with SF_6^- ion chemistry due to the ion-cluster issue [Slusher et al, 2001]. The degree of the interference from water vapor was tested by looking at the ion signal of HO_2NO_2 with humidified UHP nitrogen (Figure 2.5). These tests indicated that the CIMS has a background of less than 15 pptv of HO_2NO_2 at dew points less than 268 K. At higher dew points the background rapidly increased. For this reason, only HO_2NO_2 data at dew point

s less than 268 K were reported. The threshold dew point is much higher than the one assessed by Slusher et al. [2001] (250 K) before a CDC was adapted in the CIMS system.

2.2.2.2.2 HCl

The relative sensitivity of HCl to SO_2 was measured with a standard gas mixture of HCl (20 ppmv ± 20% balanced by UHP N_2, Matheson Tri Gas, Montgomeryville, PA). The mixing ratio of the standard gas mixture was measured with a UV-Visible absorption cell identical to that of Neumann et al. [2003] using an absorption cross section for HCl at 185 nm of 3.15×10^{-19} cm^2/molecule (personal communication with James B. Burkholder NOAA). The assessed mixing ratio of the standard is 5.3 ppmv (±22 %), which is significantly lower than the denoted mixing ratio by the manufacturer.

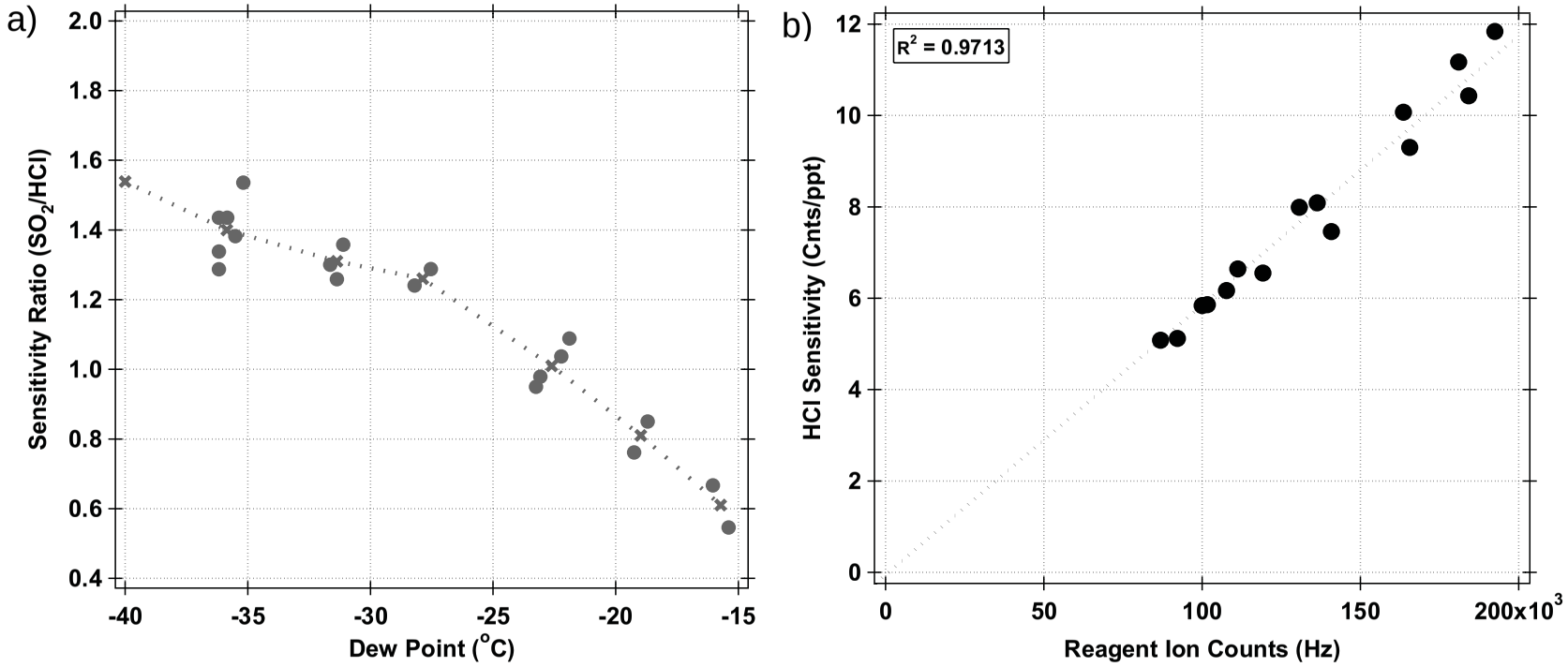

Figure 2.6 a) The correlation between the dew point and the sensitivity ratio (SO_2/HCl) , used for the mixing ratio estimation from the raw data when dew point was under -15 ^oC. b) The correlation between the HCl sensitivity and reagent ion counts. The strong correlation is used for the mixing ratio estimation the range of dew point higher than -15^oC

The intercomparison between the SO_2 (Scott Marrin, SO_2 247 ppbv $\pm$ 5 %) and the HCl standard mixture proved that the HCl sensitivity does not depend on pressure or dew point over the range encountered during the INTEX-B mission. However, the ratio of sensitivities depends on the dew point because of the strong dependency of the SO_2 sensitivity on humidity as shown in Figure 2.6a. The linear relation between HCl and SO_2 sensitivities below -15^{o}C was used to determine HCl sensitivities. However, above dew points of -15^{o}C, the strong correlation between the sensitivity of HCl and reagent ion counts ($^{34}SF_6^-$) as shown in Figure 2.6b (R^2 = 0.9713) was utilized. An uncertainty in the observed HCl levels was estimated to be 33% with calibration uncertainty dominating. The uncertainty is determined by accuracies of standard (SO_2, 5% and HCl, 10%) and dew point measurements in the field (5%) and the post-mission calibration (18%). In addition, the statistical error at the 2σ level of calibration signals (1 second average) is considered as 25%. The LLOD for HCl was estimated to be 2 pptv for a signal to noise ratio of one with the noise defined as 2σ of the background signal (30 seconds average)

2.3 Calculations and Model Validations

This study conducted several calculations and compared measured results with model products to test our current understanding of tropospheric chemistry. Calculation schemes for the steady state and the time dependent calculation of HO_2NO_2 are explained in this section. In addition, a summary of the radiative transfer model for near-IR solar radiation to estimate the IR photolysis rate of HO_2NO_2 in the free troposphere is presented. Since the photolysis rate in the IR region was the only parameter

unconstrained by measurements, the radiative transfer model calculations were essential to evaluate potential differences between calculations and observations.

2.3.1 Steady State Calculation

HO_2NO_2 levels were estimated using a simple model and the steady-state approximation. This assumes sources and sinks of short lived species, such as radicals, are in balance. Since the lifetime of HO_2NO_2 during the INTEX-mission is shorter than five hours throughout the troposphere, the application of the steady-state assumption to HO_2NO_2 is reasonable. For this study, we use R 2.14 for the source and R 2.-14, R 2.15 and R2.16 for the sinks to calculate HO_2NO_2 with the steady-state assumption ($[HO_2NO_2]_{SS}$).

$$HO_2 + NO_2 \leftrightarrow HO_2NO_2 \qquad \text{R 2.14, R 2.-14}$$

$$HO_2NO_2 + OH \rightarrow \text{products} \qquad \text{R 2.15}$$

$$HO_2NO_2 + h\nu \rightarrow \text{products} \qquad \text{R 2.16}$$

$[HO_2NO_2]ss$ is given by the following equation:

$$[HO_2NO_2]_{SS} = \frac{k_1[HO_2][NO_2]}{J_2 + k_{-1} + k_3[OH]}$$

Where k_1, k_{-1}, k_3 are rate constants and J_2 is the photolysis rate of HO_2NO_2. The rate constants are from Sander et al., [2006], and the concentrations of OH, NO_2, and HO_2 are taken from observations [Singh et al., 2006] or from the output of the NASA Langley photochemical model. Since radiation measurements during the INTEX mission were conducted only for the UV-Visible wavelength region, the photolysis rate for R 2.5 is assessed by adding the commonly accepted IR photolysis constant for HO_2NO_2 in the

troposphere of 10^{-5} /sec to the measured photolysis rate. The assessment of this assumed value was conducted by radiative transfer model calculations over the near-IR.

The calculations, described above are conducted with the code of IGOR-PRO (WaveMetrics, Inc.,OR USA) as shown in APPENDIX A.

2.3.2 Time Dependent Model

Time dependent model calculations were also performed to assess the deviation of HO_2NO_2 from steady-state for typical upper tropospheric conditions where its lifetime is of the order of five hours. This method assumed an initial injection of NO_x into the upper troposphere and followed its temporal evolution and oxidation over the course of several days in one-minute time steps. Short lived species such as radicals were predicted using the steady state assumption and the chemical scheme of Faloona et al. [2000]. In addition, longer lived species such as CO were held at median observed values. The chemical species and how they were treated in the model are listed in Table 2.4. Rate constants were taken from the JPL evaluation version 15 [Sander et al., 2006], and all photolysis rates in given local time were calculated with the TUV 4.1 model (http://cprm.acd.ucar.edu/Models/TUV/) for typical conditions of INTEX (e.g., latitude, time of day, and date). The calculated photolysis rates were found to be within 20% of observations during the INTEX mission. Based on the schemes above, the calculations were performed with the MATLAB (The MathWorks, Inc) code, presented in APPENDIX B

Table 2.4 The summary of chemical species, considered in the time dependent model in this study according to three different ways of dealing the chemical species.

Category	Species
Constrained	O_3, CH_4, CO, CH_2O CH_3OOH, H_2O_2, $CH_3C(O)CH_3$, H_2O
Steady state	OH, HO_2, CHO , $O(^1D)$, CH_3O_2, $CH_3C(O)O_2$
Time dependent	NO, NO_2, HNO_3, HO_2NO_2, PAN, NO_3, N_2O_5

2.3.3 Near-IR Flux Calculation

Although the estimated overtone photolysis rate (10^{-5}/sec) in the upper troposphere and the lower stratosphere has been suggested as a good estimation by a series of HO_x budget studies and lab experiments [Evans et al., 2003; Roehl et al., 2002; Salawitch et al., 2002; Zhang et al., 2000; Wennberg et al., 1999], this value was calculated from the actinic flux at the top of the atmosphere without considering surface albedo on the given spectral region [Roehl et al., 2002]. For this reason we performed actinic flux calculations over the near-IR region to estimate the uncertainty of this overtone photolysis rate using Santa Barbara DISTORT Atmospheric Radiative Transfer model (SBDART). The SBDART model applies the calculation scheme of the plane-parallel radiative transfer for the estimation of the spectral range of 0-50000 cm^{-1} with a spectral resolution of 20 cm^{-1}. A more detail description of SBDART can be found in Richiazzi et al. [1998]. With the actinic flux, calculated by SBDART, the overtone photolysis rate of HO_2NO_2 is calculated on the bands of $2\nu_1$ (6900 cm^{-1}) and $3\nu_1$ (10090 cm^{-1}) that account for more than 92% of the overtone photolysis of HO_2NO_2 [Roehl et al., 2002]. In addition, the calculation used the quantum yield and the absorption cross-section of Roehl et al. [2002].

2.4 References

Avery, M. A., Westberg, D. J., Fuelberg, H. E., Newell, R. E., Anderson, B. E., Vay, S. A., Sachse, G. W., and Blake, D. R.: Chemical tansport the ITCZ in the central Pacific during El Nino-Southern Oscillation cold phase event March-April 1999, Journal of Geophysical Research, 106, 32539-32554, 2001.

Bandy, A. R., Thornton, D. C., and Driedger III, A. R.: Airborne measurements of sulfur dioxide, dimethyl sulfide, carbon disulfide, and carbonyl sulfide by isotope dillution gas chromatography/mass spectrometry, Journal of Geophysical Research, 98, 23432-23433, 1993.

Bey, I., Jacob, D. J., Yantosca, M., Logan, J. A., Field, B. D., Fiore, A. M., Li, Q., Liu, H. Y., Mickley, L. J., and Schultz, G.: Global modeling of tropospheric chemistry with assimilated meteorology: Model description and evaluation, Journal of Geophysical Reserach, 106, 23073-23095, 2001.

Blake, N. J., Blake, D. R., Atlas, E., Flocke, F., and Rowland, F. S.: Latitudinal, vertical, and seasonal variatoins of C1-C4 alkyl nitrates in the troposphere over the Pacific Ocean during PEM-Tropics A and B: Oceanic and continental sources, Journal of Geophysical Research, 108, 8242,doi:8210.1029/2001JD001444,002003, 2003.

Brune, W. H., Stevens, P. S., and Mather, J. H.: Measuring OH and HO_2 in the troposphere by laser-induced fluorescence at low pressure, Journal of the Atmospheric Sciences, 52, 3328-3336, 1995.

Burris, J., Heaps, W., Gary, B., Hoegy, W., Lait, L., McGee, T., and Gross, M.: Lidar temperature measurements during the TOTE/VOTE mission, Journal of Geophysical Research, 103, 3505-3510, 1998.

Crawford, J., Davis, D., Olson, J., Chen, G., Liu, S., Gregory, G., Barrick, J., Sachse, G., Sandholm, S., Heikes, B., Singh, H., and Blake, D.: Assessment of upper tropospherix HO_x sources over the tropical Pacific based on NASA GTE/PEM data: Net effect on HO_x and other photochemical parameters, Journal of Geophysical Research, 104, 16255-16273, 1999.

Crounse, J. D., McKinney, K. A., Kwan, A. J., and Wennberg, P. O.: Measurement of gas-phase hydroperoxides by chemical ionization mass spectrometry, Analytical Chemistry, 78, 6726-6732, 2006.

Dibb, J. E., Talbot, R. W., Scheuer, E., Seid, G., DeBell, L., Lefer, B., and Ridley, B.: Stratospheric influence on the northern North American free troposphere during TOPSE: ^{7}Be as a stratospheric tracer, Journal of Geophysical Research, 108, 8363,doi:8310.1029/2001JD001347, 2003.

Evans, J. T., Chipperfield, M. P., Oelhaf, H., Stowasser, M., and Wetzel, G.: Effect of near-IR photolysis of HO_2NO_2 on stratospheric chemistry, Geophysical Research

Letter, 30, 1223,doi:1210.1029/2002GL016470, 2003.

Faloona, I., Tan, D., Brune, W. H., Jagle, L., Jacob, D. J., Kondo, Y., Koike, M., Chatfield, R., Pueschel, R., Ferry, G., Sachse, G., Vay, S., Anderson, B., Hannon, J., and Fuelberg, H.: Observation of HO_x and its relationship with NO_x in the upper troposphere during SONEX, Journal of Geophysical Research, 105, 3771-3783, 2000.

Hennigan, C. J., Sandholm, S., Kim, S., Stickel, R. E., Huey, L. G., and Weber, R. J.: Influence of Ohio River valley emissions on fine particle sulfate measured from aircraft over large regions of the eastern United States and Canada during INTEX-NA, Journal of Geophysical Research, 111, doi:10.1029/2006JD007282, 2006.

Huey, L. G.: Measurement of trace atmospheric species by chemical ionization mass spectrometry: Speiciation of reactive nitrogen and future directions, Mass Spectrometry Reviews, 26, 166-184, 2007.

Huey, L. G., Hanson, D. R., and Howard, C. J.: Reactions of SF_6^- and I^- with atmospheric trace gases, Journal of Atmospheric Chemistry, 99, 5001-5008, 1995.

Kenley, R. A., Trevor, P. L., and Lan, B. Y.: Preparation and thermal decomposition of Pernitric Acid ($HOONO_2$) in aqueous media, Journal of the American Chemical Socieity, 103, 2203-2206, 1981.

Lamarque, J.-F., Kiehl, J. T., Hess, P. G., Collins, W. D., Emmons, L. K., Ginoux, P., Luo, C., and Tie, X. X.: Response of a coupled chemistry-climate model to changes in aerosol emissions Global impact on the hydrological cycle and the tropospheric budens of OH, ozone, and NO_x, Geophysical Research Letter, 32, doi:10.1029/2005GL023419, 2005.

Lee, M., O'Sullivan, D., Noone, K. B., and Heikes, B. G.: HPLC method for determination of H_2O_2, C1 and C2 hydrogenproxides in the atmosphere, Journal of Atmospheric and Oceanic Technology, 12, 1060-1070, 1995.

Neuman, J. A., Ryerson, T. B., Huey, L. G., Jakoubek, R., Nowak, J. B., Simons, C., and Feshenfeld, F. C.: Calibration and evaluation of nitric acid and ammonia permeation tubes by UV optical absorption, Environmetal Science and Technology, 37, 2975-2981, 2003.

Podolske, J. R., Sachse, G. W., and Diskin, G. S.: Calibration and data retrieval algorithms for the NASA Lagley/Ames Diode Laser Hygrometer for the NASA Transport and Chemical Evolution Over the Pacific (TRACE-P) mission, Journal of Geophysical Research, 108, 8792,doi:8710.1029/2002JD003156, 2003.

Ricchiazzi, P., Yang, S., Gautier, C., and Sowle, D.: SBDART: A research and teaching software tool for plane-parallel radiative transfer in the Earth's atmosphere, Bulletin of the American Meteorological Society, 79, 2101-2114, 1998.

Roehl, C. M., Nizkorodov, S. A., Zhang, H., Blake, G., and Wennnberg, P. O.: Photodissociation of peroxynitric acid in the Near-IR, Journal of Physical Chemistry A, 106, 3766-3772, 2002.

Roller, C., Fried, A., Walega, J., Weibring, P., and Tittel, F.: Advances in hardware, system diagnostics software, and aquisition procedures for high performance airborne tunable diode laser measurements of formaldehyde, Applied Physics B-Lasers and Optics 82, 247-264, 2006.

Röttgen, M. A., K., J., Antonietti, J.-M., Heiz, U., Rauschenbach, S., and Kern, K.: Conical octopole ion guide: Design, focusing, and its application to the deposition of low energetic clusters, Review of Scientific Instruments, 77, 013302, 2006.

Ryerson, T. B., Huey, L. G., Knapp, K., Neuman, J. A., Parrish, D. D., Sueper, D. T., and Feshenfeld, F. C.: Design and initial characterization of an inlet for gas-phase NO_y measurements from aircraft, Journal of Geophysical Research, 104, 5483-5492, 1999.

Sachse, G. W., Hill, G. F., Wade, L. O., and Perry, M. G.: Fast-response, high-precision carbon monoxide sensor using a tunable diode laser absorption technique, Journal of Geophysical Research, 92, 2071-2081, 1987.

Salawitch, R. J., Wennberg, P. O., Toon, G. C., Sen, B., and Blavier, J.-F.: Near IR photolysis of HO_2NO_2: Implications for HOx, Geophysical Research Letter, 29, doi:10.1029/2002GL0150006, 2002.

Sander, S. P., Friedl, R. R., Ravishankara, A. R., Golden, D. M., Kolb, C. E., Kurylo, M. J., Molina, M. J., Moortgat, G. K., Keller-Rdek, H., Finlayson-Pitts, B. J., Wine, P. H., Huie, R. E., and Orkin, V. L.: Chemical kinetics and photochemical data for use in atomspheric studies, Evaluation Number 15, JPL Publication 06-02, 2006.

Shetter, R. E., and Muller, M.: Photolysis frequency measurements on the NASA DC-8 during the PEM-Tropics mission using actnic flux spectrometry: Instrumentation description and some results, Journal of Geophysical Research, 104, 5647-5661, 1999.

Shinozuka, Y., Clarke, A. D., Howell, S. G., Kapustin, V., McNaughton, C., Zhou, J., and Anderson, B. E.: Aircraft profiles of aerosol microphysics and optical properties over North America: Aerosol optical depth and its association with PM 2.5 and water uptake, Journal of Geophysical Research, doi:10.1029/2006JD007918, 2007.

Singh, H. B., Brune, W. H., Crawford, J., and Jacob, D.: Overview of the summer 2004 Intercontinental Chemical Transport Experiment-North America (INTEX-A), Journal of Geophysical Research, 111, doi:10.1029/2006JD007905, 2006.

Singh, H. B., Salas, L., Herlth, D., Kolyer, R., Czech, E., Avery, M., Crawford, J. H., Pierce, R. B., Sachse, G. W., Blake, D. R., Cohen, R. C., Bertram, T. H., Perring,

A., Wooldridge, P. J., Dibb, J., Huey, G., Hudman, R. C., Turquety, S., Emmons, L. K., Flocke, F., Tang, Y., Carmichael, G. R., and Horowitz, L. W.: Reactive nitrogen distributions and partitioning in the North American troposphere and lowermost stratosphere, Journal of Geophysical Research, 112, doi:10.1029/2006JD07664, 2007.

Slusher, D. L., Huey, L. G., Tanner, D. J., Flocke, F., and Roberts, J. M.: A thermal dissociation-chemical ionization mass spectrometry (TD-CIMS) technique for the simultaneous measurement of peroxyacyl nitrates and dinitrogen pentaoxide, Journal of Geophysical Reserach, 109, doi:10.1029/2004JD004670, 2004.

Slusher, D. L., Pitteri, S. J., Haman, B. J., Tanner, D. J., and Huey, L. G.: A chemical ionization technique for measurement of pernitric acid in the upper troposphere and the polar boundary layer, Geophysical Research Letters, 28, 3875-3878, 2001.

Tanner, D. J., Jefferson, A., and Eisele, F. L.: Selected ion chemical ionization mass spectrometric measurements of OH, Journal of Geophysical Research, 102, 6415-6425, 1997.

Thornton, J. A., Wooldridge, P. J., and Cohen, R. C.: Atmospheric NO_2: In situ lase-induced fluorescence detection at parts per trillion mixing rations, Analytical Chemistry, 72, 528-539, 2000.

Vay, S. A., Woo, J.-H., Anderson, B. E., Thornhill, K. L., Blake, D. R., Westberg, D. J., Kiley, C. M., Avery, M. A., Sachse, G. W., Streets, D. G., Tsutsumi, Y., and Nolf, S. R.: Influence of regional-scale antrhopogenic emissions on CO_2 contributions over the western North Pacific, Journal of Geophysical Reserach, 108, 8801,doi:8810.1029/2002JD003094, 2003.

Wennnberg, P. O., Salawitch, R. J., Donaldson, D. J., Hanisco, T. F., Lanzendorf, E. J., Perkins, K. K., Lloyd, S. A., Vaida, V., Gao, R. S., Hintsa, E. J., Cohen, R. C., Swartz, W. H., Kusterer, T. L., and Anderson, D. E.: Twilight observation suggest unknown sources of HO_x, Geophysical Research Letters, 26, 1373-1376, 1999.

Wulfmeyer, V., Bauer, H. S., Grzeschik, M., Behrendt, A., Vandenberqhe, F., Browell, E. V., Ismail, S., and Ferrare, R. A.: Four-dimensional variational assimilatoin of water vapor differential absorption lidar data: The first case study within IHOP 2002, Monthly Weather Review, 134, 209-230, 2006.

Zhang, H., Roehl, C. M., Sander, S. P., and Wennberg, P. O.: Intensity of the second and third OH overtones of H_2O_2, HNO_3, and HO_2NO_2, Journal of Geophysical Research, 105, 14593-14598, 2000.

[1]CHAPTER 3

MEASUREMENT OF HO_2NO_2 IN THE FREE TROPOSPHERE DURING THE INTERCONTINENTAL CHEMICAL TRANSPORT EXPERIMENT–NORTH AMERICA 2004

3.1 Introduction

Pernitric acid (HO_2NO_2) is formed in the atmosphere by an association reaction that couples the HO_x and NO_x families [Niki et al., 1977]:

$$HO_2 + NO_2 + M \leftrightarrow HO_2NO_2 + M \qquad \text{R3.1, R3.-1}$$

The thermal decomposition of HO_2NO_2 , R3.-1, is a strong function of temperature with the lifetime for this process varying from approximately 20 seconds in the boundary layer to 8 hours at 8 km. Consequently, at lower and mid latitudes HO_2NO_2 is only expected to build up to significant concentrations in the upper troposphere, where photolysis and reaction with OH are expected to be the dominant loss processes.

$$HO_2NO_2 + h\nu \rightarrow \text{Products} \qquad \text{R3.2}$$

$$OH + HO_2NO_2 \rightarrow H_2O + NO_2 + O_2 \qquad \text{R3.3}$$

The potential impact of HO_2NO_2 on upper tropospheric photochemistry (z = 8-12 km) has been discussed by several investigators [Brune et al., 1999; Wennberg et al., 1999; Faloona et al., 2000; Jaeglé et al., 2000]. In particular, Jaeglé et al. [2000] noted the importance of HO_2NO_2 as a sink for HO_x at intermediate levels of NO_x (100 - 500 pptv)

---

[1]Adopeter part from Kim, S et al.: Measurement of HO_2NO_2 in the free troposphere during the INTEX-NA 2004, Journal of Geophysical Research, Vol112, D12S01, doi:10.1029/2006JD007676, 2007. Reproduced by permission of American Geophysical Union. Copyright 2007 American Geophysical Union.

via R3.3. However, these studies were unconstrained by observations of HO_2NO_2. The only previous direct measurements of HO_2NO_2 are in the South Pole boundary layer during Austral Summer 2000 and 2003 [Slusher et al., 2001; Sjostedt et al, 2004]. These results demonstrated that HO_2NO_2 was present in significant levels (on average 25 pptv in 2000; 42 pptv in 2003) and could be the dominant sink for HO_x via deposition to the snowpack and R3.3. The only in situ airborne HO_2NO_2 data were obtained during the TOPSE campaign from the NCAR C-130 at altitudes of 0 to 7 km. Murphy et al. [2003] derived levels of $HO_2NO_2 + CH_3ONO_2$ from their sum of peroxy nitrates channel (ΔPN) by subtracting independent measurements of peroxy acyl nitrates (PANs). They compared the derived HO_2NO_2 to photochemical calculations (with and without an overtone photolysis rate of 10^{-5} sec^{-1}) and demonstrated the importance of the overtone photodissociation channel as a loss mechanism for HO_2NO_2 [Roehl et al, 2002; Wennberg et al, 1999]. Observations of pernitric acid by remote sensing have been reported but are confined to the stratosphere (20 – 40 km) [Rinsland et al., 1996; Sen et al., 1998]. However, Stiller et al. [2007] recently reported satellite borne measurements of HO_2NO_2 profiles in the altitude range of 6 km to 62 km with an altitude resolution of 3 km and the instantaneous field of view of 30 km × 3 km using the Michelson Interferometer for Passive Atmospheric Sounding (MIPAS) mounted on the Environmental Satellite (ENVISAT) of the European Space Agency (ESA).

This work presents the first direct in situ observations of HO_2NO_2 in the free troposphere. These measurements were performed in the summer of 2004 with a chemical ionization mass spectrometer from the NASA DC-8 during the Intercontinental Chemical Transport Experiment-North America (INTEX-NA) field experiment. The

INTEX-NA study sought to characterize and investigate the transport and transformation of both aerosol and gas-phase species over large spatial scales and altitude ranges. Flights were based out of California, Illinois, and New Hampshire. The sampling domain included much of the U.S., parts of Canada, and areas off the eastern and western coasts of North America. A detailed description of the DC-8 payload and the INTEX-NA campaign is presented by Singh et al. [2006] and in Chapter II. In this work our understanding of the chemistry of HO_2NO_2 over the altitude range of 4-12 km is investigated by comparison of observations with highly constrained steady state calculations and photochemical models.

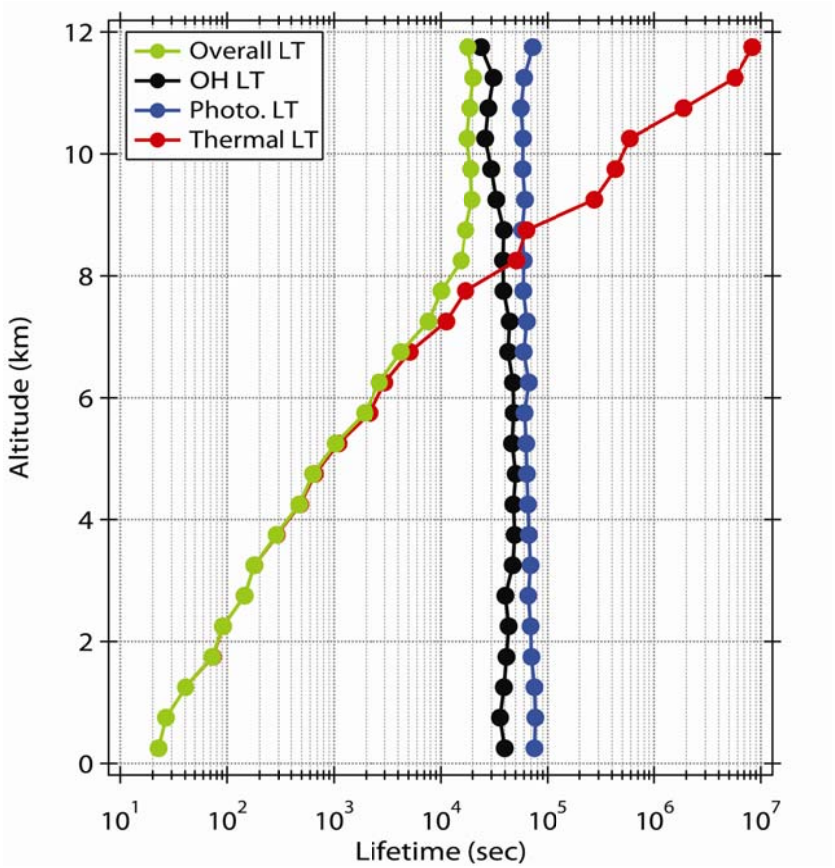

Figure 3.1 Vertical distribution of the total lifetime of HO_2NO_2 (green) and individual lifetimes with respect to thermal decomposition (red), photolysis (blue), and OH reaction (black). The calculated values are based on INTEX-NA observations except for the overtone photolysis rate (10^{-5} s^{-1})

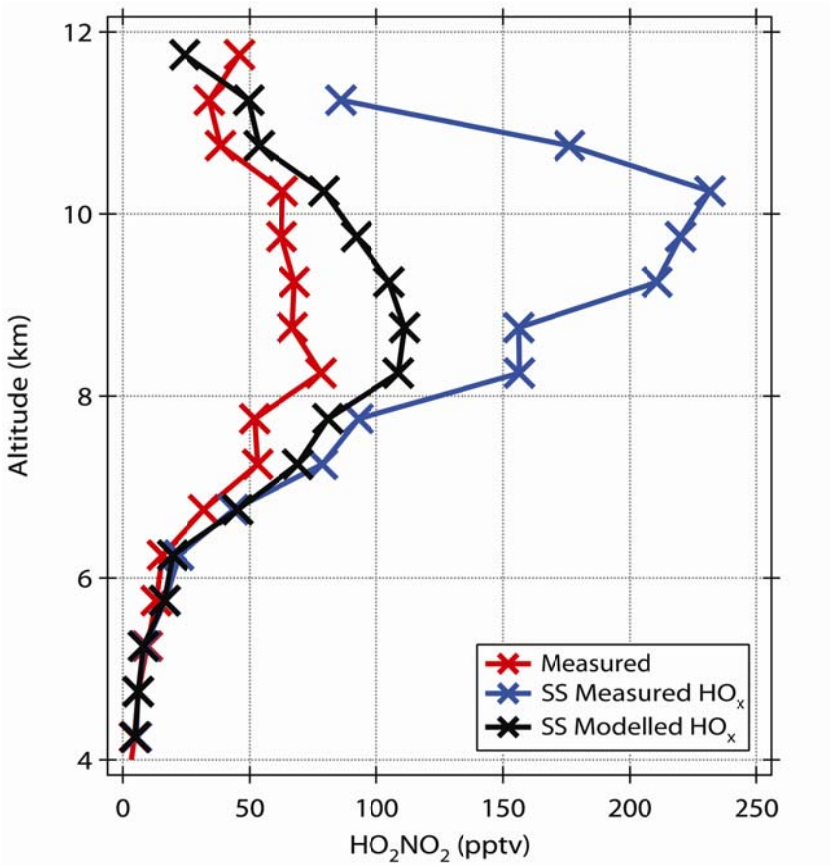

Figure 3.2 Vertical distribution of observed HO_2NO_2 (red) and predictions based on model predicted (black) and observed (blue) HO_x.

3.2. Results and Analysis

All reported data and analyses are based on a one-minute average merged data set (ftp://ftp-air.larc.nasa.gov/pub/INTEXA/DC8_AIRCRAFT/). The median observed HO_2NO_2 altitude profile for the INTEX-NA mission is presented in Figure 3.2, and the statistics of the vertical distribution are reported in Table 3.1. Median values of steady state calculations of HO_2NO_2 based on both observed and model predicted (the NASA Langley box model [Crawford et al., 1999; Olson et al., 2004]) HO_x are also graphed in Figure 3.2. The observed HO_2NO_2 mixing ratio profile shows a maximum of ~76 pptv between 8 and 9 km. Pernitric acid mixing ratios decrease below this altitude as expected due to large thermal dissociation rates. Above 10 km, levels decrease primarily due to a weakening of the source strength. The mean concentration of pernitric acid in the upper troposphere (8 ~ 12 km) was 67±37 pptv (2467 data points, 1σ), which accounted for approximately 5% of the total reactive nitrogen (NO_y) budget and approximately 10% of the HO_x sink in this region [Singh et al., 2007].

Table 3.1 Vertical distribution of observed HO_2NO_2 from 1-min averaged data for INTEX-NA 2004

Altitude, km	Median, pptv	Average, pptv	1 σ, pptv
4.25	8.0	12.3	15.9
4.75	11.4	15.8	20.7
5.25	13.4	31.3	62.7
5.75	15.6	20.5	15.5
6.25	20.4	25.6	18.4
6.75	32.2	38.9	24.0
7.25	53.7	59.2	32.4
7.75	51.9	61.5	39.3
8.25	78.2	77.5	39.6
8.75	66.8	75.1	39.9
9.25	67.8	75.8	41.4
9.75	62.6	65.0	32.5
10.25	63.0	66.1	29.7
10.75	38.7	44.1	25.2
11.25	34.1	41.0	23.8
11.75	46.0	46.8	10.7

In the mid troposphere (4km - 8km) both of the calculated profiles are in reasonable agreement with observations (Figure 3.2). This is more clearly illustrated in Figure 3.3, which presents scatter plots of the steady state calculations versus observations. The calculations based on observed HO_x (Figure 3.3a, R^2= 0.61, slope = 1.23, intercept = 4.8 pptv) and on model predicted HO_x (Figure 3.3b, R^2= 0.66, slope = 0.97 intercept = 7.0 pptv) are both well correlated to the observations. The median ratios for the calculations relative to the observations are 1.3 for observed HO_x and 1.1 for model predicted HO_x. This level of agreement is well within the 30% error bar of the HO_2NO_2 measurement alone. These results indicate that we have a reasonable understanding of the chemistry of HO_2NO_2 in this region, where thermal decomposition dominates the lifetime (Figure 3.1). Very similar results were also derived using k_{-1} from the recent work of Gierczak et al., [2005]. Correlations between calculations and

observations were essentially identical with calculated values rising by a factor of 1.5. However, these results are still within the uncertainty of the analysis.

In the upper troposphere (8-12 km) the agreement between the steady state calculations and observations is not as good as at lower altitudes. The HO_2NO_2 calculations based on model predicted HO_x are still highly correlated with the observations (Figure 3.4b, R^2=0.63, slope = 0.80, intercept = 35.8 pptv) but with a significant offset that yields a median ratio of calculated to observed of 1.3. Conversely, the correlation between HO_2NO_2 calculations based on observed HO_x and observations is significantly weaker (Figure 3.4a, R^2=0.10, slope = 1.75, intercept = 102.2 pptv) with a median ratio of calculated to observed of 2.9. These results indicate that our ability to predict HO_2NO_2 with simple steady state models at higher altitudes, where its lifetime is longer and controlled by photochemical processes (Figure 3.1), is not as good as at low altitudes. There is also a difference between upper tropospheric HO_x observations and predictions, especially around 10 km, with the pernitric acid observations more in accord with the photochemical model results.

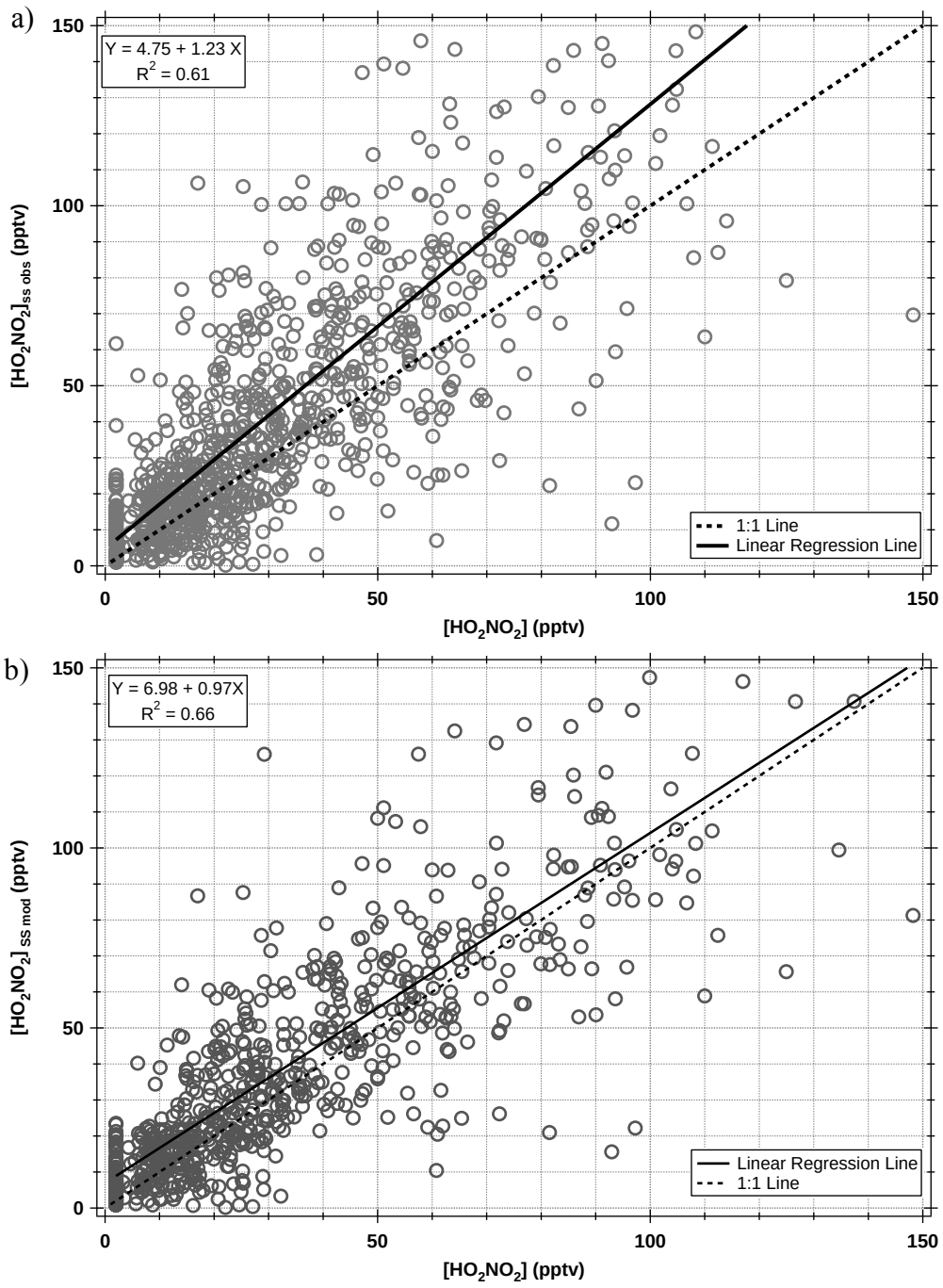

Figure 3.3 Scatter plot of mid tropospheric (5.5-7.5 km) HO_2NO_2 steady state calculations versus observed HO_2NO_2. The calculations are based on (a) observed and (b) model HO_x

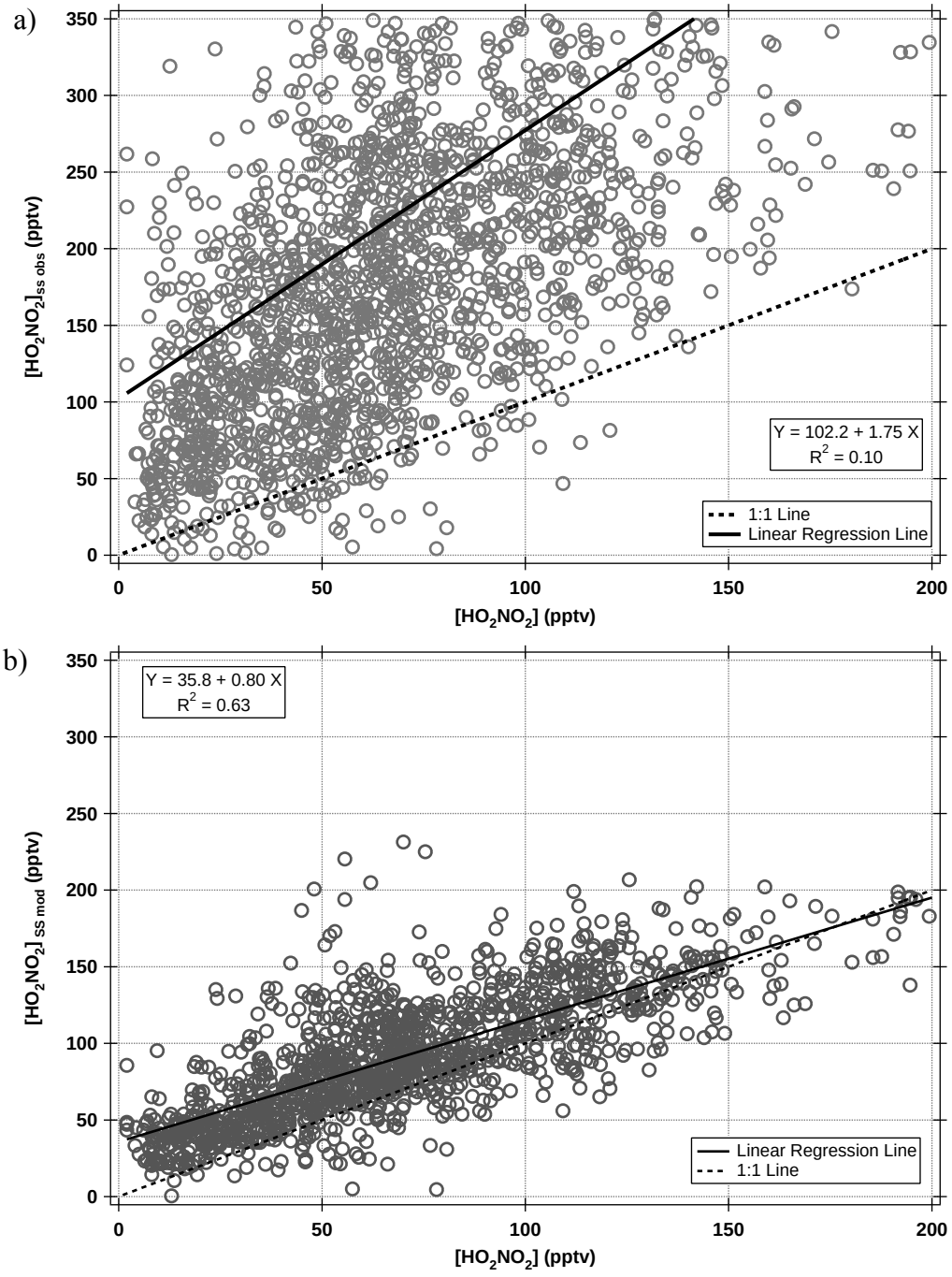

Figure 3.4 Scatter plot of upper tropospheric (8 – 12 km) HO_2NO_2 steady state calculation versus observed HO_2NO_2. The calculations based on (a) observed and (b) model HO_x. The offset presented by the intercept of the regression result probably comes from an intrinsic error of the steady state assumption of HO_2NO_2.

At altitudes of 8-10 km the ratio of photochemical model predictions to observations (M/O) for OH and HO_2 are 1.8 and 1.0, respectively. In the altitude range of 10-12 km the M/O ratio for OH and HO_2 are 1.5 and 0.5, respectively. Consequently, there is a discrepancy between the measured and predicted HO_2 to OH ratio that increases with altitude. However, this difference is primarily due to the high levels of NO_x that also were observed to increase with altitude [Bertram et al., 2007]. The predicted ratio of $[HO_2]/[OH]$ decreases much more strongly as a function of NO_x than the observations as shown in Figure 3.5.

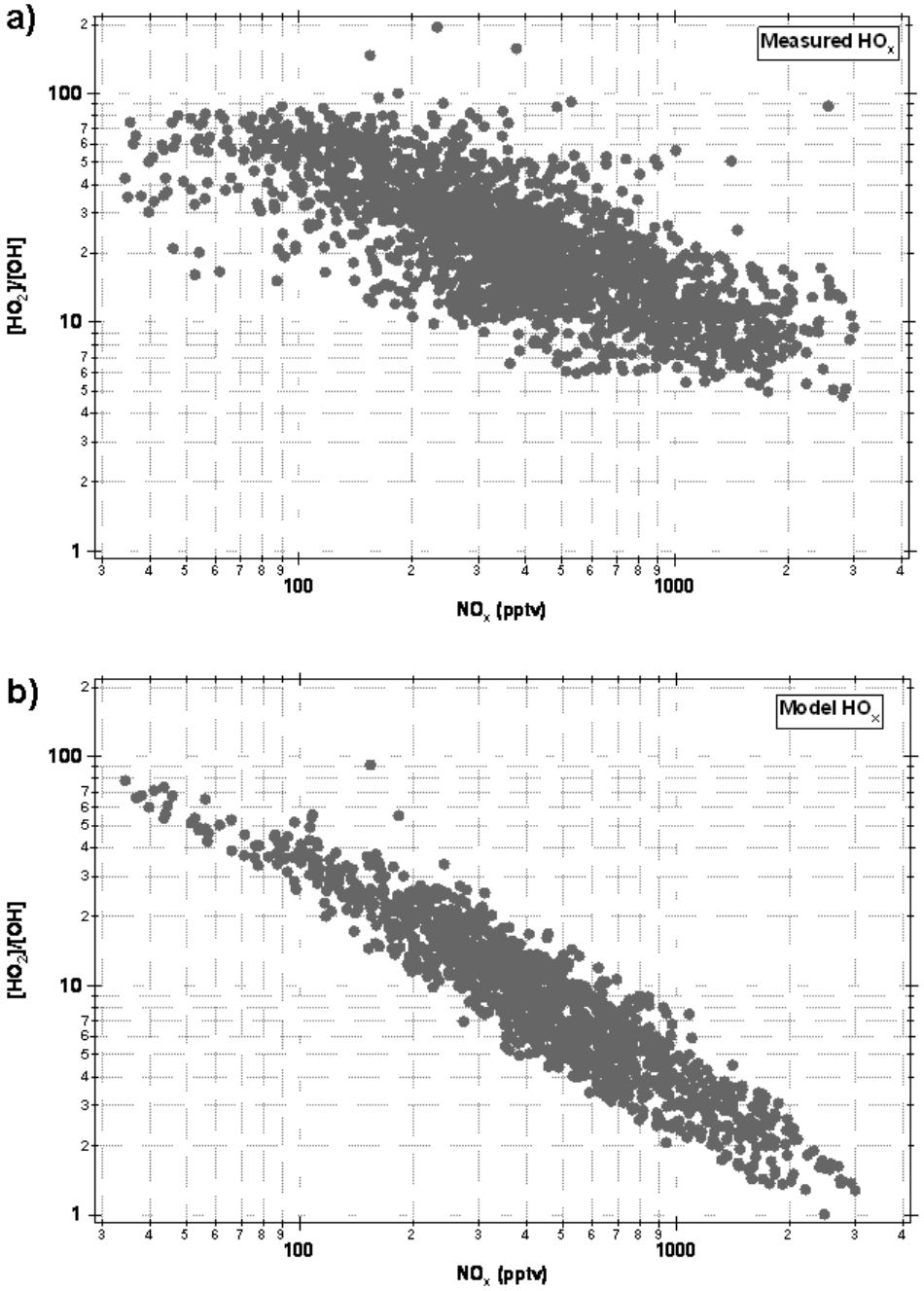

Figure 3.5 Correlation plots between $[HO_2]/[OH]$ and $[NO_x]$ (a) from observed HO_x and (b) from model predicted HO_x. Due to lack of NO data, the photo-stationary state of $NO\text{-}NO_2\text{-}O_3$ is applied

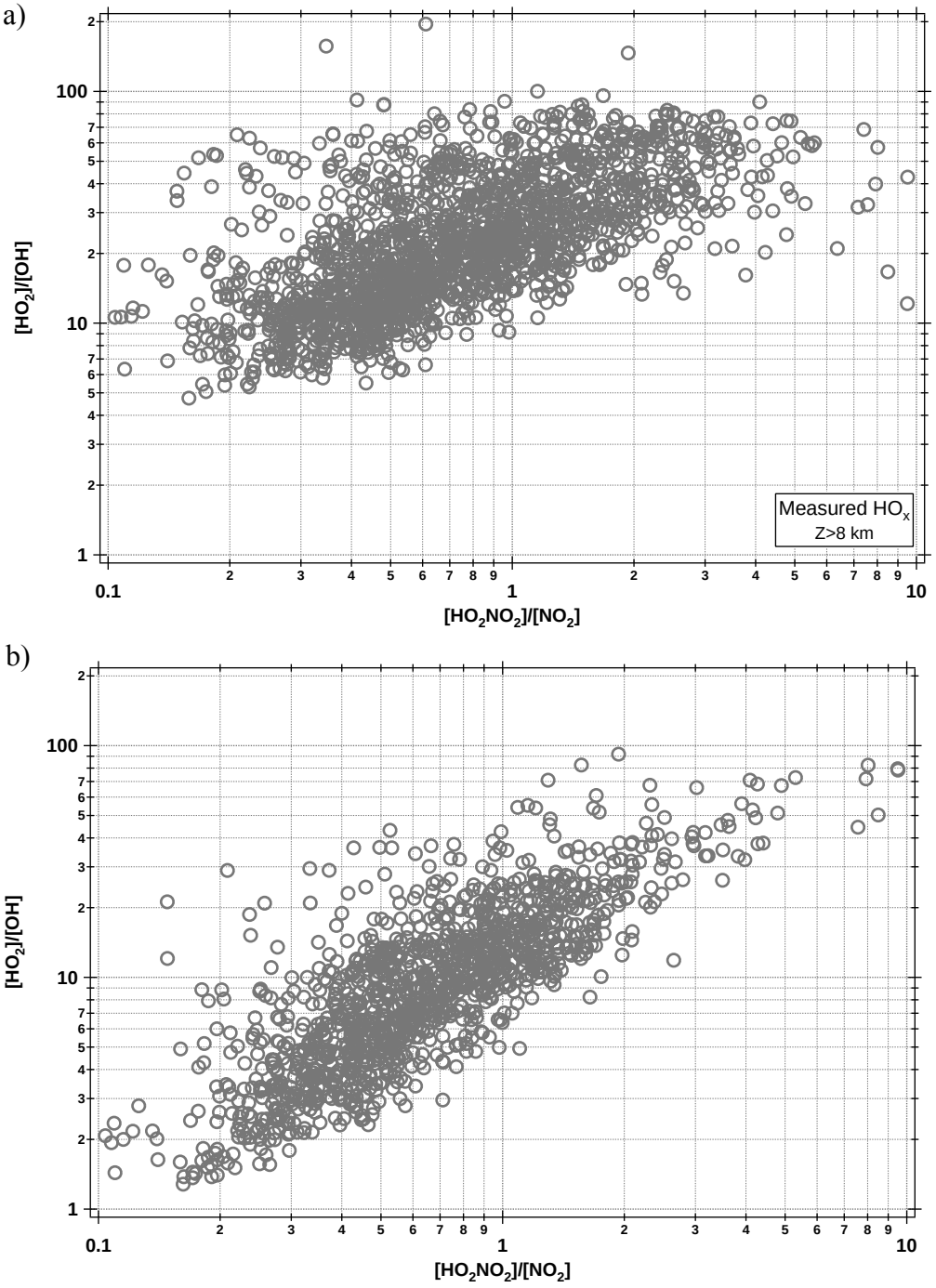

Figure 3.6 Correlation plots between $[HO_2NO_2]/[NO_2]$ and $[HO_2]/[OH]$ (a) from observed HO_x and (b) from model predicted HO_x.

At higher altitudes where thermal decomposition of pernitric acid is negligible the ratio of HO_2NO_2 to NO_2 should have a strong dependence on the $[HO_2]/[OH]$ ratio. This is evident from the steady state equation for those conditions where reaction with OH (R3.3) is the dominant loss. For the INTEX-NA mission the HO_2NO_2 loss due to OH dominates in the upper troposphere according to model predictions. However, if the model is incorrect the correlation between $[HO_2]/[OH]$ and $[HO_2NO_2]/[NO_2]$ should still be significant due to the dependence of OH levels on photolysis rates. Thus the observed $[HO_2NO_2]/[NO_2]$ ratio provides an independent check of the $[HO_2]/[OH]$ ratio. A strong correlation ($R^2 = 0.6$) is observed between model predicted $[HO_2]/[OH]$ (Figure 3.6b) and observed $[HO_2NO_2]/[NO_2]$; however, the correlation decreases significantly with observed HO_x (Figure 36a, $R^2=0.2$). The weaker correlation with the observations is primarily due to the insensitivity of the observed $[HO_2]/[OH]$ ratio to higher NO_x levels which corresponds to lower ratios of $[HO_2NO_2]/[NO_2]$. Consequently, the observed HO_2NO_2 levels are more consistent with the predicted $[HO_2]/[OH]$ ratio.

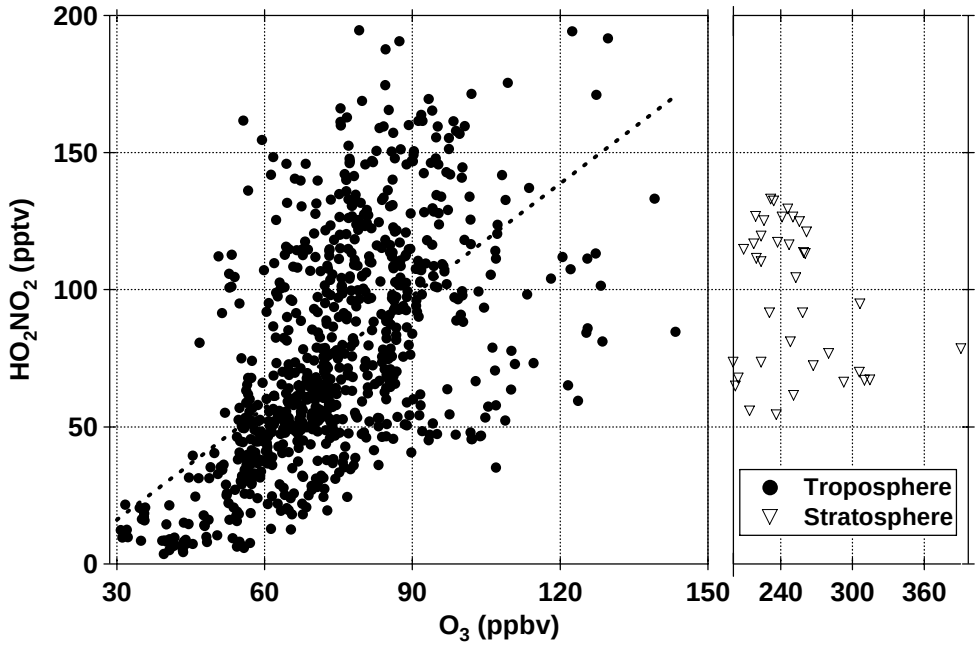

Figure 3.7 Scatterplot of HO_2NO_2 and O_3 in the altitude range of 8.5 to 9.5 km. Solid circles represent air, primarily of tropospheric origin, and open triangle present air with the significant stratospheric influence. Note the x axis has a change in scale at 150 ppbv of ozone

Finally, the INTEX-NA data set allows the investigation of the impact of high levels of ozone on the CIMS system. A potential problem with the SF_6^- CIMS system for measurement of HO_2NO_2 is a positive interference due to high ozone levels [Slusher et al., 2001]. This interference has been characterized in the laboratory and was found to be unimportant at levels of ozone up to several hundred ppbv [Slusher et al., 2001] but this has not been confirmed by field observations. The potential effect was investigated by examining the relationship of observed HO_2NO_2 and O_3. Figure 3.7 plots observed HO_2NO_2 versus O_3 in the altitude range of 8.5 – 9.5 km (i.e., highest HO_2NO_2) for both periods when the air was primarily of tropospheric (O_3<150 ppbv, H_2O>120ppmv) and stratospheric (O_3>200 ppbv, H_2O<100ppmv) origin. There is a moderate correlation (R^2=0.33) between pernitric acid and ozone at lower ozone levels for the tropospheric air

masses. At the higher ozone levels in the stratospherically influenced air masses there is essentially no correlation. This indicates that O_3 at levels of up to 250 ppbv are not a significant interference to the HO_2NO_2 measurement. The correlation between ozone and HO_2NO_2 in the tropospheric air masses is likely due to ozone production via the reaction of HO_2 with NO which is closely related to pernitric acid formation (R3.1). This suggests that HO_2NO_2 in this altitude range may be a good marker for recent ozone production.

3.3 Discussion

Measurements of HO_x, NO_x, and HO_2NO_2 were consistent at altitudes below 7.5 km where thermal decomposition dominates the loss of pernitric acid. The thermal decomposition rates derived from Sander et al. [2006] and Gierzcak et al. [2005] are both in reasonable agreement with the lower altitude observations. These results indicate that the uncertainty in the HO_2NO_2 lifetime due to the thermal decomposition rate, k_{-1}, is less than a factor of two at temperatures greater than 250 K.

Above 8 km the observations of HO_x and HO_2NO_2 are less compatible with our understanding of photochemistry. The results indicate that the formation rate of HO_2NO_2 is overestimated or the loss rates are underestimated. Alternatively these results may suggest that the steady state calculations are problematic in this altitude range and the agreement between the model HO_x calculations and observed HO_2NO_2 is fortuitous. There is strong evidence that the rate constant (k_1) for the formation of HO_2NO_2 is accurately known. The most recent study on the rate constant by Christensen et al. [2004] concluded that their results agree within 15% of the previous value, based on several prior studies, over a wide range of temperature and pressure. There has been speculation

that the reaction of HO_2 with NO_2 could produce other products such as HONO, but this has been shown to be unimportant by Tyndall et al. [1995]. The rate constant, k_3, for the reaction of HO_2NO_2 with OH also appears to be known to better than 50% over a wide temperature range (218-335 K) [Jimenez et al., 2004; Smith et al., 1984]. This uncertainty is too little to bring the observed HO_x and HO_2NO_2 at higher altitudes into agreement. For these reasons, we have investigated other potential loss processes, reassessed our estimate of overtone photolysis rates, and performed time-dependent photochemical calculations to assess the magnitude of the deviation from steady state.

Pernitric acid could be lost by heterogeneous loss or uptake in the upper troposphere on either background sulfate aerosol or cirrus clouds [Evans et al., 2003; Saathoff et al., 2001; Leu et al., 1999; Zhang et al., 1997; Li et al., 1996]. However, we found no evidence for a relationship between aerosol surface area and HO_2NO_2 levels indicating that reaction on sulfate aerosol is not an important loss process. Evaluating the impact of cirrus clouds on pernitric acid levels is more problematic due to their relatively short lifetime (~1 hour). There were a few flight legs during the campaign in which the DC-8 sampled in cirrus clouds as evidenced by detection of large particles (>20 μm dia.). There was no obvious diminishment of pernitric acid in these air masses, but these data are limited and do not allow for a robust conclusion. For this reason, we think cirrus cloud processing of HO_2NO_2 is still an open question especially since pernitric acid has been shown to efficiently stick to ice at low temperatures [Li et al., 1996].

The upper limit of the overtone photolysis rate of HO_2NO_2 in the upper troposphere of the typical INTEX condition is estimated to assess the degree of uncertainty in the overtone photolysis rate. Overtone photolysis rates of HO_2NO_2 were

estimated by calculating actinic fluxes using the SBDART (Santa Barbara DISORT Atmospheric Radiative Transfer) model [Ricchiazzi et al., 1998] and cross sections and quantum yields from Roehl et al. [2002]. Calculations of both direct and diffuse fluxes were performed for typical INTEX conditions as listed in Table 3.2.

Table 3.2 Parameters for actinic flux calculations using SBDART

Local time	28 July, Local noon
Latitude	38^{o}N
Surface type	Sand
Atmosphere profile	US 62
Boundary layer type	Rural

Note that sand was chosen as the surface to maximize the infrared albedo. A total photolysis rate of 8.0 x 10^{-6} s^{-1} was calculated which compares favorably with the value of 8.3 x 10^{-6} s^{-1} derived by Roehl et al. [2002] from the direct flux at the top of the atmosphere. These calculations indicate the photolysis rate (10^{-5} s^{-1}) used in the steady state analysis is reasonable but is probably an upper limit. As the dominant overtone photolysis band, $2\nu_1$, for HO_2NO_2 overlaps a water transition [Rothman et al., 2005] the upward flux in this spectral range over clouds, ocean, and snowpack will be attenuated due to a decreased albedo in the near-IR. It is also worth noting that only one measurement [Roehl et al., 2002] of the quantum yield and cross section for the $2\nu_1$ band is available and should probably be confirmed.

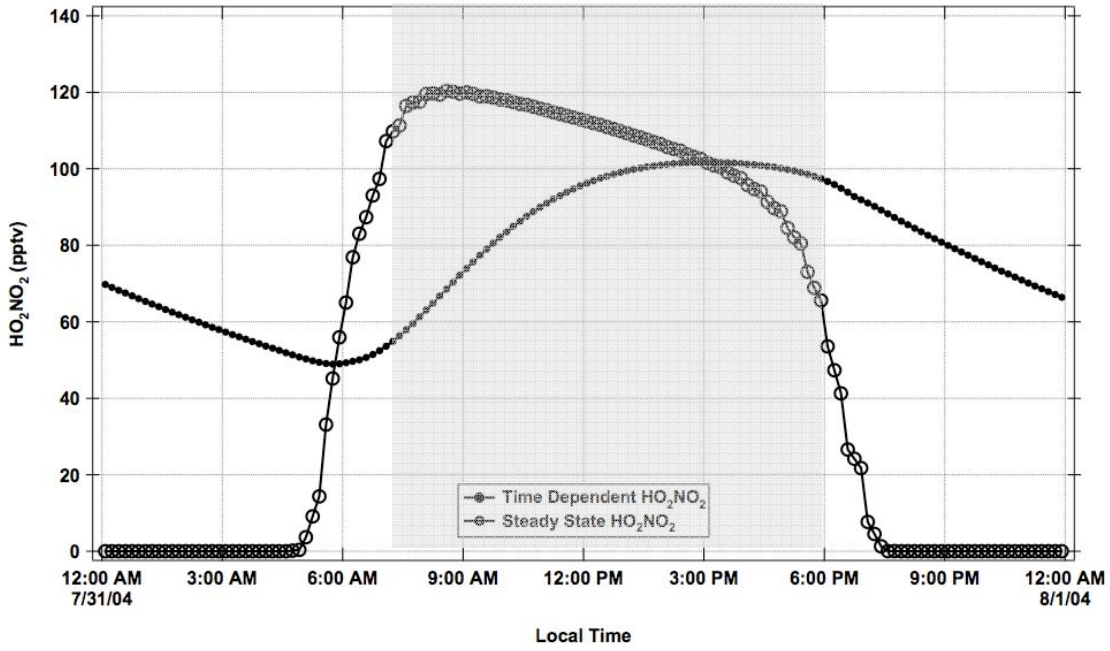

Figure 3.8 Temporal plot of HO_2NO_2 calculated using time-dependent (solid circle with solid line) and steady state HO_2NO_2 (open circle with dashed line) models. Shaded time zone is a typical flight time during INTEX-NA from 0800 to 1800 LT.

The error in the HO_2NO_2 calculations was investigated by using a time-dependent photochemical model to estimate the deviation from steady state. Figure 3.8 shows a temporal plot of HO_2NO_2 at 9 km, for typical INTEX-NA conditions (28 July, latitude~40ºN), calculated using steady state and time-dependent methods. The time-dependent results are for the second day after a fresh injection of NO_x into the upper atmosphere reflecting the relatively fresh air-masses sampled during INTEX-NA [Bertram et al., 2007; Fuelberg et al., 2007]. However, the comparison of the time-dependent and steady state results was not found to depend strongly on the number of days after the NO_x injection. In fact, the steady state values were found to be within 50% of the time-dependent calculations within approximately five hours after a fresh injection of NO_x. The shaded area in Figure 3.7 is the typical flight time from 8 a.m. to 5 p.m. The

largest difference is in the morning where the steady state model over-predicts HO_2NO_2 by ~50%. The disagreement diminishes through the day until there is a slight underestimation by the steady state model in the late afternoon. These effects were observed to a small extent in the data as the ratio of model predictions to observations before noon was approximately 10% greater than in the afternoon. On average the steady state model over-predicts the time-dependent results by 12% during typical DC-8 flight times. At higher altitudes the disagreement between steady state and time-dependent calculations is lower as HO_2NO_2 does not undergo significant thermal decomposition through the night. Consequently, steady state methods seem to be valid for predicting HO_2NO_2 levels in the upper troposphere with less than a 50% inherent error bar.

Clearly, the measured HO_2NO_2 and HO_x are not consistent with our current understanding of photochemistry in the upper troposphere. One possible explanation is that there are unidentified measurement errors in either or both the HO_x and HO_2NO_2 measurements. These potential errors must be greater at either high altitude or high NO_x levels, but at this point we are unaware of any mechanisms for these errors. Alternatively, a higher loss rate for pernitric acid would bring observations of HO_2NO_2 and HO_2 into better agreement. Figure 3.9a presents the vertical profile of the needed HO_2NO_2 first order rate constant for the additional loss needed to bring observed HO_2NO_2 and HO_x into accord. This additional loss rate generally increases with altitude with a maximum near 11 km. The needed loss rate is of a large magnitude and is unlikely to be explained by any single mechanism. One potential mechanism that could account for some of the additional loss is photolysis via weak electronic transitions as discussed by Mathews et al. [2005]. Finally, we determined if the measured OH and the model predicted

$[HO_2]/[OH]$ ratio are consistent with the observed HO_2NO_2. This was done with a steady state analysis using observed OH and HO_2 derived from the predicted HO_x ratio. The median altitude profile for this data is shown in Figure 3.9b and shows excellent agreement with the observed profile. These data demonstrate that the observed HO_2NO_2 are inconsistent with the observed HO_x ratio but not the observed OH levels.

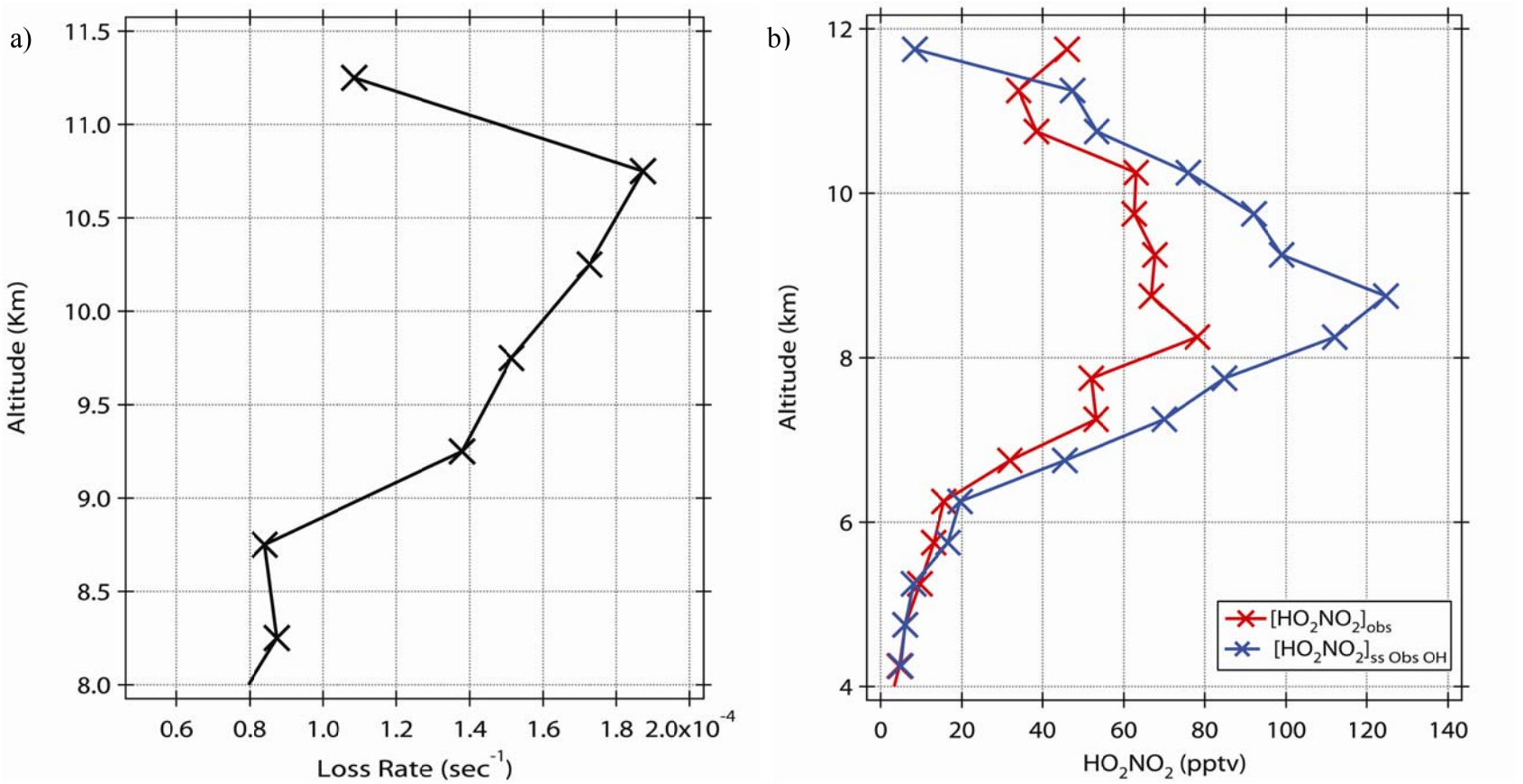

Figure 3.9 (a) Altitude profile of the first-order rate constant for the additional loss of HO_2NO_2 derived from measured HO_x. (b) Vertical profile of observed ($[HO_2NO_2]_{obs}$) and predicted ($[HO_2NO_2]_{SS\ Obs\ OH}$). The predicted HO_2NO_2 is derived from a steady state analysis using observed OH levels and the model predicted ratio of $[HO_2]$ to [OH]

3.4 Summary

Our understanding of HO_2NO_2 in the free troposphere is examined with the first direct in situ observations from the NASA DC-8 during INTEX-NA 2004. Photochemical models and observed HO_x levels can explain the HO_2NO_2 in the mid troposphere (4.5-8 km) where thermal decomposition is dominant. In the upper troposphere (8-12 km) there is a significant discrepancy between model predicted and observed HO_x. There is also significant disagreement between steady state calculations of HO_2NO_2 that use measured HO_2 levels and observations of HO_2NO_2 in the upper troposphere. Conversely, pernitric acid levels are reasonably well predicted by steady state calculations using photochemical model predicted HO_2 levels. Time dependent modeling of HO_2NO_2 levels indicates that treating pernitric acid as in steady state is valid in the upper troposphere within the uncertainty of steady state calculations. The discrepancy between the observed HO_2 and HO_2NO_2 levels would be diminished if there is an unidentified loss process for HO_2NO_2 whose magnitude increases with altitude. This suggests that further investigation of potential HO_2NO_2 loss processes may be needed.

3.5 References

Bertram, T. H., Perring, A. E., Wooldridge, P. J., Crounse, J. D., Kwan, A. J., Wennnberg, P. O., Scheuer, E., Dibb, J., Avery, M., Sachse, G., Vay, S., Crawford, J. H., McNaughton, C. S., Clarke, A., Pickering, K. E., Fuelberg, H., Huey, G., Blake, D. R., Singh, H. B., Hall, S. R., Shetter, R. E., Fried, A., Heikes, B. G., and Cohen, R. C.: Direct measurements of the convective recycling of the upper troposphere, Science, 315, 816 - 820, 2007.

Brune, W. H., Tan, D., Faloona, I. F., Jaglé, L., Jacob, D. J., Heikes, B. G., Snow, J., Kondo, Y., Shetter, R., Sachse, G. W., Anderson, B., Gregory, G. L., Vay, S., Singh, H. B., Davis, D. D., Crawford, J. H., and Blake, D. R.: OH and HO_2 chemistry in the North Atlantic free troposphere, Geophysical Research Letters, 26, 3077-3080, 1999.

Christensen, L. E., Okumura, M., Sander, S. P., Friedl, R. R., Miller, C. E., and Sloan, J. J.: Measurements of the rate constant of $HO_2 + NO_2 + N_2 \rightarrow HO_2NO_2 + N_2$ using near-infrared wavelength-modulation spectroscopy and UV-visible absorption spectroscopy, Journal of Physical Chemistry A, 108, 80-91, 2004.

Crawford, J. H., Davis, D., Olson, J., Chen, G., Liu, S., Gregory, G., Barrick, J., Sachse, G., Sandholm, S., Heikes, B., Singh, H., and Blake, D.: Assessment of upper tropospheric HO_x sources over the tropical Pacific based on NASA GTE/PEM data: Net effect on HOx and other photochemical parameters, Journal of Geophysical Research, 104, 16255-16273, 1999.

Evans, M. J., Jacob, D. J., Atlas, E., Cantrell, C. A., Eisele, F., Flocke, F., Fried, A., Mauldin, R. L., Ridley, B. A., Wert, B., Talbot, R., Blake, D., Heikes, B., Snow, J., Walega, J., Weinheimer, A. J., and Dibb, J.: Coupled evolution of BrO_x-ClO_x-HO_x-NO_x chemistry during bromine catalyzed ozone depletion events in the arctic boundary layer, Journal of Geophysical Reserach, 108, 8368,doi:8310.1029/2002JD002732, 2003.

Faloona, I., Tan, D., Brune, W. H., Jaglé, L., Jacob, D. J., Kondo, Y., Koike, M., Chatfield, R., Pueschel, R., Ferry, G., Sachse, G., Vay, S., Anderson, B., Hannon, J., and Fuelberg, H.: Observation of HO_x and its relationship with NO_x in the upper troposphere during SONEX, Journal of Geophysical Reserach, 105, 3771-3783, 2000.

Fuelberg, H. E., Porter, M. J., Kiley, C. M., Holland, J. J., and Morse, D.: Meteorological conditions and anomalies during the Intercontinental Chemical Transport Experiment-North America, Journal of Geophysical Reserach, 112, doir:10.1029/2006JD007734, 2007.

Gierczak, T., Jimenez, E., Riffault, V., Burkholder, J. B., and Ravishankara, A. R.: Thermal decomposition of HO_2NO_2 (peroxynitric acid, PNA):Rate coefficient and determination of the enthalpy of formation, Journal of Physical Chemistry A, 109,

586-596, 2005.

Jaglé, L., Jacob, D. J., Brune, W. H., Faloona, I., Tan, D., Heikes, B., Kondo, Y., Sachse, G. W., Anderson, B., Gregory, G. L., Singh, H. B., Pueschel, R., Ferry, G., Blake, D. R., and Shetter, R. E.: Photochemistry of HO_x in the upper troposphere at northern midlatitudes, Journal of Geophysical Reserach, 105, 3877-3892, 2000.

Jimenez, E., Gierczak, T., Stark, H., Burkholder, J. B., and Ravishankara, A. R.: Reaction of OH with HO_2NO_2 (pernitric acid): Rate coefficient between 218 and 225 K and product yields at 298 K, Journal of Atmospheric Chemistry A, 108, 1139-1149, 2004.

Leu, M.-T., and Zang, R.: Solubilities of $CH_3C(O)O_2NO_2$ and HO_2NO_2 in water and liquid H_2SO_4, Geophysical Research Letters, 26, 1129-1132, 1999.

Li, Z., Friedl, R. R., Moore, S. B., and Sander, S. P.: Interaction of peroxynitric acid with solid H_2O ice, Journal of Geophysical Reserach, 101, 6759-6802, 1996.

Mathews, J., Sinha, A., and Francisco, J. S.: The importance of weak absorption features in promoting tropospheric radical production, Proceedings of the National Academy of Sciences, 102, 7449-7452, 2005.

Murphy, J. G., Thornton, J. A., Wooldridge, P. J., Day, D. A., Rosen, R. S., Cantrell, C., Shetter, R., Lefer, B., and Cohen, R. C.: Measurements of the sum of HO_2NO_2 and $CH_3O_2NO_2$ in the remote troposphere, Atmospheric Chemistry Physics, 4, 377-384, 2003.

Niki, H., Marker, P. D., Savage, C. M., and Breitenbach, L. P.: Fourier transformation IR sepctroscopy obseravtion of pernitric acid formed via $HOO + NO_2 \rightarrow HOONO_2$, Chemical Physic Letters, 45, 564-566, 1977.

Olson, J. R., Crawford, J. H., Chen, G., Fried, A., Evans, M. J., Jordon, C. E., Sandholm, S. T., Davis, D. D., anderson, B. E., Avery, M. A., Barrick, J. D., Blake, D. R., Brune, W. H., Eisele, F. L., Flocke, F., Harder, H., Jacob, D. J., Kondo, Y., Lefer, B. L., Martinez, M., Mauldin, R. L., Sachse, G. W., Shetter, R. E., Singh, H. B., Talbot, R. W., and Tan, D.: Testing fast photochemical theory during TRACE-P based on measurements of OH, HO_2, and CH_2O, Journal of Geophysical Research, 109, D15S10, 2004.

Ricchiazzi, P., Yang, S., Gautier, C., and Sowle, D.: SBDART: A research and teaching software tool for plane-parallel radiative transfer in the Earth's atmosphere, Bulletin of the American Meteorological Society, 79, 2101-2114, 1998.

Rinsland, C. P., Gunson, M. R., Salawitch, R. J., Michelsen, H. A., Zander, R., Newchurch, M. J., Abbas, M. M., Abrams, M. C., Manney, G. L., Chang, A. Y., Irion, F. W., Goldman, A., and Mahieu, E.: ATMOS/ATLAS-3 measurements of stratospheric chlorine and reactive nitrogen partitioning inside and outside the November 1994 Antarctic vortex, Geophysical Research Letters, 23, 2365-2368,

1996.

Roehl, C. M., Nizkorodov, S. A., Zhang, H., Blake, G., and Wennnberg, P. O.: Photodissociation of peroxynitric acid in the Near-IR, Journal of Physical Chemistry A, 106, 3766-3772, 2002.

Rothman, L. S., Jacquemart, D., Barbe, A., Chris Benner, D., Birk, M., Brown, L. R., Carleer, M. R., Chackerian Jr, C., Chance, K., Coudert, L. H., Dana, V., Devi, V. M., Flaud, J.-M., Gamache, R. R., Goldman, A., Hartmann, J.-M., Jucks, K. W., Maki, A. G., Mandin, J.-Y., Massie, S. T., Orphal, J., Perrin, A., Rinsland, C. P., Smith, M. A. H., Tennyson, J., Tolchenov, R. N., Toth, R. A., Vander Auwera, J., Varanasi, P., and Wagner, G.: The HITRAN 2004 molecular spectroscopic database, Journal of Quantitative Sepctroscopy and Radiative Transfer, 96, 139-204, 2005.

Saathoff, H., Naumann, K.-H., Riemer, N., Kamm, S., Mohler, O., Schurath, U., Vogel, H., and Vogel, B.: The loss of NO_2, HNO_3, NO_3/N_2O_5, and $HO_2/HOONO_2$ on soot aerosol: A chamber and modeling study, Geophysical Research Letters, 28, 1957-1960, 2001.

Sander, S. P., Friedl, R. R., Ravishankara, A. R., Golden, D. M., Kolb, C. E., Kurylo, M. J., Molina, M. J., Moortgat, G. K., Keller-Rdek, H., Finlayson-Pitts, B. J., Wine, P. H., Huie, R. E., and Orkin, V. L.: Chemical kinetics and photochemical data for use in atomspheric studies, Evaluation Number 15, JPL Publication 06-02, 2006.

Sen, B., Toon, G. C., Osterman, G. B., Blavier, J.-F., Margitan, J. J., Salawitch, R. J., and Yue, G. K.: Measurements of reactive nitrogen in the stratosphere, Journal of Geophysical Reserach, 103, 3571-3585, 1998.

Simth, C. A., Molina, L. T., Lamb, J. J., and Molina, M. J.: Kinetics of the reaction of OH with pernitric acid and nitric acids, International Journal of Chemical Kinetics, 16, 41-55, 1984.

Singh, H. B., Brune, W. H., Crawford, J., and Jacob, D.: Overview of the summer 2004 Intercontinental Chemical Transport Experiment-North America (INTEX-A), Journal of Geophysical Reserach, 111, doi:10.1029/2006JD007905, 2006.

Singh, H. B., Salas, L., Herlth, D., Kolyer, R., Czech, E., Avery, M., Crawford, J. H., Pierce, R. B., Sachse, G. W., Blake, D. R., Cohen, R. C., Bertram, T. H., Perring, A., Wooldridge, P. J., Dibb, J., Huey, G., Hudman, R. C., Turquety, S., Emmons, L. K., Flocke, F., Tang, Y., Carmichael, G. R., and Horowitz, L. W.: Reactive nitrogen distributions and partitioning in the North American troposphere and lowermost stratosphere, Journal of Geophysical Reserach, 112, doi:10.1029/2006JD07664, 2007.

Sjostedt, J. J., Tanner, D. J., Dibb, J. E., Buhr, M., Warshawsky, M., Davis, D., Chen, G., Mauldin, R. L., Eisele, F., and Arimoto, R.: Measurements of HO_2NO_2 and HNO_3 at South Pole during ANTCI 2003, Eos, Trans. AGU, 85(47), Fall Meet. Suppl.,

Abstract A24A-02, 2004.

Slusher, D. L., Pitteri, S. J., Haman, B. J., Tanner, D. J., and Huey, L. G.: A chemical ionization technique for measurement of pernitric acid in the upper troposphere and the polar boundary layer, Geophysical Research Letters, 28, 3875-3878, 2001.

Stiller, G. P., von Clarmann, T., Bruhl, C., Fischer, H., Funke, B., Glatthor, N., Grabowski, U., Hopfner, M., Jockel, P., Kellmann, S., Kiefer, M., Linden, A., Lopez-Puertas, M., Mengistu Tsidu, G., Milz, M., Steck, T., and Steil, B.: Global distributions of HO_2NO_2 as observed by the Michelson Interferomenter for Passive Atmospheric Sounding (MIPAS), Journal of Geophysical Reserach, 112, doi:10.1029/2006JD007212, 2007.

Tyndall, G. S., Orlando, J. J., and Calvert, J. G.: Upper limit for the rate coefficient for the reaction $HO_2 + NO_2 \rightarrow HONO + O_2$, Environmental Science and Technology, 29, 202-206, 1995.

Wennnberg, P. O., Salawitch, R. J., Donaldson, D. J., Hanisco, T. F., Lanzendorf, E. J., Perkins, K. K., Lloyd, S. A., Vaida, V., Gao, R. S., Hintsa, E. J., Cohen, R. C., Swartz, W. H., Kusterer, T. L., and Anderson, D. E.: Twilight observation suggest unknown sources of HO_x, Geophysical Research Letters, 26, 1373-1376, 1999.

Zang, R., Leu, M.-T., and Keyser, L. F.: Heterogeneous chemistry of HO_2NO_2 in liquid sulfuric acid, Journal of Physical Chemistry A, 101, 3324-3330, 1997.

CHAPTER 4

HCl OBSERVATIONS OVER THE NORTH PACIFIC OCEAN

4.1. Introduction

Hydrochloric acid (HCl) is produced in the troposphere and stratosphere by different mechanisms. In the remote troposphere the major source of HCl is thought to be dechlorination of sea-salt aerosol by acids such as HNO_3 and H_2SO_4 [Erickson, 1959a and b; Kerminen et al., 1998]. HCl is very soluble in water and can be lost to cloud drops and aerosols of non-acidic composition [Keene et al., 1999] on the time scale of a day in the remote marine boundary layer (MBL). Conversely, the lifetime of HCl with respect to photolysis and reaction with OH is relatively long (~20 days with $[OH]_{AVG} = 10^6$ molecules/cm^3) in the troposphere [Sander et al., 2006]. For this reason, tropospheric HCl chemistry is expected to be most active in the marine boundary layer (MBL). This is especially true in the polluted MBL where very high levels of HCl have been predicted (~400 pptv; Spicer et al., 1998). These high levels have been attributed to the interaction of N_2O_5 with sea salt to produce high levels of Cl_2 [Behnke et al., 1997; Schweitzer et al., 1998; Rossi, 2003]. Cl_2 will rapidly photolyze to produce chlorine atoms that produce HCl by reaction with methane and other volatile organic compounds (VOC). Elevated Cl_2 in the urban MBL has been speculated to lead to enhanced ozone production [Finley and Saltzman, 2006; Tanaka et al, 2003; Chang et al., 2002; Spicer et al., 1998].

Direct observations of HCl in the MBL and lower troposphere are limited in terms of frequency and geographical coverage. However, HCl has been measured sporadically in a variety of locations [Graedel and Keene 1995]. These measurements indicate HCl

mixing ratios in the remote MBL (0 – 200 m) of 100-300 pptv with levels decreasing to 50-100 pptv in the remote marine free troposphere (1 km – 6 km; Vierkorn-Rudolph et al., 1984). In the urban influenced troposphere ppbv levels of HCl have been reported in various locations [Keene et al., 2007; Graedel and Keene, 1995]. Keene et al.,[1999] calculated the global tropospheric budget of HCl, based on the data from Greedel and Keene,[1995], and reported that large unknown sources are needed to explain the distribution of HCl in the troposphere. However, this conclusion was based on data from analytical methods (filter techniques), which have been identified to potentially have positive artifacts such as NOCl, $ClNO_2$, $ClNO_3$ and chlorinated aerosols. Therefore, most of these studies report HCl*, which includes NOCl, $ClNO_2$, and $ClNO_3$, rather than HCl.

The magnitude of HCl production in the troposphere by Cl reactions with VOC is not well constrained due to the uncertainty in Cl levels. A series of studies have applied indirect methods using chemical proxies such as observations of C_2Cl_4 and VOC ratios to estimate Cl number densities [Singh et al., 1996a, 1996b; Wingenter et al., 1996; Rudolph et al., 1996, 1997; Jobson et al., 1998; Wingenter et al., 1999]. These estimates range from 720 atoms/cm^3 [Wingenter et al., 1999] to 10^5 atoms/cm^{-3}[Singh et al., 1996a; Wingenter et al., 1996]. Recently, Arsene et al. [2007] and Wingenter et al. [2005] reported 6×10^3- 4.7×10^4 atoms/cm^{-3} and 5.7×10^4 atoms/cm^{-3}, respectively.

In the stratosphere HCl is produced primarily by the reaction of Cl radicals with CH_4 [Lin et al., 1978]. The source of stratospheric chlorine is the photodissociation of chlorofluorocarbons (CFCs) [Molina and Rowland, 1974]. HCl is the most abundant form of inorganic chlorine in the stratosphere due to its long photochemical lifetime (of the order of 30 days at 20 km; Webster et al., 1994). However, HCl can be lost via

heterogeneous processes in the stratosphere. [Hanson et al., 1994; Hanson and Ravishakara, 1991, 1993, and 1994; Tolbert et al., 1988]. Lelieveld et al., [1999] reported a mean mixing ratio of ~ 450 pptv of HCl at 12.3 km in the late Arctic winter (Feburary 1995; Kiruna, Norway) from observations with a quadrupole mass spectrometer. Webster et al.,[1994], also, reported in situ HCl measurements in the stratosphere using a tunable diode laser spectrometer integrated on the NASA ER-2 research aircraft during the SPADE(Stratospheric Photochemistry, Aerosols, and Dynamics Expedition) mission. These research flights covered a latitude range of 15- 60^{o}N and altitudes below 20km in spring and fall of 1992 and 1993. HCl levels of 500 pptv to 1ppbv of HCl were observed over a pressure range of 50 to 70 mb. In addition, the study also found that model predictions of the HCl fraction of inorganic chlorine (Cl_y = HCl, ClO, and $ClONO_2$) in the stratosphere was systematically higher than observations although the model predicted Cl_y within the uncertainty of the measurement.

Remote sensing has been used to measure the global distribution of HCl in the stratosphere. The Halogen Occultation Experiment (HALOE) indicated ~1ppbv of HCl at 10 mb with no obvious variation as a function of season or latitude [Russell III et al., 1996].

Recently, Marcy et al.[2004] demonstrated the utility of HCl measurements for examining the transport of stratospheric O_3 to the troposphere. They found a very high degree of correlation between HCl and O_3 in the upper troposphere and lower stratosphere during the Cirrus Regional Study of Tropical Anvils and Cirrus Layers-Florida Area Cirrus Experiment (CRYSTAL FACE) mission. They also found the observed relationship was consistent with the IMPACT (Interactive Modeling Project for

Atmospheric Chemistry) model of stratospheric chemistry. Consequently, they proposed using the observed HCl/O_3 ratio to calculate the fraction of stratospheric ozone in an air parcel. However, this method relies on the assumption that HCl in the free troposphere is only of stratospheric origin which is inconsistent with the observations of Graedel and Keene [1995].

In this work we present observations of HCl from the NASA DC-8 during the Anchorage, AK deployment of the Intercontinental Chemical Transport Experiment-Phase B (INTEX-B). This phase of the mission consisted of five flights over the North Pacific as shown in Figure 1. Each science mission consisted of level flight legs and multiple spiral vertical profiles from the MBL to the UT. The comprehensive vertical coverage allows us to examine HCl levels over the entire troposphere. These data are analyzed using correlations with other measured species and a 3D chemical transport models to probe our understanding of the sources and distribution of HCl in the troposphere.

4.2. Results and Discussion

All reported data and analyses are based on a 1 minute merged dataset unless otherwise noted. The median and the mean profiles of HCl for five science flights of the INTEX-B mission are presented in Figure 4.1, accompanied with median profile of O_3 and HNO_3. In addition, in Table 4.1, we report the statistics of the vertical distribution of HCl. In general, we found high HCl episodes (up to 140 pptv) in the upper troposphere (8-12km) interspersed with observations of low levels near our detection limit of 2 pptv. In the MBL HCl levels above 20 pptv were routinely observed. In the mid troposphere (4

- 8 km), HCl was measured below 15 pptv more than 90% of the time (90%). However, one case of strong stratospheric influence was identified by HCl enhancement along with enhanced O_3. There was also evidence for one episode of dechlorination in the mid troposphere. The vertical distribution of HCl in this study is significantly different from that of Keene et al. [1999] and Graedel and Keene [1995]. The observed values in both the MBL and mid troposphere are lower by a factor of 5-10 than the previous studies. The observations of very low background levels of HCl in the UT/LS are consistent with the results reported by Marcy et al. [2004]

Table 4.1 Vertical distribution of HCl from five science flights during the Anchorage deployment of the INTEX campaign (in pptv)

Altitude	Average	Median	1 σ	min.	Max.
0.25	32.1	24.4	20.9	5.8	105.1
0.75	22.8	17.5	18.0	8.1	82.6
1.25	18.3	14.1	17.0	2.0	72.0
1.75	16.9	11.2	14.6	2.0	72.2
2.25	18.0	13.8	14.0	2.0	80.7
2.75	8.3	6.3	12.6	2.0	64.8
3.25	7.4	8.6	5.8	2.0	29.3
3.75	6.9	5.8	6.5	2.0	28.2
4.25	5.5	2.0	5.8	2.0	25.2
4.75	6.1	2.0	6.1	2.0	25.5
5.25	6.0	2.0	7.1	2.0	24.1
5.75	6.8	6.7	6.0	2.0	23.5
6.25	4.4	2.0	4.5	2.0	22.0
6.75	5.0	2.0	5.8	2.0	20.7
7.25	8.1	2.0	11.4	2.0	56.0
7.75	5.9	2.0	8.7	2.0	55.0
8.25	9.8	2.0	13.6	2.0	55.2
8.75	27.7	14.2	33.5	2.0	115.4
9.25	6.6	2.0	11.0	2.0	55.9
9.75	26.2	2.0	31.8	2.0	89.4
10.25	54.5	62.3	43.5	2.0	140.9

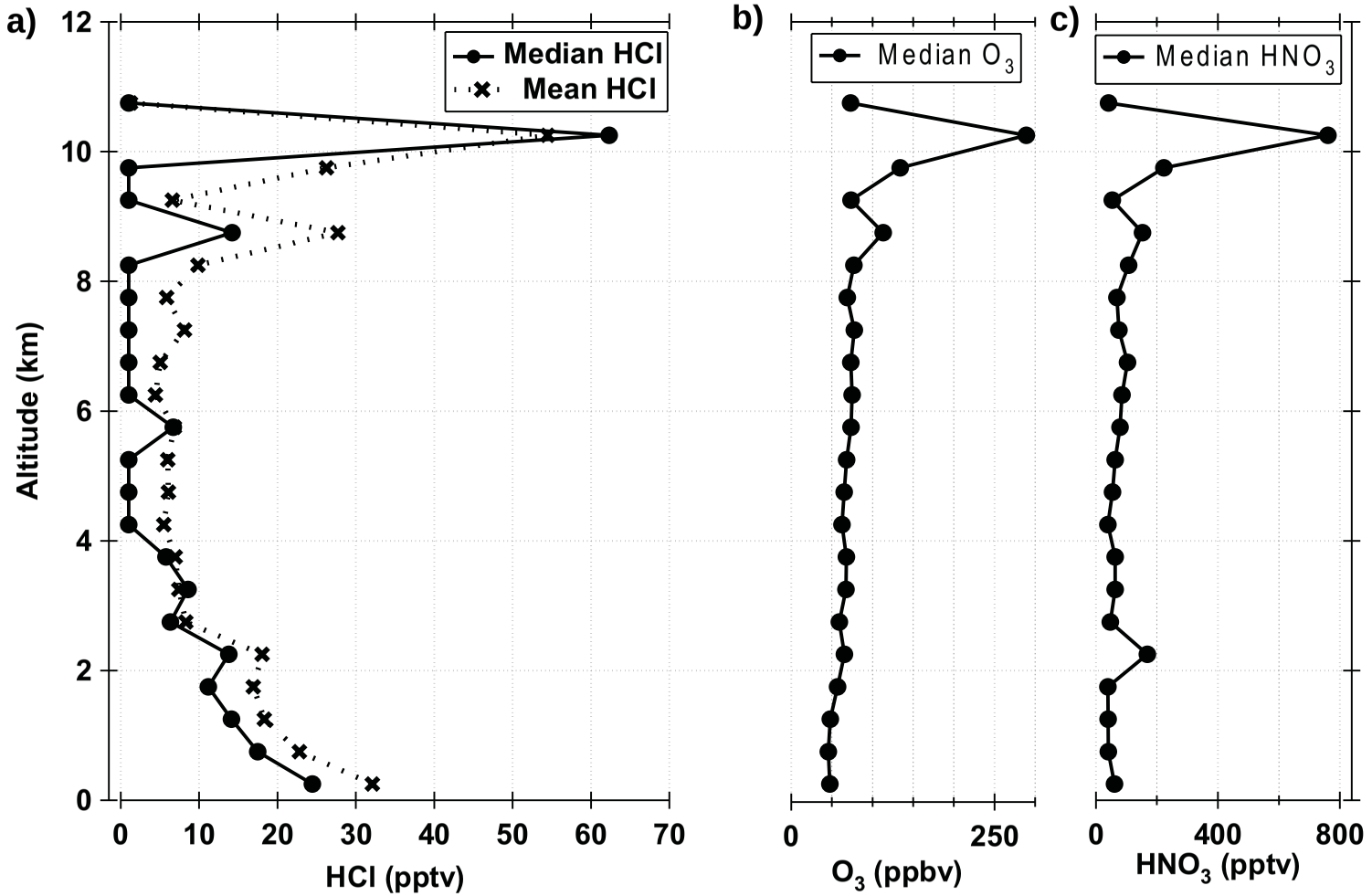

Figure 4.1 The median and mean profile of HCl, a) and the median profile of O_3 b) and HNO_3 c) for five science flights during the Anchorage deployment of the INTEX campaign

4.2.1 The Upper Troposphere (8-12 km)

High levels of HCl in the upper troposphere were strongly associated with stratospheric influences. This is illustrated in Figures 4.2c and 4.2d, which show a strong negative correlation of HCl with tropospheric tracers (N_2O and CFCs), and Figure 4.2a and 4.2b which show a strong positive correlation of HCl with stratospheric tracers (O_3 and HNO_3).The correlation with O_3 (Figure 4.2a) illustrates that the background level of HCl (i.e. w/o stratospheric influence) in the upper troposphere is low and that HCl is a good tracer for recent stratospheric influence. HCl also shows a strong positive (R^2 = 0.773) correlation with Be-7, another stratospheric tracer [Dibb et al., 2003].

The method of Marcy et al. [2004] was employed to assess the extent of stratospheric influence on the upper troposphere during the Anchorage deployment of INTEX-B. This method utilizes the O_3-HCl correlation (Figure 4.3) and sets a stratospheric end member (O_3: 160 ppbv and HCl: 30 pptv). Above the end member the air is categorized as pure stratospheric. Air parcels with HCl below detection limit are categorized as pure tropospheric air. In between these limits the air is characterized as a mixture of both. The analysis suggests that in the upper troposphere (8-12 km) during INTEX-B pure stratospheric air was sampled ~30 % of the time and air with significant stratospheric influence was observed 15 % of the time.

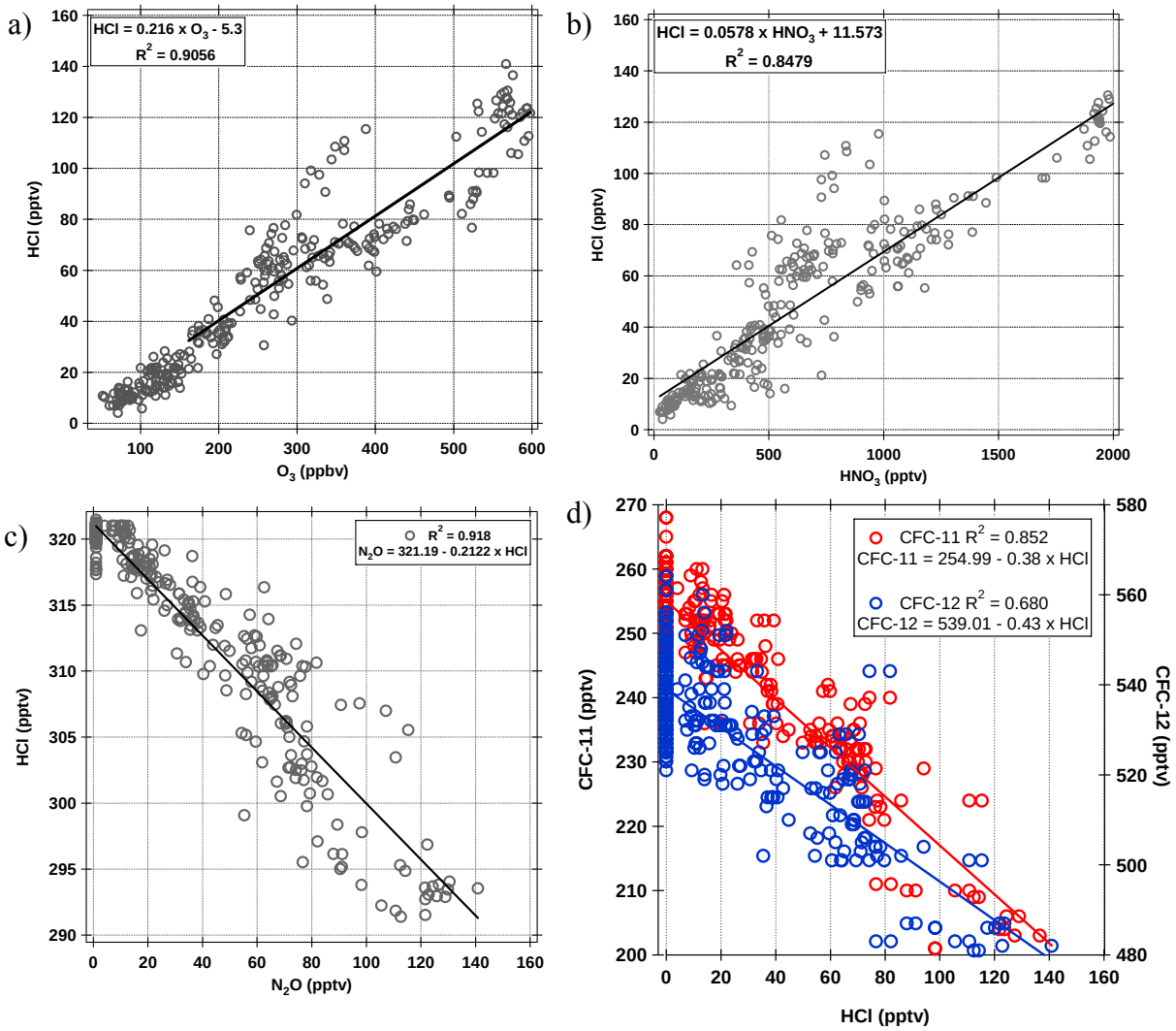

Figure 4.2 The correlation of HCl with a) O_3,b) HNO_3 c), N_2O and d) CFCs in the upper troposphere (8-12 km).

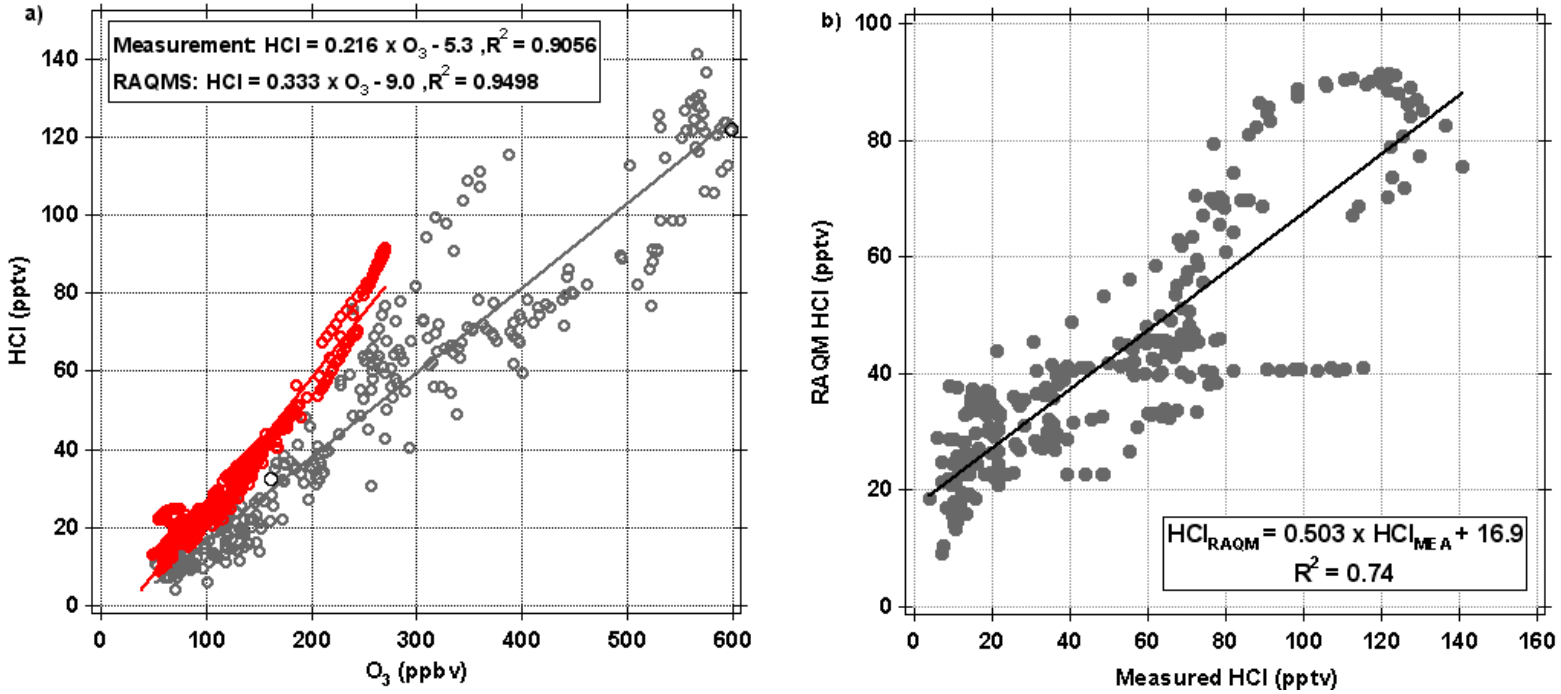

Figure 4.3 a) The correlation of HCl with O_3 in the upper troposphere from in situ measurements (black open circles) and RAQMS model results (red open circles). Regression lines of each result are also presented. The simple analysis for the stratospheric influence is also illustrated in the figure (see the text for more detail) b) A correlation plot between measured and RAQM HCl

Figure 4.3a also contains the predicted correlation of HCl with O_3 by the Realtime Air Quality Modeling System (RAQMS) model [Pierce et al., 2003] in the upper troposphere. The model systematically overestimated the slope of the correlation by ~50% which is only slightly larger than the estimated measurement error. Marcy et al. [2004] found even better agreement between their observations and the Interactive Modeling Project for Atmospheric Chemistry and Transport (IMPACT) model [Eckman et al., 1995; Pierce et al., 2000; Al-Saadi et al., 2001]. These studies indicate that the IMPACT chemical scheme can predict the HCl/O_3 relationship with at least reasonable accuracy. Marcy et al. [2004] did report a significantly higher ratio of (0.45) HCl/O_3 than in this work (0.21). However, that study was conducted in the summer in the subtropics (24^oN -39^oN) in a higher altitude range (11-18km).

Figure 4.3b presents a strong correlation (R^2 = 0.72) between measured and RAQMS HCl in the upper troposphere. However, the linear regression analysis presents a slope of ~ 0.5 with a significant offset (16 pptv). Overall, RAQMS predicted HCl is ~30% lower than measured HCl in the high concentration range (> 60 pptv). Therefore, the overestimated HCl/O_3 ratio from RAQMS may reflect discrepancies between modeled and measured O_3 rather than HCl. This positive offset in the data also suggests that the RAQMS model always predicts a finite amount of stratosphere-troposphere exchange since no other source of chlorine is available in the model. This is not compatible with the observations and indicates that the mixing parameterization in the models may need to be modified. However, in general the RAQMS model appears to do a reasonable job of capturing stratospheric transport.

4.2.2 The MBL and the Lower Troposphere (0 – 4 km)

The median levels of HCl (Figure 4.1) increase at altitudes below 4 km and reach up to 20 pptv in the MBL (z < 1km). These observations are much lower than recent measurements in the relatively clean Hawaii MBL of 30 – 250 pptv [Pszenny et al., 2004]. Figures 4.4a and 4.4b show the correlation of HCl with HNO_3 and SO_2 in the MBL (z < 1 km), respectively. Both species shows a good correlation with HCl except for a few outliers associated with either volcanic influence, from the Veniaminof volcano, located in the Aleutian Island chain, or anthropogenic pollution near the western U.S. coast. These positive correlations with HNO_3 and SO_2, the major precursor of H_2SO_4, are consistent with HCl production from the acidification of seasalt aerosol (assuming that HCl has a relatively short lifetime in the MBL).

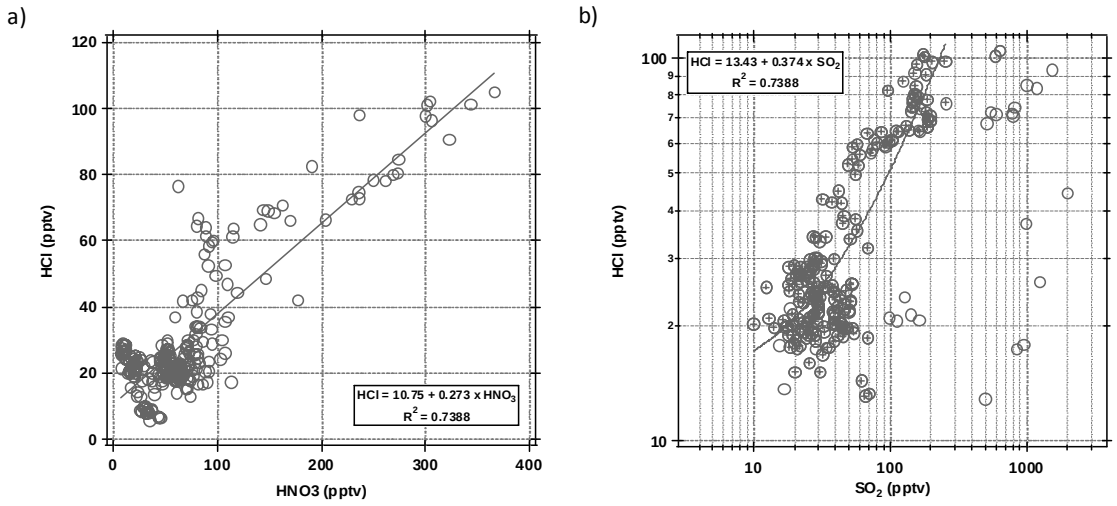

Figure 4.4 The correlation of HCl with a) HNO_3 and b) SO_2 in the MBL

However, at very low levels of HNO_3 and SO_2, reasonably high levels of HCl were still observed (~20pptv). These low levels of HCl in the absence of HNO_3 and SO_2 could be produced by the reactions of Cl atoms with VOCs. A simple calculation to estimate the number density of Cl atoms needed to produce this amount of HCl is conducted using the assumption that HCl is in steady state. Three HCl loss pathways: aerosol uptake, oceanic deposition, and reaction with OH, are considered. Lifetimes for each loss process are estimated based on the INTEX-B data summarized in Table 4.2. These assumptions give the equation below for calculation of the Cl atom number density.

$$[Cl] = \frac{[HCl] \times (k_{OH} + k_{Dry-Deposition} + k_{Aerosol-Uptake})}{k_1[Ethane] + k_2[Propane] + k_{34}[Ethyne] + k_4[Methane] + k_5[DMS]}$$

Table 4.2 The summary of input parameters for the calculation of Cl atom

Species	Concentrations	k_{Cl}
Ethane	1497 pptv	5.58×10^{-11} molecules/cm^3 s
Propane	242 pptv	1.40×10^{-10} molecules/cm^3 s
Ethyne	257 pptv	5.81×10^{-11} molecules/cm^3 s
Methane	1.86 ppmv	7.01×10^{-14} molecules/cm^3 s
DMS	7 pptv	1.93×10^{-10} molecules/cm^3 s
Loss Pathways		Rates
k_{OH}		1/21 day^{-1}
$k_{Aerosol\ Uptake}$		1/0.5 day^{-1}
$k_{Dry\text{-}Deposition}$		1/0.5 day^{-1}

The input parameters (Table 4.2) are based on observations from the INTEX dataset and rate constants from the JPL compilation [Sander et al., 2006]. The result of the calculation is 2.8×10^3 atmos/cm^3. This estimate is in the lower range [Singh et al., 1996b; Rudolph et al., 1996, 1997; Jobson et al., 1998; Wingenter et al., 1999; Wingenter et al., 2005; Arsene et al., 2007] of those previous studies and is not compatible with

higher order estimates of greater than 10^5 atom cm^{-3} [Singh et al., 1996a; Wingenter et al., 1996]. This may reflect that the sampling environment of this study was a relatively remote high latitude region and the spring season with suppressed photo chemistry.

During the INTEX-B campaign, most boundary layer legs were conducted in unpolluted regions. However, one flight in the MBL south of Seattle did intercept moderate levels of pollution (Figure 4.5). Consequently, enhancements of HCl might be expected due to both dechlorination and NO_x activated processes as suggested by a series of studies (e.g. Spicer et al., 1997) and recent measurement results [Keene et al., 2007]. However, large enhancements of HCl were not observed in the polluted air mass. Although, the sampling duration was very short (~ 10 minutes) and was over a limited geographic area.

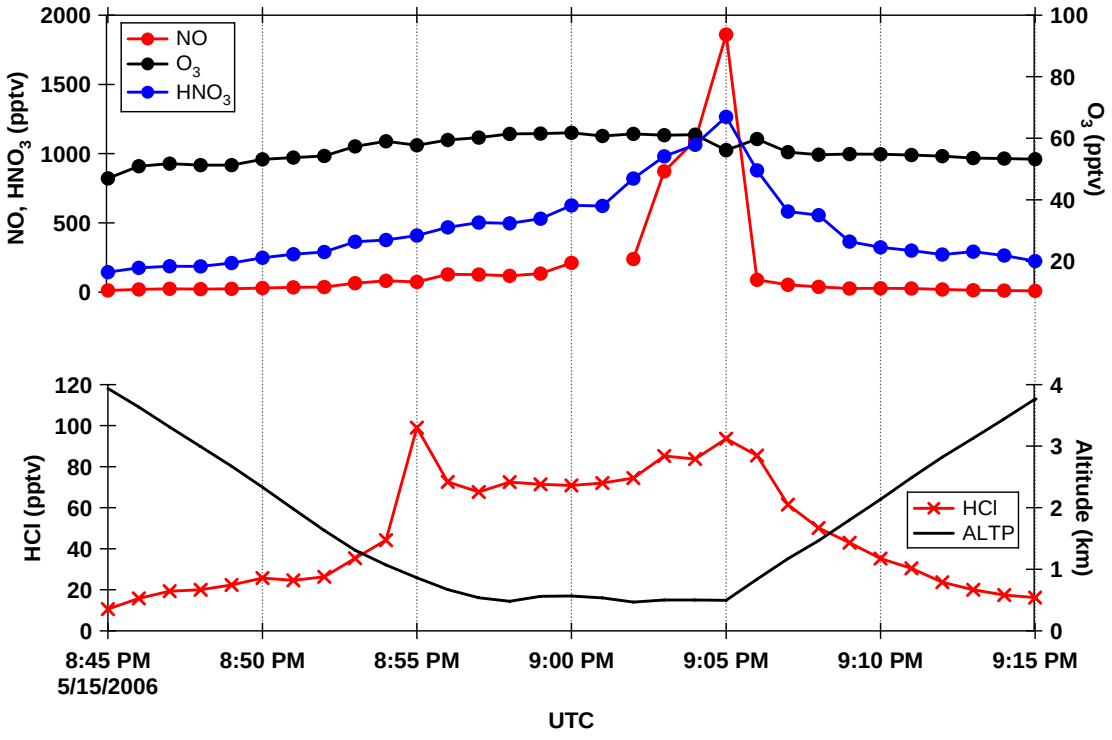

Figure 4.5 Temporal variations of HCl, O_3, NO, and altitude for the coastal boundary layer sampling near Seattle, WA. Any obvious enhancement of HCl was not detected even in the high NOx environment. (see text for more detail).

4.2.3 The Mid Troposphere (4 – 8 km)

Figure 4.6 presents the correlation between O_3 and HCl in the mid-troposphere (4 – 8 km). Although HCl levels in the mid-troposphere were usually low (< 2 pptv 55%, and <15 pptv 90%), significant levels of HCl were observed that were associated with stratospheric influence and had a similar ratio of O_3 to HCl at higher altitudes (~ 7.5 km). However, Figure 4.7 also shows that HCl enhancements (more than 20 pptv) can be observed with no stratospheric influence (i.e. no enhancement in O_3 and incompatible back trajectories). To investigate the origin of the non-stratospheric HCl in the mid troposphere we examined two aircraft spirals in similar geographical locations with contrasting HCl. These profiles are shown in Figure 4.7 with spiral 1 having undetectable HCl and spiral 2 with significant HCl in the mid troposphere.

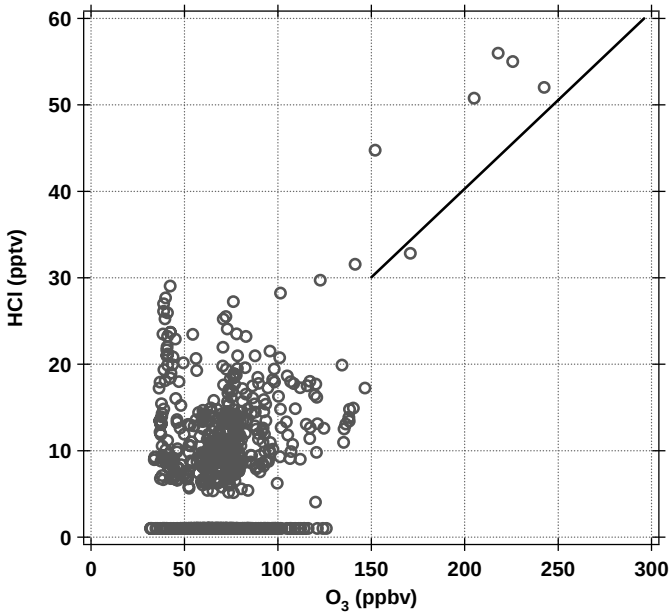

Figure 4.6 The correlation of HCl with O_3 in the mid troposphere (4-8km). The line represents the HCl-O_3 regression line of the stratosphere in Figure 4.3.

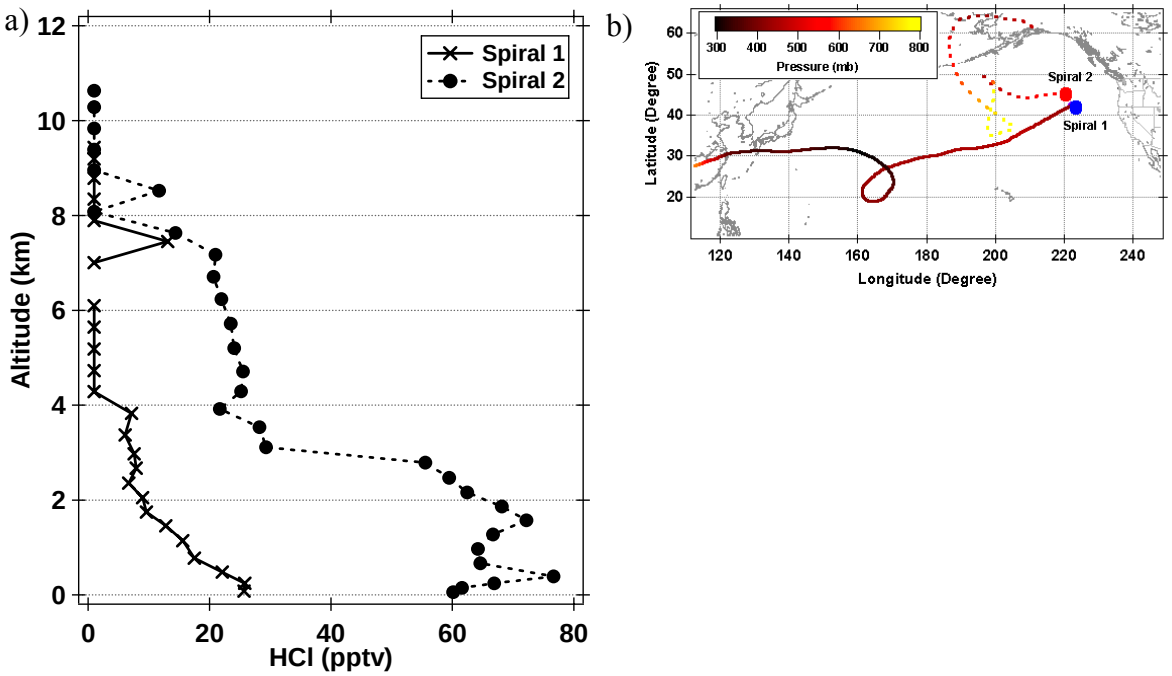

Figure 4.7 a) HCl profiles, measured two different spiral samplings. b) Sampling sites of spiral samplings and 7day back trajectories

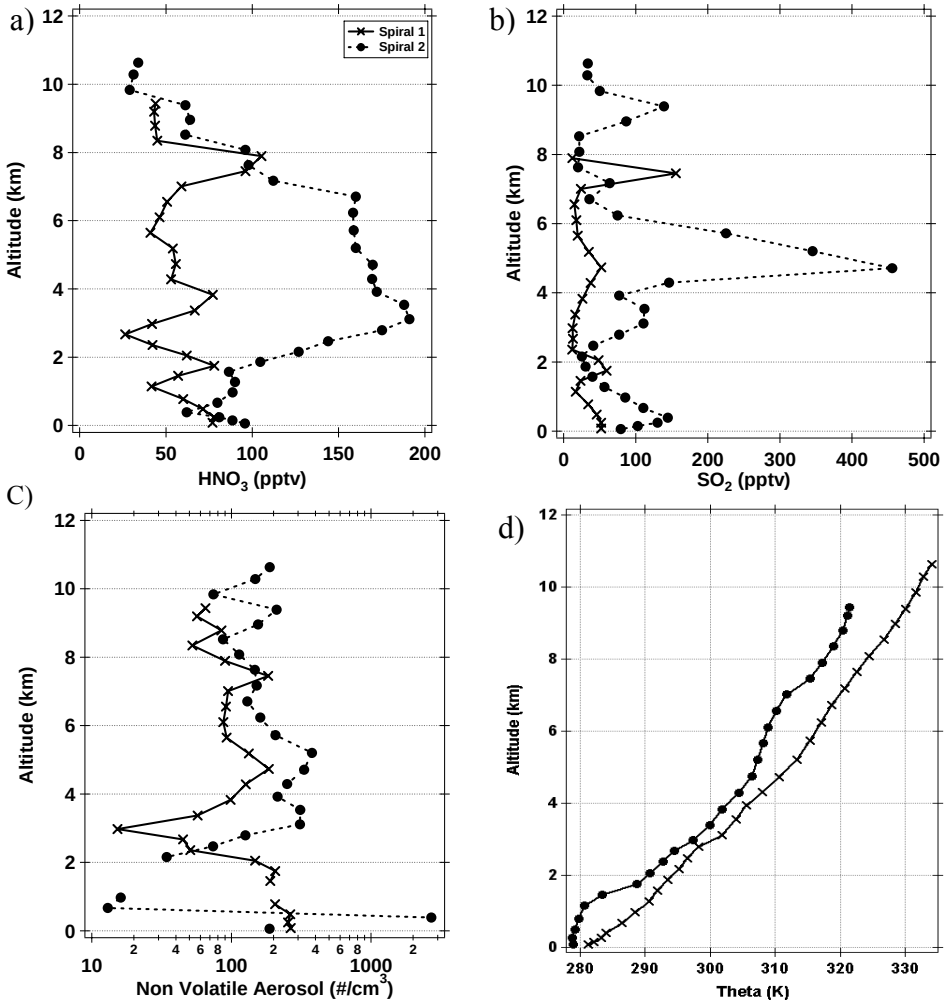

Figure 4.8 Profiles of a) HNO_3, b) SO_2, and c) non volatile aerosols d) potential temperature. Consistently, the mid troposphere of spiral 2 depicts enhanced pollutions.

The transport of HCl to the mid troposphere from the MBL could explain the enhancement in spiral 2. However, backtrajectory analyses show that this air mass had resided in the mid troposphere for ~5 days without any influence from either the stratosphere or the MBL. Moreover, chemical tracers such as O_3 for the stratosphere, and CH_3I and CH_3NO_3 for the MBL were not enhanced in the mid troposphere during spiral 2. In addition, the potential temperature profile (Figure 4.8 d) suggests that the mid troposphere of spiral 2 is stratified. In fact they are very similar levels to that observed in the non-enhanced spiral 1. Consequently, we are skeptical that the HCl in the mid-troposphere has a recent MBL origin. However, there is evidence for enhanced levels of non-volatile aerosol in spiral 2 as shown in Figure 4.8. The optical properties of the nonvolatile aerosol (the ratio of refractory aerosols to total aerosols and the aerosol depolarization) indicate that is primarily dust of Asian origin. There is evidence from recent field studies that dust particles can absorb significant amounts of chlorine when passing through the MBL [Sullivan et al., 2007; Ooki and Uematsu, 2005; Zhang and Iwasaka, 2001]. This dust could undergo dechlorination later by exposure to strong acids such as nitric and sulfuric. High levels of HNO_3 and SO_2 are observed in spiral two that are consistent with the air mass having been in contact with urban areas such as Shanghai, China as indicated by a 7-day back trajectory analysis in Figure 4.7 b). For these reasons, we speculate that the mid-tropospheric HCl in this case is produced by dechlorination of dust particles activated by anthropogenic pollution. It is doubtful if this mechanism is a large source of HCl to the atmosphere. However, this mechanism should be recognized as a potential interference to using HCl as a stratospheric tracer in free

troposphere. In addition, the production of HCl from dust particles provides a mechanism to transform the chemical composition of the aerosol.

4.3 Summary

Airborne measurements of HCl during the Anchorage deployment of the INTEX-B field mission provide a unique dataset from the MBL to the lower stratosphere over the North Pacific Ocean. In the upper troposphere (z >8km), HCl serves as a good tracer for recent stratospheric influence due to its very low background concentration (less than 2 pptv). A simple analysis using the HCl/O_3 correlation illustrates that ~ 50% of the air above 8 km (up to 12 km) was either stratospheric air (~ 30%) or recent stratospheric influenced air (~ 15%). The RAQMS model systematically overestimated the HCl/O_3 correlation by 50%. In addition, the model underestimated measured HCl ~30% in high HCl range (HCl > 60 pptv) although both measured and model predicted HCl show a strong correlation ($R^2 = 0.72$) in the upper troposphere.

In the remote MBL HCl levels were consistently above 20 pptv (up to 400 pptv).and strongly correlated with HNO_3. This is consistent with dechlorination of seasalt aerosols by gas phase acids as the major source of HCl in the MBL. One sampling leg (~ 15 minutes) in a polluted coastal boundary layer (south of Seattle, WA) did not show significant enhancements of HCl relative to the remote MBL which is in contrast with other studies. The background level of HCl in the MBL was used to estimate average Cl atom number density of 3×10^3 atoms/cm^3, which is consistent with the lower range of previous studies.

In the mid troposphere (4-8 km), HCl was almost always below our detection limit of 2 pptv, which is consistent with recent in situ measurement of HCl in the upper troposphere by Marcy et al. [2004] However, on a few occasions HCl associated with enhanced O_3, was detected due to recent stratospheric influences. In addition, enhanced HCl not of stratospheric origin was detected in the in the mid troposphere. This HCl appears to have been produced by dechlorination of Asian dust aerosols.

The measured HCl profiles in this work indicate that above the MBL that background tropospheric levels of HCl are very low (< 2pptv). This is consistent with the findings of Marcy et al. [2004] but is inconsistent with the profile of Keene et al. [1999]. However, profiles obtained in this study are over a limited geographic region (Northern Pacific Ocean) which may be a reason for the disagreement with the work of Keene et al. [1999]. Consequently, observations by the method presented in this paper over a wider geographic range would be useful to sort out this difference.

4.4 References

Al-Saadi, J. A., R. B. Pierce, T. D. Fairlie, M. M. Kleb, R. S. Eckman, W. L. Grose, M. Natarajan, and J. R. Olson: Response of middle atmosphere chemistry and dynamics to volcanically elevated sulfate aerosol: Theree-dimensional coupled model simulation, Journal of Geophysical Research, 106, 27255-27275,2001.

Arsene, C., A. Bougiatioti, M. Kanakidou, B. Bonsang, N. Mihalopoulos: Tropical OH and Cl levels deduced from non-methane hydrocarbon measurements in a marine site, Atmospheric Chemistry and Physics, 7, 4661-4673, 2007.

Behnke, W., C. George, V. Scheer, and C. Zetzsch: Production and decay of $ClNO_2$ from the reaction of gaseous N_2O_5 with NaCl solution: Bulk and aerosol experiments, Journal of Geophysical Research, 102(D3), 3795-3804,1997.

Chang, S., E. C. McDonald-Buller, Y. Kimura, G. Yarwood, J. D. Neece, M. Russell, P. Tanaka, and D. Allen: Sensitivity of urban ozone formation to chlorine emission estimates, Atmospheric Environment, 36, 4991-5003,2002.

Dibb, J. E., R. W. Talbot, E. Scheuer, G. Seid, and L. DeBell: Stratospheric influence on the northern North American free troposphere during TOPSE: ^{7}Be as a stratospheric tracer, Journal of Geophysical Research, 108(D4), 8368,doi:8310.1029/2001JD001347,2003.

Davis, D., G. Chen, A. Bandy, D. Thornton, F. Eisele, L. Mauldin, D. Tanner, D. Lesnschow, H. Fuelberg, B. Huebert, J. Heath, A. Clarke, and D. Blake: Dimethyl sulfide oxidation in the equatorial Pacific: Comparison of model simulations with field observations for DMS, SO_2, H_2SO_4(g), MSA(g), and NSS, Journal of Geophysical Research, 104(D5), 5765-5784,1999.

Eckman, R. S., W. L. Grose, R. E. Turner, W. T. Blackshear, J. M. Russell III, L. Froidevaux, J. W. Waters, J. B. Kumer, and A. E. Roche: Stratospheric trace constituents simulated by a three-dimensional general circulation model, Journal of Geophysical Research, 100, 13951-13966,1995.

Erickson, E.: The yearly circulation of chloride and sulfur in nature; meteorological, geochemical and pedological implications, Part I., Tellus, 11, 375-403,1959.

Erickson, E.: The yearly circulation of chloride and sulfur in nature; meteorological, geochemical and pedological implications, Part II., Tellus, 12, 63-109,1959.

Finlayson-Pitts, B. J.: The tropospheric of sea salt; A molecular-level view of the chemistry of NaCl and NaBr, Chemistry Review, 103, 4801-4822,2003.

Finley, B., and E. Saltzman: Measurement of Cl_2 in coastal urban air, Geophysical Research Letters, 33, L11809,doi:11810.11029/12006GL025799,2006.

Friedlander, S. K.: Chemical element balances and identification of air pollution sources, Environmental Science and Technology, 7(3), 235-240,1973.

Graedel, T. E., D. T. Hawkins, and L. D. Claxton: Atmospheric chemical compounds: sources, occurences, and bioassay, 732 pp., Academic, San Diego, CA,1986.

Graedel, T. E., and W. C. Keene: Tropospheric budget of reactive chlorine, Global Biogeochemical Cycles, 9(1), 47-77,1995.

Hanson, D. R., and A. R. Ravishankara: The reaction probabilities of $CONO_2$ and N_2O_5 on 40 to 75% sulfuric acid solutions, Journal of Geophysical Research, 96, 17307-17314,1991.

Hanson, D. R., and A. R. Ravishankara: Reaction of $CLONO_2$ with HCl on NAT, NAD, and frozen sulfuric acid and hydrolysis of N_2O_5 and $ClONO_2$ on frozen sulfuric acid, Journal of Geophysical Research, 98, 22931 - 22936,1993.

Hanson, D. R., and A. R. Ravishankara: Reactive uptake of $ClONO_2$ onto sulfuric acid due to reaction with HCl and H_2O, Journal of Physical Chemistry, 98, 5728-5735,1994.

Hanson, D. R., A. R. Ravishankara, and S. Solomon: Heterogeneos reactions in sulfuric acid aerosols: A framework for model calculations, Journal of Geophysical Research, 99, 3615-3629,1994.

Jobson, B. T., D. Parrish, P. Goldan, W. Kuster, F. C. Feshenfeld, D. R. Blake, N. J. Blake, and H. Niki: Spatial and temporal variability of nonmethane hydrocarbon mixing ratios and their relation to photochemical lifetime, Journal of Geophysical Research, 103, 13557-13567,1998.

Keene, W. C., M. Aslam, K. Khalil, D. J. Erickson, A. McCulloch, T. E. Graedel, J. M. Lobert, M. L. Aucott, S. L. Gong, D. B. Harper, G. Kleiman, P. Midgley, R. M. Moore, C. Seuzaret, W. T. Sturges, C. M. Benkovitz, V. Koropalov, L. A. Barrie, and Y. F. Li: Composite global emissions of reactive chlorine from anthropogenic and natural resorces; Reactive Chlorine Emissions Inventory, Journal of Geophysical Research, 104(D7), 8429-8440,1999.

Keene, W. C., J. Stutz, A. P. Pszenny, J. R. Maben, E. V. Fischer, A. M. Smith, R. von Glasow, S. Pechtl, B. C. Sive, and R. K. Varner: Inorganic chlorine and bromine in coastal New England air during summer, Journal of Geophysical Research, 112(D10S12), doi:10.1029/2006JD007689,2004.

Kerminen, V.-M., K. Teinila, R. Hillamo, and T. Pakkanen: Substitution of chloride in sea-salt paticles by inorganic and organic anions, Journal of Aerosol Science, 29(8), 929-942,1998.

Knipping, E. M., and D. Dabdub: Modeling Cl_2 formation from aqueous NaCl particles: evidence for interfacial reactions and importance of Cl_2 decomposition in alkaline solution, Journal of Geophysical Research, 107, 4360,doi:4310.1029/2001JD000867,2002.

Lelieveld, J., A. Bregman, H. A. Scheeren, J. Strom, K. S. Carslaw, H. Fischer, P. C. Siegmund, and F. Arnold: Chlorine activation and ozone destruction in the northern lowermost stratosphere, Journal of Geophysical Research, 104(D7), 8201-8212,1999.

Lin, C. L., M. T. Leu, and W. B. DeMore: Rate constant for the reaction of atomic chlorine with methane, The Journal of Physical Chemistry, 82(16), 1772-1777,1978.

Marcy, T. P., D. W. Fahey, R. S. Gao, P. J. Popp, E. C. Richard, T. L. Thompson, K. H.

Rossenlof, E. A. Ray, R. J. Salawitch, C. S. Atherton, D. J. Bergmann, B. A. Ridley, A. J. Weinheimer, M. Loewenstein, E. M. Weinstock, and M. J. Mahoney: Quantifying stratospheric ozone in the upper troposphere with in situ measurements of HCl, Science, 304(5668), 261-265,2004.

Molina, M. J., and F. S. Rowland: Stratospheric sink for chlorofluoromethanes:Chlorine-atom catalysed destruction of ozone, Nature, 249, 810-812,1974.

Molina, M. J.: Role of chlorine in stratospheric chemistry, Pure and Applied Chemistry, 68(9), 1749-1756,1996.

Nassar, R., P. F. Bernath, C. D. Boone, C. Clerbaux, P. F. Coheur, G. Dufour, L. Froidevaux, E. Hahieu, J. C. McConnell, S. D. McLeod, D. P. Murtagh, C. P. Rinsland, K. Semeniuk, R. Skelton, K. A. Walker, and R. Zander: A global inventory of stratospheric chlorine in 2004 based on measurements by the Atmospheric Chemistry Experiment Fourier Transform Spectrometer (ACD-FTS), Journal of Geophysical Research, 111(D22312), doi:10.1029/2006JD007395,2006.

Ooki, A., and M. Uematsu: Chemical interactions between mineral dust particles and acid gases during Asian dust events, Journal of Geophysical Research, 110(D03201), doi:10.1029/2004JD004737,2005.

Pierce, R. B., J. A. Al-Saadi, R. S. Eckman, T. D. Fairlie, W. L. Grose, M. M. Kleb, M. Natarajan, and J. R. Olson: Dynamic climatology of the NASA Langley Research Center Interactive Modeling Project for Atmospheric Chemistry and Transport (IMPACT) model, Journal of Geophysical Research, 105(D23), 29109-29134,2000.

Pierce, R. B., J. A. Al-Saadi, T. Schaack, A. Lenzen, T. Zapotocny, D. G. Johnson, C. Kittaka, M. Buker, M. H. Hitchman, G. Tripoli, T. D. Fairlie, J. R. Olson, M. Natarajan, J. Crawford, J. Fishman, M. Avery, E. Browell, J. Creilson, Y. Kondo, and S. T. Sandholm: Regional Air Quality Modeling System (RAQMS) predictions of the tropospheric ozone budget over east Asia, Journal of Geophysical Research, 108(D21), 8825, doi:8810.1029/2002JD003176,2003.

Pszenny, A. A. P., J. Moldanova, W. C. Keene, R. Sander, J. R. Maben, M. Martinez, P. J. Crutzen, D. Perner, and R. G. Prinn: Halogen cycling and aerosol pH in the Hawaiian marine boundary layer, Atmospheric Chemistry and Physics, 4, 147-168,2004.

Rossi, M. J.: Heterogeneous reactions on salts, Chemistry Review, 103, 4823-4882,2003.

Rudolph, J., R. Koppmann, and C. Plass-Dulmer: The budget of ethane and tetrachloroethene: Is there evidence for an impact of reactions with chlorine atoms in the troposphere?, Atmospheric Environment, 30, 1887-1894,1996.

Rudolph, J., B. Ramacher, C. Plass-Dulmer, K.-P. Muller, and R. Koppmann: The indirect determination of chlorine atom concentration in the troposhere from changes in the patterns of non-methane hydrocarbons, Tellus, 49B, 592-601,1997.

Russell III, J. M., L. E. Deaver, M. Luo, J. H. Park, L. L. Gordley, A. F. Tuck, G. C. Toon, M. R. Gunson, W. A. Traub, D. G. Johnson, K. W. Jucks, D. G. Murcray, R. Zander, I. G. Nolt, and C. R. Webster: Validation of hydrogen chloride measurements made by the Halogen Occultation Experiment from the UARS platform, Journal of

Geophysical Research, 101(D6), 10151-10162,1996.

Sander, S. P., R. R. Friedl, A. R. Ravishankara, D. M. Golden, C. E. Kolb, M. J. Kurylo, M. J. Molina, G. K. Mootgat, B. J. Finlayson-Pitts, P. H. Wine, R. E. Huie, and V. L. Orkin (2006), Chemical kinetics and photochemical data for use in atmospheric studies,Evaluation Number 15, JPL Publication 06-2.

Schweitzer, F., P. Mirabel, and C. George: Multiphase chemistry of N_2O_5, $ClNO_2$ and $BrNO_2$, Journal of Physical Chemistry A, 102, 3942-3952,1998.

Singh, H. B., G. L. Gregory, B. Anderson, E. Browell, G. W. Sachse, D. D. Davis, J. Crawford, J. D. Bradshaw, R. Talbot, D. R. Blake, D. Thornton, R. Newell, and J. Merrill: Low ozone in the marine boundary layer of the tropical pacific ocean;Photochemical loss, chlorine atoms, and entrainment, Journal of Geophysical Research, 101, 1907-1914,1996.

Singh, H. B., A. N. Thakur, Y. E. Chen, and M. Kanakidou: Tetrachloroethylene as an indicator of low Cl atom concentrations in the troposphere, Geophysical Research Letters, 23, 1529-1532,1996.

Spicer, C. W., E. G. Chapman, B. J. Finlayson-Pitts, R. A. Plastridege, J. M. Hubbe, and J. D. Fast: Unexpected high concentrations of molecular chlorine in coastal air, Nature, 394, 353-356,1998.

Sullivan, R. C., S. A. Guazzotti, D. A. Sodeman, and K. A. Prather: Direct observations of the atmospheric processing of Asian mineral dust, Atmospheric Chemistry and Physics, 7, 1213-1236,2007.

Tanaka, P. L., D. D. Riemer, S. Chang, G. Yarwood, E. C. McDonald-Buller, E. C. Apel, J. J. Orlando, P. J. Silva, J. L. Jimenez, M. R. Canagaratna, J. D. Neece, C. B. Mullins, and D. T. Allen: Direct evidence for chlorine-enhanced urban ozone formation in Houston, Texas, Atmospheric Environment, 37, 1393-1400,2003.

Tolbert, M. A., M. J. Rossi, and D. M. Golden: Heterogeneous interactions of chlorine nitrate hydrogen chloride and nitric acid with sulfuric acid surfaces at stratospheric temperatures, Geophysical Research Letters, 15, 847-850,1988.

Vierkorn-Rudolph, B., K. Bachmann, B. Schwarz, and F. X. Meixner: Vertical profiles of hydrogen chloride in the troposphere, Journal of Atmospheric Chemistry, 2, 47-63,1984.

Webster, C. R., R. D. May, L. Jaegle, H. Hu, S. P. Sander, M. R. Gunson, G. C. Toon, J. M. Russell III, R. M. Stimpfle, J. P. Koplow, R. J. Salawitch, and H. A. Michelsen: Hydrochloric acid and the chlorine budget of the lower stratosphere, Geophysical Research Letters, 21(23), 2575-2578,1994.

Wingenter, O. W., M. K. Kubo, N. J. Blake, J. Smith, T. W., D. R. Blake, and F. S. Rowland: Hydrocarbon and halocarbon measurements as photochemical and dynamical indicators of atmospheric hydroxyl, atomic chlorine, and vertical mixing obtained during Lagrangian flights, Journal of Geophysical Research, 101, 4331-4340,1996.

Wingenter, O. W., D. R. Blake, N. J. Blake, C. Sive, F. S. Rowland, E. Atlas, and F.

Flocke: Tropospheric hydroxyl and atomic chlorine concentrations, and mixing timescales determined from hydrocarbon and halocarbon measurements mad over the Southern Ocean, Journal of Geophysical Research, 104, 21819-21818,1999.

Wingenter, O. W., B. C. Sive, N. J. Blake, D.R. Blake, and F. S. Rowland: Atomic chlorine concentrations derived from ethane and hydroxyl measurements over the equatorial Pacific Ocean, Journal of Geophysical Research, 104, 21819-21828, 1999.

Zhang, D., and Y. Iwasaka: Chlorine deposition on dust particles in marine atmosphere, Geophysical Research Letters, 28(18), 3613-3616,2001.

CHAPTER 5

MEASUREMENT OF SO_2 IN THE TROPOSPHERE DURING THE INTEX CAMPAIGN

5.1 Introduction

Most of the SO_2 in the troposphere originates from anthropogenic activities (~70%) in North America, Europe, and Asia [Stern, 2005]. Efforts to reduce SO_2 emissions have led to a gradual decrease of SO_2 in Western Europe and the U.S. since the early 1990s and Asia since the late 1990s [Stern, 2005]. The decrease of global SO_2 emissions is estimated to be in the range of 13 % [Streets et al., 2006] to 23 % [Stern., 2005] from the mid 1980s to 2000. However, recent studies indicate SO_2 emissions from Asia have increased since early 2000 and are expected to increase a total of 22% from 2000 to 2020 mostly due to emissions from China [Ohara et al., 2007]

SO_2 in the troposphere is oxidized by either reaction with the OH radical or multi-phase processes to ultimately produce sulfate aerosol [Stockwell and Calvert, 1983; Wine et al., 1984; Hoffmann and Jacob, 1983; Hegg, 1985]. Sulfate aerosol has been studied intensively due to its importance for the radiation balance of the atmosphere [Haywood and Boucher, 2000]. However, due to inaccuracies and differences in model treatments of chemical and physical processes of the SO_2 oxidation processes the estimated radiative forcing from the direct effect of sulfate aerosols has a significant uncertainty (-0.4±0.2 W m^{-2}) [Forster et al., 2007].

Since the lifetime of SO_2 in the troposphere from oxidation processes is relatively short (several days for gas phase oxidation by OH to several hours for liquid phase

oxidation; Berresheim et al. [1995]), it is probable that a large fraction of the SO_2 in the polluted boundary layer would be oxidized to sulfate before transport to the free troposphere [Charlson et al., 1992]. However, a limited number of airborne measurements suggest that significant amounts of anthropogenic SO_2 can be transported to the upper troposphere by various processes [Raes et al., 2000; Thornton et al., 1999; Thornton et al., 1997a; Thornton et al., 1997b; Thornton et al., 1996]. In spite of those findings, airborne in situ measurements of SO_2, the most effective way to investigate free tropospheric distributions of SO_2, have been limited compared with other gaseous species due to technical difficulties in measuring trace level (pptv) with high temporal frequencies [Brasseur et al., 1999]. The limited airborne SO_2 measurements during NASA airborne campaigns had been mostly conducted by the GC-MS method, described by Bandy et al. [1993]. The method has a very low detection limit (~2pptv), but has a relatively long sampling frequency (~ 3min) [e.g. Thornton et al., 1999].

Free tropospheric SO_2 distributions from airborne field campaigns were used to evaluate deep convection and Asian SO_2 transport to the North Pacific [Thornton et al., 1997a, 1997b]. In addition, Shon et al.[2001] and Davis et al.[1999] also used the marine boundary layer (MBL) dataset in the tropical region from the Aerosol Characterization Experiment 1 (ACE 1) and Pacific Exploratory Missions (PEM)-Tropics A, respectively, to estimate the conversion efficiency of DMS (dimethyl sulfide) to SO_2. In the clean MBL, DMS, released by marine algae [Lovelock et al., 1972] has been established as a major natural source of SO_2 through its oxidation processes; mainly by OH during the daytime and NO_3 during the nighttime [Barnes et al., 1989; Hynes and Wine 1989; Butkovskaya and Lebras, 1994; Barone et al., 1996; Sorensen et al., 1996; Turnipseed et

al., 1996; Patroescu et al., 1999]. Although laboratory and chamber studies have been conducted to quantify the SO_2 yield from DMS oxidation processes, Berresheim et al. [1995] pointed out that there are large difficulties applying these results in the natural environment due to the difference in complexity of the laboratory and atmosphere. For this reason, in situ observations have been utilized to estimate the overall efficiency of DMS conversion to SO_2. Both studies using airborne measurements of SO_2, DMS and other relevant parameters illustrated that the "best estimated" yield of SO_2 from DMS is ~ 0.7. [Davis et al., 1999; Shon et al., 2001]

Singh et al [1997] reported concentrations of stratospheric SO_2 in the range of 30-60 pptv during the PEM-West campaign. Stratospheric SO_2 is of interest as it is the source of stratospheric sulfate aerosols, first described by Junge et al. [1961]. Volcanic plumes can directly inject a significant amount of SO_2 in the stratosphere. However, Crutzen et al [1976] and following studies have indicated that the main source of the sulfate aerosols in the stratosphere is SO_2 from the photolysis of OCS. OCS is chemically inert in the troposphere and has both natural (ocean) and anthropogenic (biomass burning) sources. An ice core study suggests that anthropogenic sources contribute around 25% of modern OCS in the atmosphere [Aydin et al., 2002]. However, Chin and Davis [1995] and 3D modeling studies [Pitari et al., 2002; Timmreck, 2001] indicate that OCS can only explain around half of the stratospheric sulfur source and deep convection of tropospheric SO_2 may be the other major source for stratospheric sulfate an important source

During the Transport and Chemical Evolution Over the Pacific (TRACE-P) field program, SO_2 was measured by the atmospheric pressure chemical ionization mass

spectrometry technique with improved time resolution (sampling frequencies > 1Hz) [Thornton et al., 2002; Tu et al., 2003; Tu et al., 2004] to facilitate studies about the long range transport and the boundary layer dynamics of SO_2. During the campaign, enhanced SO_2 layers from China were occasionally found in the low turbulent mixing and the temperature inversion layer of the Yellow Sea MBL. Since those boundary dynamics were not properly simulated in a regional scale chemical transport model (CFORS/STEM2K1), the model poorly predicted SO_2 enhanced layer over the MBL [Tu et al., 2003]. Tu et al., [2004] also found that the long-range transported Asian SO_2 in the central Pacific was found in the low water vapor and low turbulence layer of the lower free troposphere (3- 4 km) after three to four days of the transport by frontal lifting.

Some studies have conducted comparisons of chemical transport model predictions of SO_2 with airborne observations. These comparisons have shown that models reasonably describe convection features and boundary layer mixing ratios of SO_2 [Chin et al., 1996; Chin et al., 2000; Park et al., 2005]. However, some studies also suggest that model treatments of cloud-SO_2 interactions may be too simplified in the model to simulate measured results [Tu et al., 2003; Tu et al., 2004; Park et al, 2004].

This study presents in situ measurements of SO_2 by a chemical ionization mass spectrometer (CIMS), integrated on the NASA DC-8 during the INTEX field campaign. The campaign consisted of two phases INTEX-NA and INTEX-B. INTEX-NA was an intensive investigation of the North American troposphere using aircraft and satellite borne measurements as well as a suite of models [Singh et al., 2006]. The measurements were mostly conducted in the eastern U.S. and its outflow regions, where deep convection and frontal uplift was very active [Bertram et al., 2007; Fuelberg et al., 2007].

The second phase of the study, INTEX-B, was conducted in March and May 2006. During the early portion of the study (March, 2006), the NASA DC-8 was deployed in Houston to sample the far and the near field polluted outflow from Mexico City as a part of the Megacity Initiative: Local and Global Research Observations (MILAGRO). In the later portion of the study (April – May, 2006), Asian outflow was sampled from aircraft deployment in Honolulu, HI and Anchorage, AK. More detailed descriptions on the INTEX project can be found in Chapter II.

The U.S. and Asia comprise ~10% and ~25% of global emissions of SO_2, respectively [Park et al., 2004]. Although, SO_2 emissions from Mexico City are not important in terms of global budget (~1%, Barth and Church [1999]), due to its unique geographical (low latitude and high altitude) and mega city characteristics, the chemical evolution of the outflow is a good test for our current knowledge of sulfur chemistry [Molina et al., 2007]. However, airborne measurements of SO_2 in those regions have been very limited [Tu, 2004]. Therefore, our SO_2 observations in combination with the comprehensive dataset of various gas phase and aerosol parameters from the INTEX campaign provide a unique opportunity to test our ability to predict sulfur levels.

In this study, we present SO_2 data, correlations of SO_2 with other measured parameters such as CO, SO_4^{2-}, and aerosol parameters, and comparisons of observations with global 3-D modeling predictions of SO_2 from the INTEX field campaign. In particular, the following topics are explored: 1) Source region characteristics of the eastern U.S. and Mexico City, 2) Outflow characteristics of the eastern U.S., Mexico City, and Asia focused on the upper troposphere, 3) Comparisons of measured SO_2 with sulfur products of global three-dimensional models (Goddard and Earth Observing

System (GEOS)-CHEM and Model for ozone and related chemical tracers (MOZART)), 4) Case studies of sulfur chemistry in the clean MBL and the lower stratosphere.

5.2 Results and Discussion

5.2.1 Boundary Layer Distributions

Figure 5.1 presents boundary layer distributions (radar altitude < 1km) of a) SO_2 , and b) $[SO_4^{2-}]/[SO_2+SO_4^{2-}]$ (defined as the sulfate ratio) during the INTEX mission, averaged on 1×1 degree grid. The Ohio Valley and the south eastern U.S. exhibit enhanced levels of SO_2 relative to other U.S. regions in correspondence with the emission inventory from EPA (U.S. EPA 2002 National Emission Inventory, http://www.epa.gov/ttn/chief/net/).

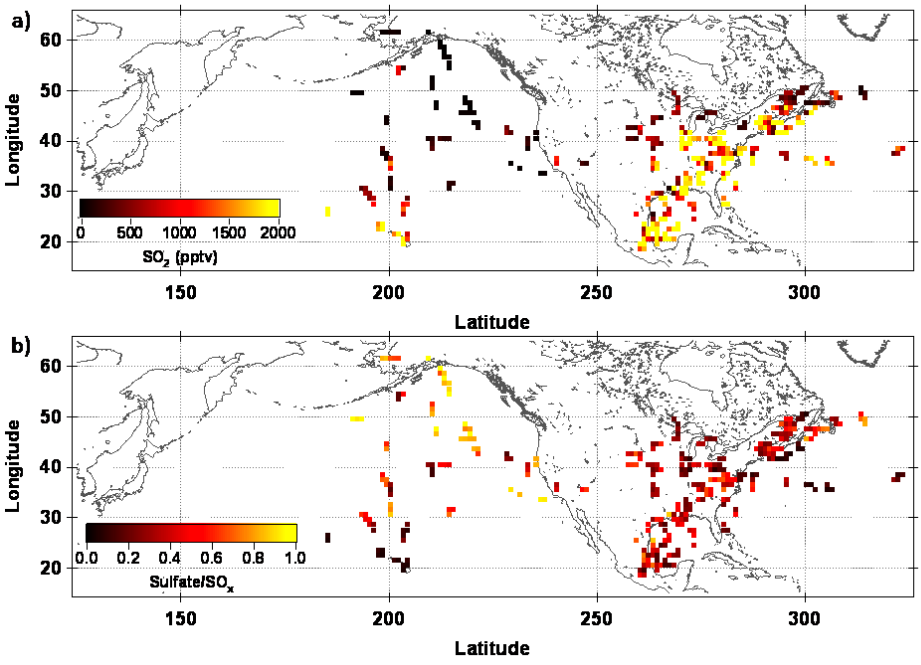

Figure 5.1 Boundary layer distributions of a) SO_2 and b) sulfate ratios ($[SO_4^{2-}]/([SO_2]+[SO_4^{2-}])$), measured during the INTEX campaign.

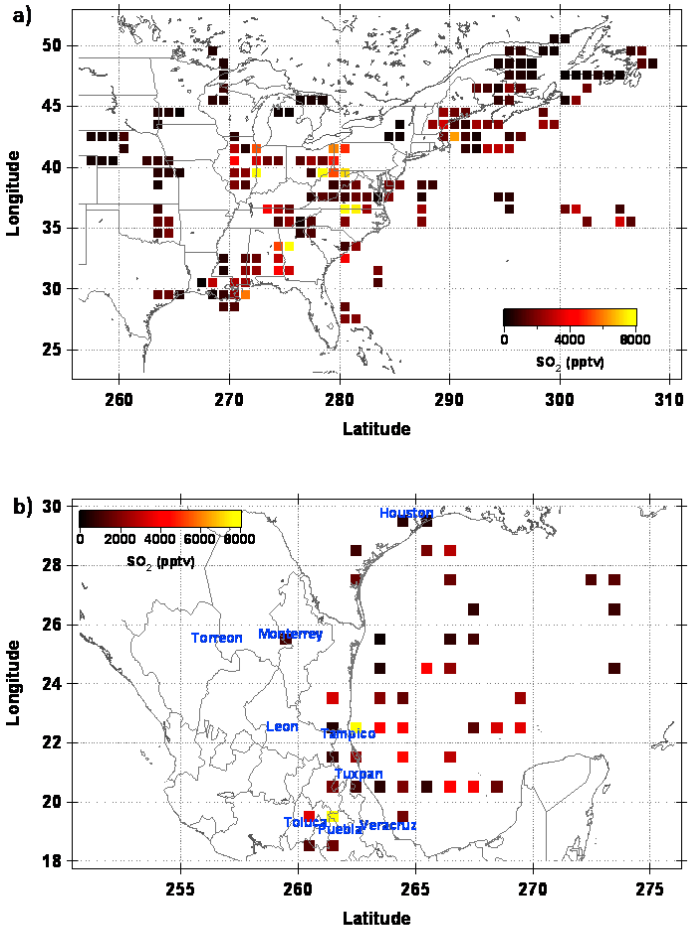

Figure 5.2 Distributions of SO_2 in the source region a) the eastern U.S. b) Mexico.

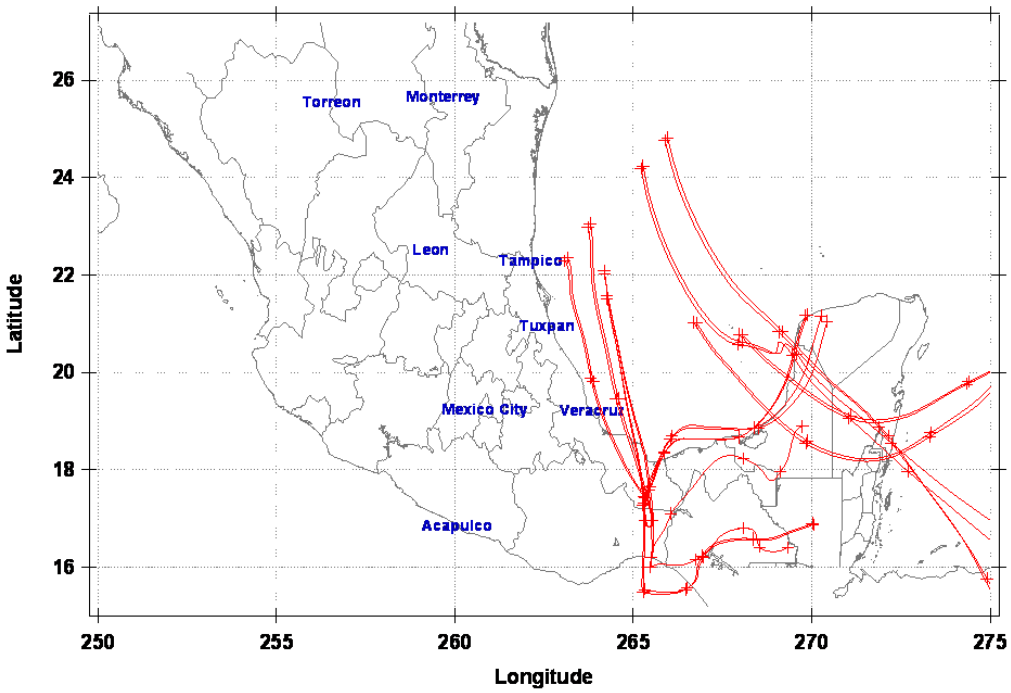

Figure 5.3 Three day back trajectories of high SO_2 plumes (SO_2 > 8 ppbv), detected in the MBL of the Gulf of Mexico.

The MBL of the Gulf of Mexico showed relatively high SO_2 (few ppbv) during the campaign (Figure 5.2b). Figure 5.3 presents three-day back trajectories of high SO_2 plumes (SO_2 > 8ppbv). The trajectories illustrate that the high SO_2 plumes originated from the boundary layer of the Yucatan Peninsula and the Veracruz area. SO_2 emissions from Veracruz due to fossil fuels have been estimated to be the highest among states in Mexico in 2002 (266,200 tons; Vijay et al., 2004). In addition, SO_2 emissions from ship traffic, estimated to be 184,700 tons/year in the EEZ (Exclusive Economic Zone) of the Gulf of Mexico [Corbett et al, at http://coast.cms.udel.edu /NorthAmericanSTEEM/ ARBCEC_SECA_task1-2ReportMay2006.pdf] are another important source in this area.

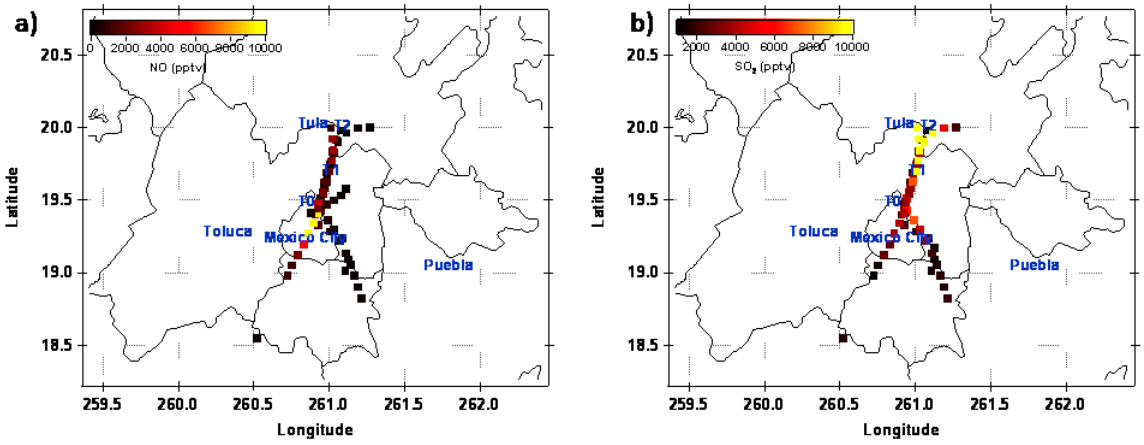

Figure 5.4 Distributions of a) NO and b) SO_2, measured during four boundary layer sampling runs in the Mexico City metropolitan area.

The SO_2 distribution in the boundary layer of the Mexico City basin appears very different from that of the NO distribution as shown in Figure 5.4. High NO is located in the center of Mexico City (Figure 5.4a). On the other hand, high SO_2 levels were found to originate from the Tula industrial complex (Figure 5.4b), which has power generation, refinery, glass manufacturing and concrete manufacturing facilities. The SO_2 emissions of Tula industrial area were estimated as 163,170 ton/year (2002; Vijay et al., 2004).

Figure 5.1 a) also depicts high SO_2 in not only the coastal region of the eastern U.S., but also in the remote Atlantic Ocean. The SO_2 levels over the Atlantic Ocean are associated with low sulfate ratios (Figure 3b), consistent with fresh emissions. This suggests that the SO_2 in the remote Atlantic originates from recent ship plumes. This is compatible with Chin et al.'s [2000] estimate that ship emissions contribute 65% of the SO_2 burden to the North Atlantic. This was echoed by Eyring et al. [2007] who suggested that high emissions from ships is the reason that global models underestimate SO_2 levels in the MBL of the North Atlantic Ocean.

High SO_2 with low sulfate ratios was also observed in the Pacific Ocean in the vicinity of the Hawaiian islands. However, back trajectories suggest that there are non-ship sources of this sulfur. One is anthropogenic sources around Oahu Island, and the other volcanic activity in the Hawaiian chains. In contrast, MBL SO_2 over the North Pacific is very low (Figure 5.1 a) and is aged with a high sulfate ratio (Figure 5.1 b). For these conditions, the dominant SO_2 source would be expected to be DMS oxidation. An analysis of SO_2 and DMS distributions in the area is presented below.

5.2.2 SO_2 Distribution in the Free Troposphere

Median profiles of SO_2 from each INTEX campaign are presented in Figure 5.5 with the 25th percentile and the 75th percentile profile. In addition Table 5.1 presents the statistics of the SO_2 vertical distribution during the INTEX campaign.

Table 5.1 Vertical distribution of observed SO2 from 1-min averaged data for a) INTEX-NA, b) INTEX-B Phase I and c) INTEX-B Phase II

a)

Altitude	Median	Mean	Max	Min	25th Percentile	75th Percentile	N
0.25	732.3	1341.6	14344.1	5.0	331.7	2060.4	399
0.75	795.1	933.8	4563.3	30.7	394.8	1401.0	121
1.25	234.1	539.9	2789.5	5.0	122.2	653.7	115
1.75	66.9	108.4	1151.7	5.0	32.7	138.6	126
2.25	44.5	78.3	1127.8	5.0	20.8	81.2	69
2.75	21.6	45.0	713.5	5.0	11.3	42.0	64
3.25	11.1	15.8	85.2	5.0	5.0	19.6	108
3.75	13.9	17.1	106.1	5.0	5.0	21.2	112
4.25	17.3	20.4	121.4	5.0	8.2	24.8	72
4.75	17.3	19.2	94.6	5.0	5.0	28.6	91
5.25	19.9	22.6	133.4	5.0	13.9	29.3	84
5.75	18.3	22.4	85.5	5.0	5.0	33.3	67
6.25	20.8	23.6	152.9	5.0	10.7	31.2	152
6.75	17.8	24.2	140.5	5.0	9.9	27.2	94
7.25	22.4	30.0	156.7	5.0	12.1	35.6	96
7.75	16.5	22.1	122.4	5.0	7.8	31.7	128
8.25	15.7	26.9	457.1	5.0	7.8	23.5	93
8.75	21.3	32.4	388.1	5.0	12.1	36.4	373
9.25	28.6	67.5	701.3	5.0	18.0	69.6	133
9.75	23.8	56.7	519.3	5.0	8.8	39.5	59
10.25	33.3	50.0	207.8	5.0	21.9	75.4	202
10.75	32.9	40.5	204.4	5.0	18.2	46.2	42
11.25	5.0	5.0	5.0	5.0	5.0	5.0	1

b)

Altitude	Median	Mean	Max	Min	25th Percentile	75th Percentile	N
0.25	2697.8	2815.1	8670.8	2.0	1172.3	4058.4	155
0.75	421.9	665.1	2541.9	2.0	191.8	928.4	34
1.25	332.4	551.0	2035.8	2.0	203.9	820.5	34
1.75	748.9	764.5	3652.5	2.0	272.0	1079.8	54
2.25	439.0	498.0	1965.7	2.0	227.8	743.8	66
2.75	315.4	583.0	2219.5	2.0	67.0	996.4	93
3.25	309.5	504.4	1609.4	2.0	123.1	759.6	68
3.75	589.6	515.7	1310.2	2.0	178.0	718.2	47
4.25	65.7	257.8	3918.3	2.0	25.9	259.4	39
4.75	2.0	187.9	3873.0	2.0	2.0	9.3	40
5.25	2.0	92.3	3538.1	2.0	2.0	2.0	46
5.75	2.0	126.8	1451.3	2.0	2.0	10.6	13
6.25	2.0	3.0	14.6	2.0	2.0	2.0	28
6.75	2.0	3.5	22.3	2.0	2.0	2.0	19
7.25	2.0	48.0	754.1	2.0	2.0	2.0	17
7.75	2.0	7.2	101.5	2.0	2.0	9.7	53
8.25	2.0	2.2	12.5	2.0	2.0	2.0	48
8.75	2.0	14.3	523.5	2.0	2.0	2.0	48
9.25	2.0	21.2	227.2	2.0	2.0	11.7	21
9.75	2.0	2.0	2.0	2.0	2.0	2.0	6
10.25	2.0	2.0	2.0	2.0	2.0	2.0	7
10.75	2.0	2.0	2.0	2.0	2.0	2.0	12
11.25	2.0	2.0	2.0	2.0	2.0	2.0	27
11.75	508.4	516.8	783.8	193.8	387.3	692.8	14

c)

Altitude	Median	Mean	Max	Min	25th Percentile	75th Percentile	N
0.25	105.4	441.0	5468.4	2.0	33.5	502.4	473
0.75	49.9	152.1	1779.1	2.0	18.5	110.5	71
1.25	43.3	82.7	728.3	2.0	2.0	86.6	70
1.75	2.0	47.6	512.8	2.0	2.0	57.3	132
2.25	22.4	71.0	3485.4	2.0	2.0	45.1	172
2.75	11.9	69.8	2091.8	2.0	2.0	34.6	93
3.25	29.5	114.6	731.2	2.0	2.0	150.1	135
3.75	23.4	52.6	310.7	2.0	2.0	84.4	122
4.25	11.0	27.4	851.4	2.0	2.0	29.8	141
4.75	16.6	45.0	658.9	2.0	2.0	61.6	256
5.25	8.9	27.2	570.8	2.0	2.0	23.7	207
5.75	2.0	40.4	458.5	2.0	2.0	34.7	127
6.25	13.7	22.0	310.2	2.0	2.0	29.8	241
6.75	11.8	32.0	326.9	2.0	2.0	39.9	120
7.25	20.5	46.2	402.5	2.0	2.0	71.8	117
7.75	2.0	20.1	235.1	2.0	2.0	23.9	237
8.25	9.7	25.8	319.7	2.0	2.0	21.8	129
8.75	14.3	17.2	132.4	2.0	2.0	22.9	192
9.25	10.0	19.1	602.4	2.0	2.0	19.9	201
9.75	2.0	17.6	1077.6	2.0	2.0	15.6	179
10.25	21.2	64.0	1499.4	2.0	11.3	47.7	405
10.75	2.0	27.1	383.3	2.0	2.0	16.8	332
11.25	9.2	30.0	306.5	2.0	2.0	47.4	129
11.75	2.0	5.9	36.7	2.0	2.0	7.8	65

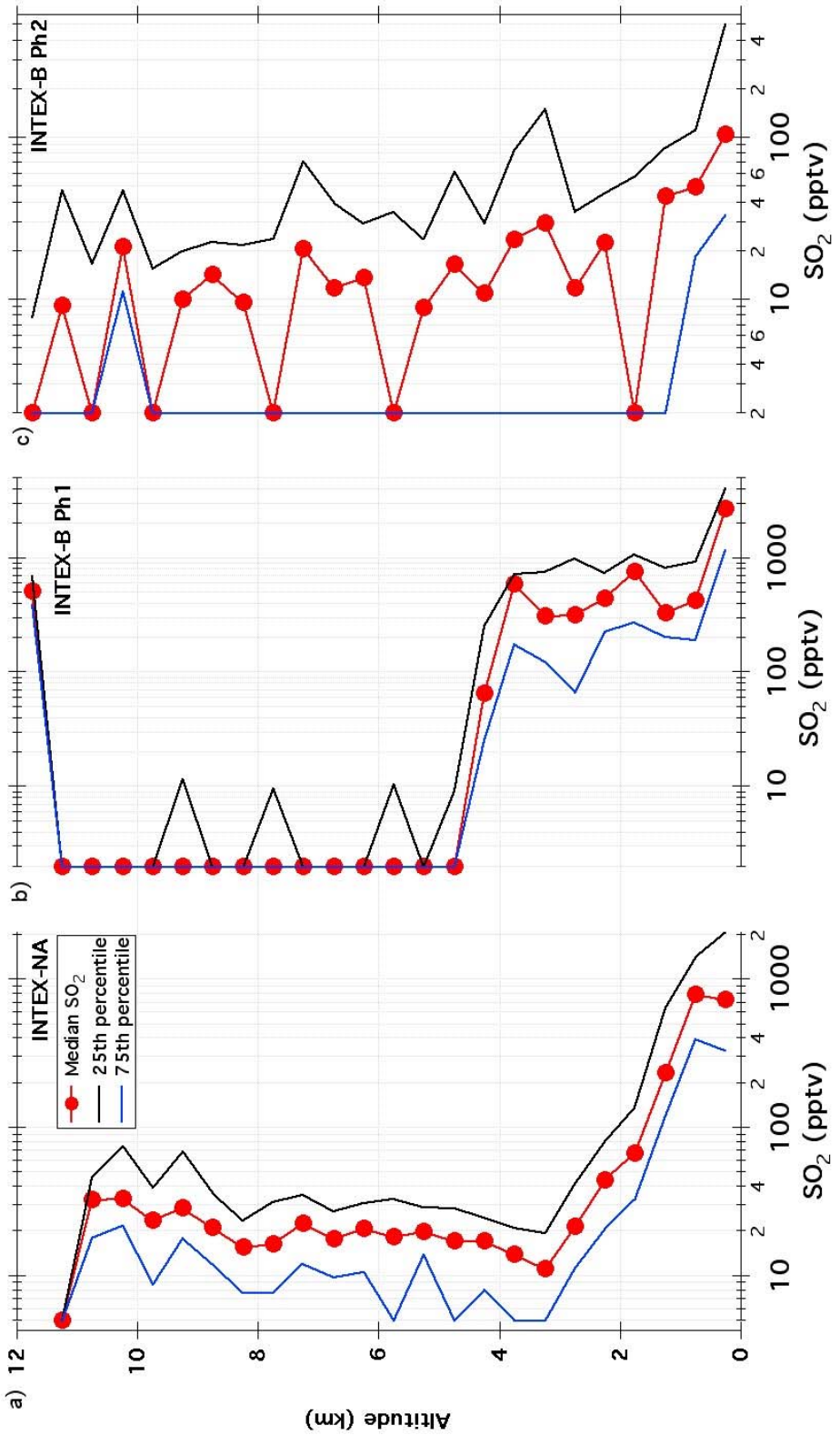

Figure 5.5 A median, a 25th percentile, and a 75th percentile profile of SO_2, measured during a) INTEX-NA, b) INTEX-B Phase I, and c) INTEX-B Phase II

5.2.2.1 The Atlantic Ocean Outflow Region – INTEX-NA

Figure 5.6 illustrates the vertical distributions of median levels of SO_2, SO_4^{2-} and the sulfate ratio in the outflow region of the eastern U.S. SO_2 in the free troposphere is consistently over a few tens of pptv up to 11km. This enhanced SO_2 throughout the free troposphere reflects active deep convection and frontal uplift events during the INTEX-NA field campaign [Bertram et al., 2007, Fuelberg et al., 2007]. The sulfate ratio profile is lower in the upper troposphere (8-12 km) than in the mid troposphere (4-8 km), which suggests that the direct injection from the boundary layer to the upper troposphere was prevalent during the INTEX-NA period.

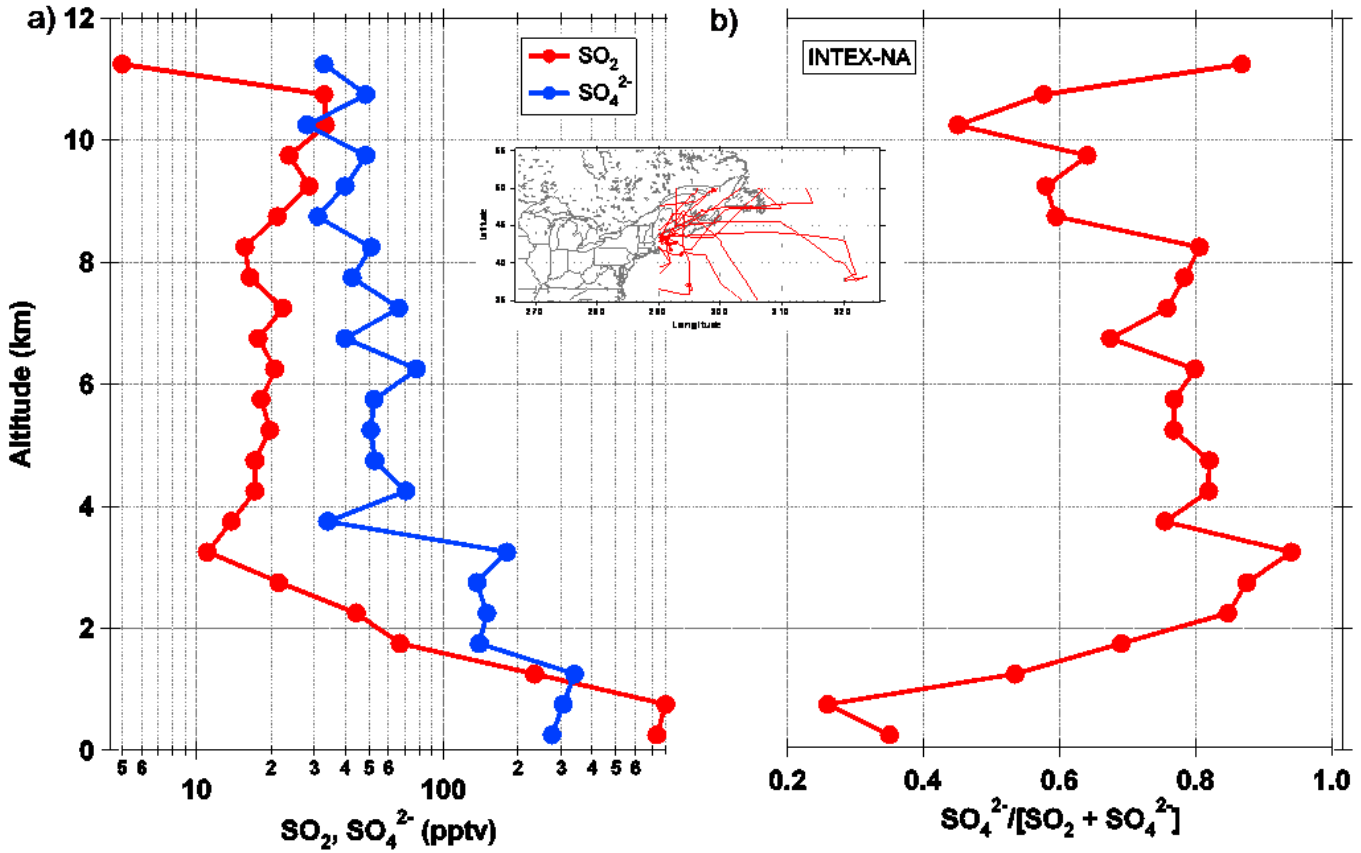

Figure 5.6 Median profiles of a) SO_2 ,SO_4^{2-}, and sulfate ratios, measured during the INTEX-NA campaign. Profiles are retrieved from the dataset of the north Atlantic region, considered as the outflow region of the eastern U.S. as shown in a subset map in the figure.

Figure 5.7a presents the correlation of SO_2 with CO. Except for biomass burning plumes, which where detected frequently during INTEX-NA low SO_2 and high CO [Singh et al., 2006], a reasonable positive correlation is found, which suggests anthropogenic origins of SO_2 in the upper troposphere [Raes et al., 2000]. Figure 8b presents a correlation between SO_2 and ultrafine aerosol (<0.01 μm) number density, which is a good indicator for deep convection [Raes et al., 2000]. Indeed, we can clearly identify two different deep convection plumes with different slopes. In contrast, poor correlation is found between ultrafine aerosols and SO_2 transported by frontal uplift.

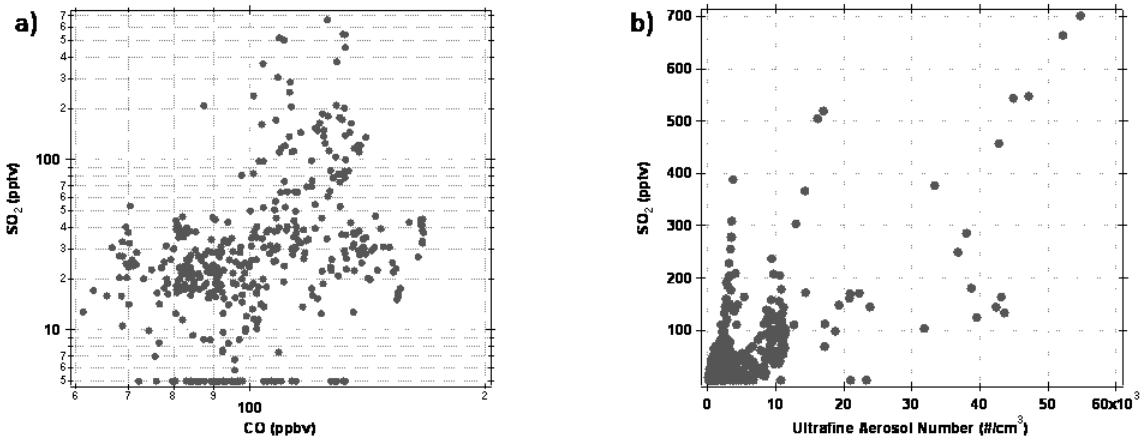

Figure 5.7 Correlation plots of SO_2 with a) CO and b) ultrafine aerosols in the upper troposphere during the INTEX-NA field campaign.

5.2.2.2 The Gulf of Mexico-INTEX-B Phase I

Figure 5.8 shows median vertical profiles of SO_2, SO_4^{2-}, and the sulfate ratio from the Gulf of Mexico. Flight tracks illustrating where data were collected are also presented in the Figure 5.8. The profiles show contrasts below and above 4km. Below 4 km, high SO_2 and relatively low sulfate ratios were detected. Conversely, above 4km, SO_2 was mostly below detection limit (2pptv) and sulfate ratios were close to 1, indicating complete aging of the sulfur.

As illustrated in Figure 5.3, high SO_2 in the MBL of the Gulf of Mexico came from the boundary layer of the Yucatan peninsula and the Veracruz region due to the counter clockwise flows driven by a prevalent high pressure system in the Gulf of Mexico. The three-day back trajectory results (Figure 5.9) for high SO_2 plumes (> 1ppbv) that DC-8 encountered over the Gulf of Mexico buffer region (1 km < z < 4 km) illustrate that those plumes are originated from inland of Mexico and transported with little vertical motion. The forward trajectories of those plumes depict that the high SO_2 air masses in the Gulf of Mexico are mostly transported into the mid troposphere of the eastern U.S. and North Atlantic.

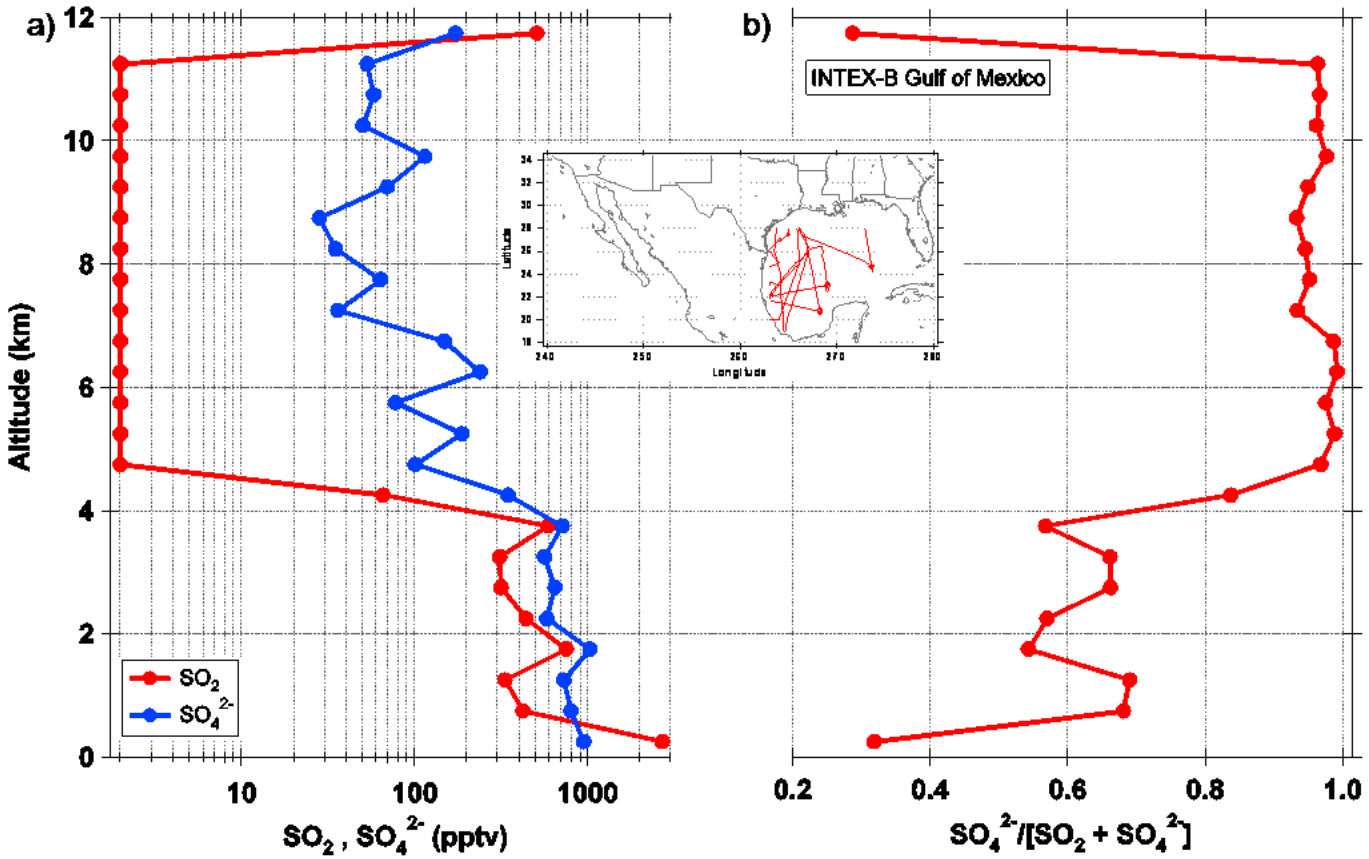

Figure 5.8 Median profiles of a) SO_2 ,SO_4^{2-}, and sulfate ratios, measured during the INTEX-B Phase I campaign. Profiles are retrieved from the dataset of the Gulf of Mexico region, considered as the outflow region of Mexico.

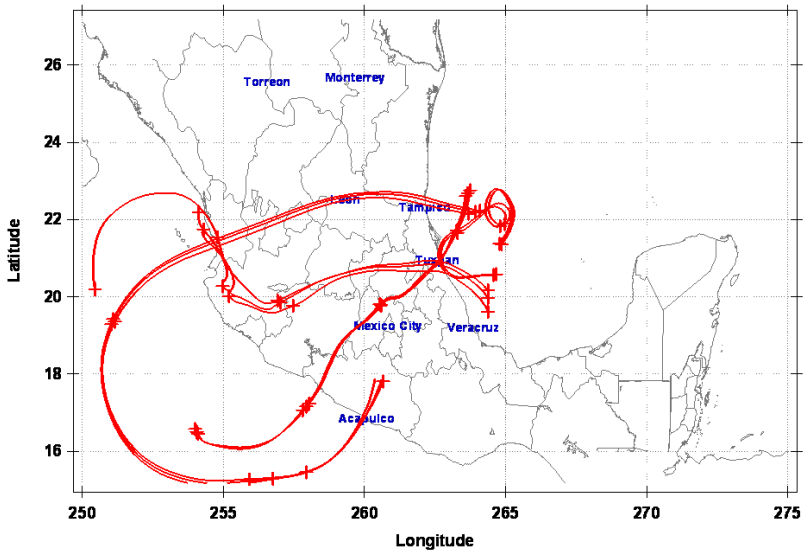

Figure 5.9 Three day back trajectories for high SO_2 plumes (> 1ppbv), sampled in 1-4 km altitude of the Gulf of Mexico.

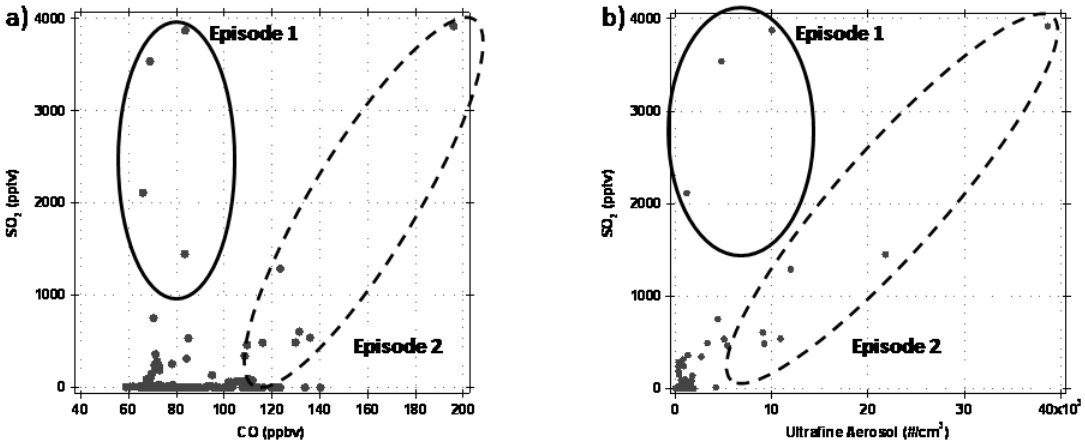

Figure 5.10 Correlation plots of SO_2 with a) CO and b) ultrafine aerosols in the mid troposphere (4-8 km) during the INTEX-B Phase I field campaign. Episode 1 (solid circle) indicates a plume, appeared to be transported from volcano and Episode 2 (dotted circle) represents a polluted origin plume.

Although SO_2 in the mid and the upper troposphere ($z > 4$ km) over the Gulf of Mexico was the under detection limit most of the time, sporadically, high SO_2 plumes were detected. Figures 5.10a and 5.10b show correlations of SO_2 with CO and ultrafine aerosols in the mid troposphere ($4km < z < 8km$) for two high SO_2 episodes with contrasting correlations. One (episode 1), associated with high CO and high ultra fine aerosol counts, and appears to be polluted deep convection plume. However, the other high SO_2 plume (episode 2) does not correlate with ultrafine aerosol counts and CO is in within its background range (60 – 80 ppbv). According to a back trajectory analysis, the plume had passed near the Popocatépetl volcano (19.0 N, 98.6 W) about one day before and was transported at the same pressure level as the top of the volcano (5452 m ASL) and sampling altitude (the pressure altitude of ~ 5km).

5.2.2.3 Asian Outflow-INTEX-B Phase II

Figure 5.11 presents vertical profiles of median SO_2, SO_4^{2-}, and the sulfate ratio for the flights in the North Pacific whose flight tracks are illustrated in the inset. Layers of enhanced SO_2 due to transport of Asian pollution were often found on low background levels. These layers were characterized by high sulfate ratios compared with those observed in convective outflow layers observed in INTEX-NA. This is consistent with longer transport times from Asia relative to the relatively fresh plumes observed in the North American study.

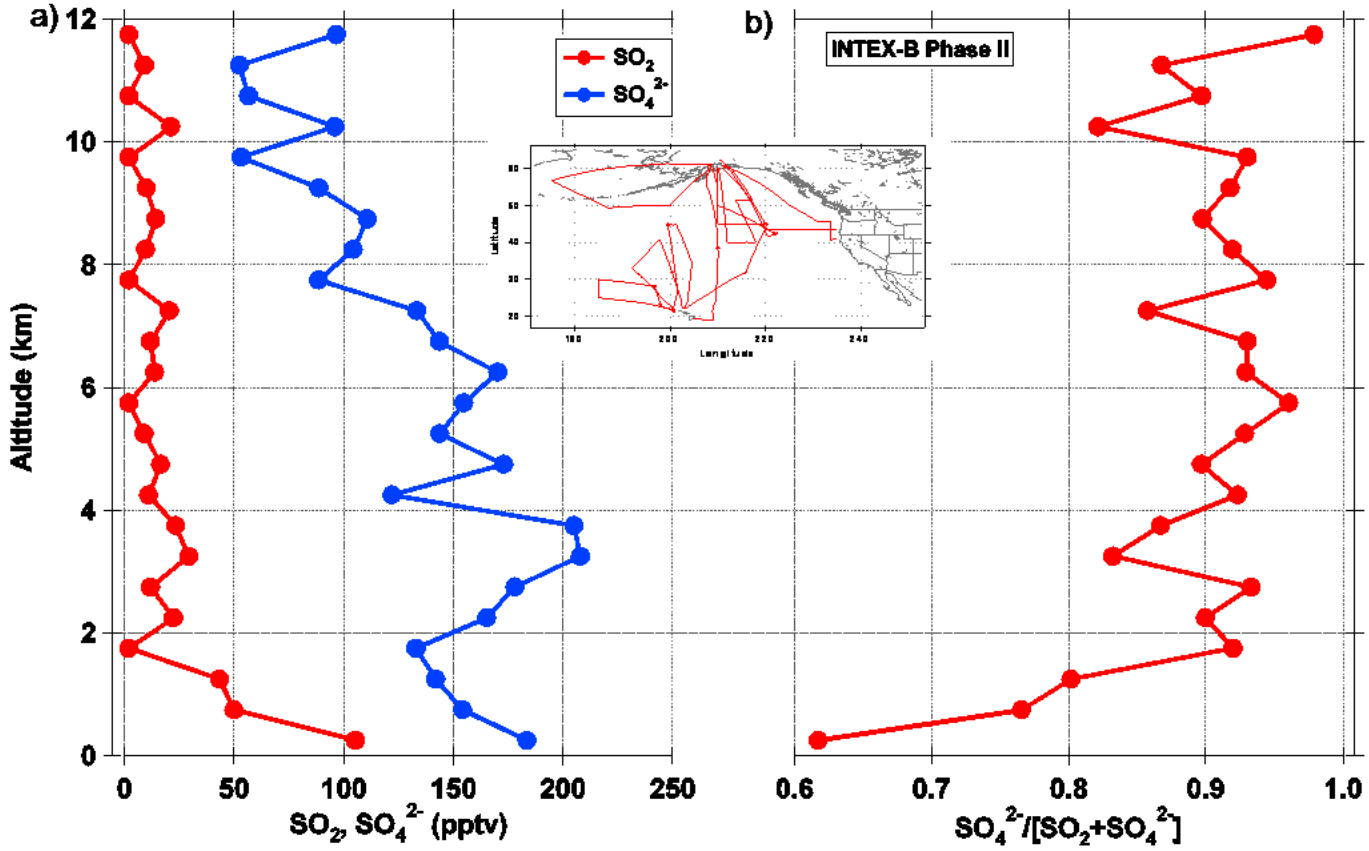

Figure 5.11 Median profiles of a) SO_2 ,SO_4^{2-}, and sulfate ratios, measured during the INTEX-B Phase II campaign. Profiles are retrieved from the dataset of the north Pacific region, considered as the outflow region of Asia.

Since the SO_2 median profile in Figure 5.11 is gathered over a wide latitude range (20^o N to 70^o N), the median profiles of SO_2 in four different latitude bins are presented in Figure 5.12. These profiles illustrate that the higher latitude free troposphere was the main SO_2 transport pathway. At high latitudes (> N 50^o), significant SO_2 enhancements (a few tens of pptv) were observed throughout the mid and upper troposphere. This pattern corresponds with a prior study [Tu et al., 2004], which found that the prevailing pathway for Asian SO_2 transport was from 50^oN to 60^oN.

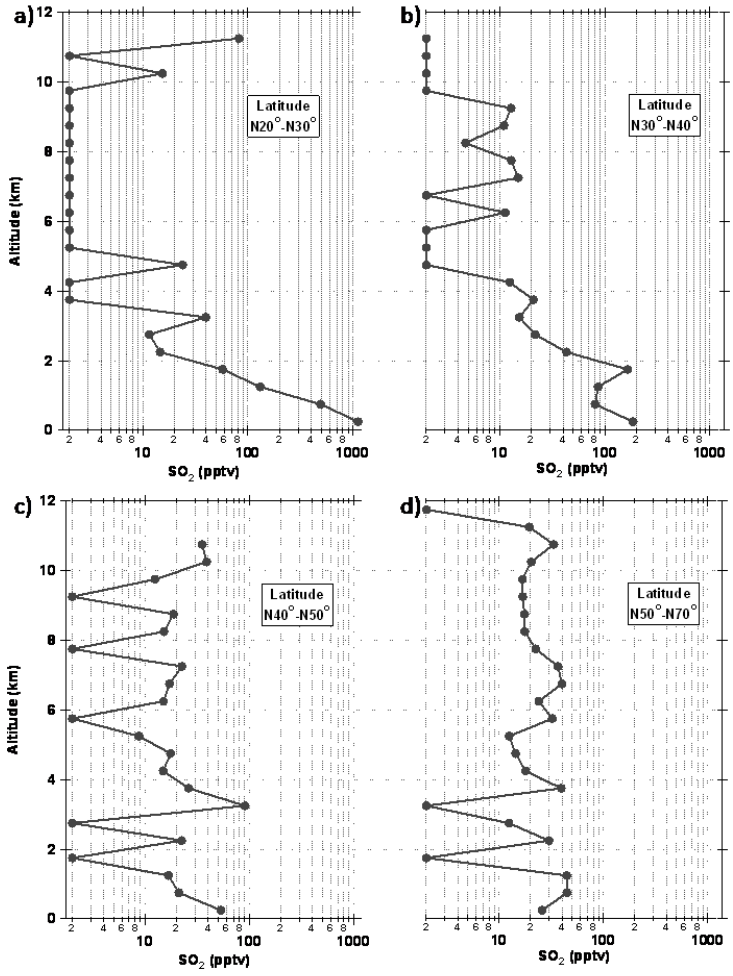

Figure 5.12 Median profiles of SO_2 as a function of latitude over the north Pacific during the INTEX-B campaign.

Figures 5.13a and b show the correlation of SO_2 with CO and ultrafine aerosols, respectively, in the upper troposphere of the North Pacific. Overall, the correlation with CO is much weaker than those from two prior campaigns. The fact may reflect the complexity of source characteristics of the Asian region. Indeed, the major anthropogenic sources in Asia such as industrial, urban, and biomass burning sources have very different ratios of SO_2 to CO as illustrated in Streets et al. [2003]. Figure 5.13b also indicates a poor correlation between SO_2 and ultrafine aerosols. Conversely, the non-volatile aerosol number density in the upper troposphere in Figure 5.14a shows a strong correlation with SO_2. For comparison purpose, the same correlation for upper tropospheric INTEX-NA data is presented in Figure 5.14b. For frontal uplift, SO_2 levels have a strong correlation with non-volatile aerosols. In contrast, for deep convection cases, SO_2 weakly correlates with non-volatile aerosols (0.01 – 7μm, T = 300 ^oC). Therefore, the high SO_2 plumes, sampled during the INTEX-B field campaign are most likely transported by frontal uplift process (the warm conveyor belt; Fuelberg et al. [2006] and references therein). In addition, the differences in the correlation with aerosol parameters in accordance with lifting processes should affect the dynamics of upper tropospheric new particle formation, which strongly depends on preexisting aerosol surface area concentrations [Kazil et al., 2007].

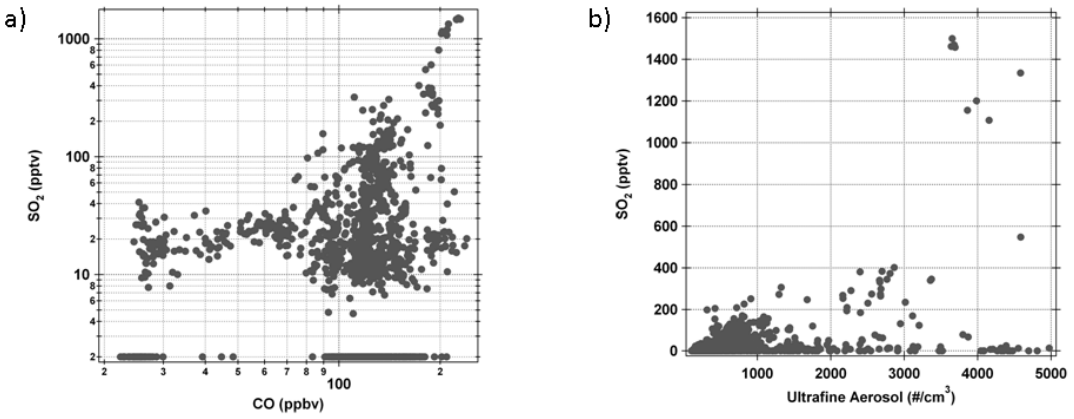

Figure 5.13 Correlation plots of SO_2 with a) CO and b) ultrafine aerosols in the upper troposphere during the INTEX-B Phase II field campaign.

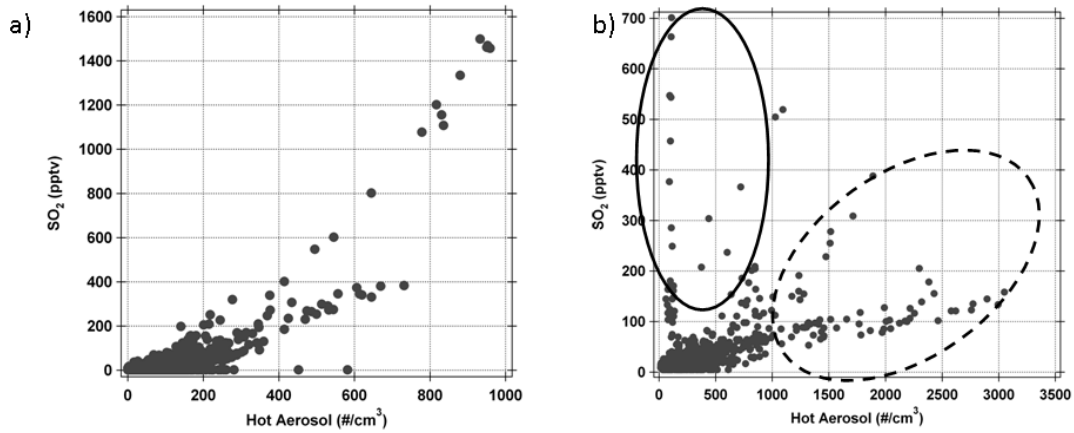

Figure 5.14 Correlation plots of SO_2 with non volatile aerosols (as denoted "Hot Aerosol" in the axis) in the upper troposphere during a) INTEX-B Phase II and b) INTEX-NA. The solid circle in Figure b) indicates high SO_2 plumes, transported by deep convection processes and the dotted circle indicates high SO_2 plumes, transported by frontal uplift processes.

5.2.3 Comparisons with 3D Model Products

This section presents the comparison of predicted SO_2 from the global 3-D chemical transport models GEOS-CHEM [Bey et al., 2001] and MOZART-4 with observations. The sulfur simulation of GEOS-CHEM is based on the Georgia Tech/Goddard Global Ozone Chemistry Aerosol Radiation Transport (GOCART) model

[Chin et al., 2000] with updated features described by Park et al. [2004] and the sulfur chemistry of MOZART-4 is based on that of Barth et al. [2000] with updated rate constants and emission data. Both models produced the SO_2 mixing ratio for every science flight track during the INTEX-field campaign with grid spacing in the horizontal of 50 km for GEOS-CHEM and 0.7 degree for MOZART-4.

First, the measured and the simulated vertical profiles of SO_2 and SO_x (SO_2 + SO_4^{2-}) in the pollution outflow region are compared to examine how the models simulate general features of the transport and oxidation processes of SO_2 in the troposphere. Then, the spatial distributions of SO_2 in the boundary layer and the free troposphere are compared.

5.2.3.1 INTEX – NA

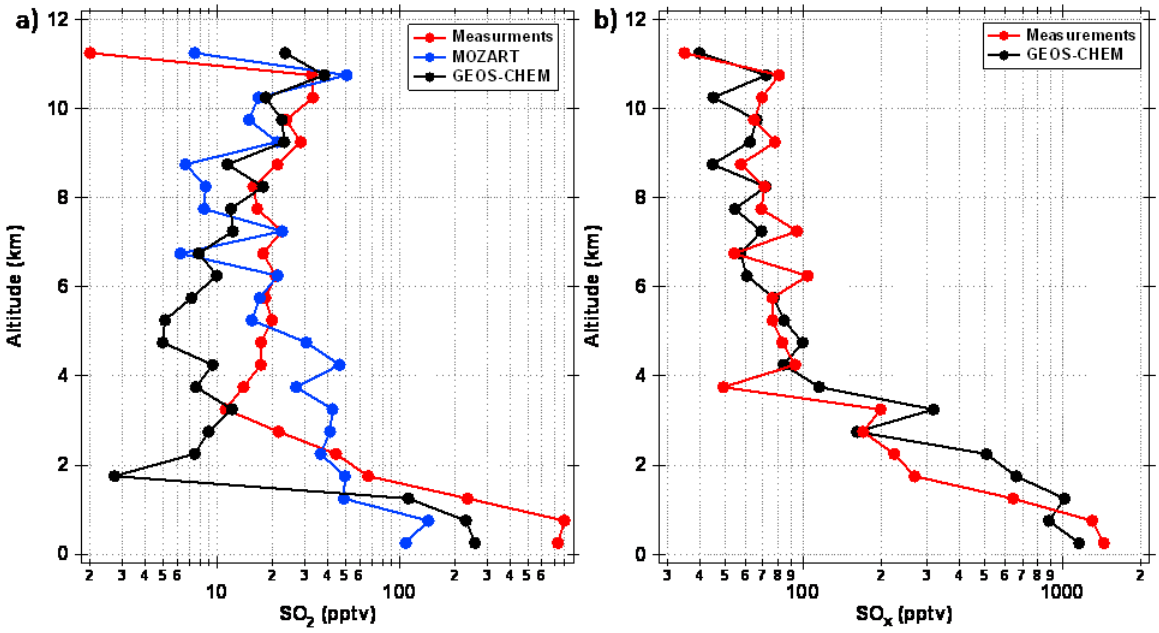

Figure 5.15 Profiles of a) SO_2 and b) SO_x (=SO_2 + SO_4^{2-}) from measurements (Red) and two model products (GEOS-CHEM: Black and MOZART: Blue) over the North Atlantic during INTEX-NA. Note SO_x profiles from MOZART are not available.

Figures 5.15 a) and b) present the median profiles of measured and simulated SO_2 and SO_x in the eastern U.S. Since MOZART SO_4^{2-} data are not available, SO_x profiles of observed and GEOS-CHEM predictions are presented. Both models reasonably simulate the SO_2 enhancements in the upper troposphere. However, in the boundary layer, both models under-predict SO_2. This underestimation is primarily due to high SO_2 observations over the Atlantic Ocean. This has also been reported in another modeling study, which suggests that poorly estimated ship traffic may be the reason for the discrepancy [Erying et al., 2007]. Overall, the SO_x profile, simulated by GEOS-CHEM shows a better agreement with the measured profile than the SO_2 profile. This suggests that the model reasonably simulates the total sulfur distribution, but the treatment of SO_2 oxidation processes may not be accurate enough to simulate the sulfur partitioning.

Figure 5.16 shows horizontal distributions of measured and simulated SO_2 in the boundary layer (radar altitude < 1km) for the INTEX-NA field campaign. Both models reasonably well simulate high SO_2 in the Ohio Valley and the southeast of the U.S. However, significant under-estimates are found in Northeast Atlantic Coast, Nova Scotia, and the open Atlantic Ocean (as discussed above).

Figure 5.17 illustrates the horizontal distributions of measured and simulated SO_2 in the upper troposphere (8-12 km) during the INTEX-NA field campaign. Measured data indicate strong enhancements of SO_2 over the North Atlantic and the North Pacific from the eastern U.S. and Asia, respectively. However, both models failed to simulate those features. Overall, GEOS-CHEM presents very little upper tropospheric SO_2. On the other

hand, MOZART predicts much broader enhancements of SO_2 in the upper troposphere all over the eastern U.S.

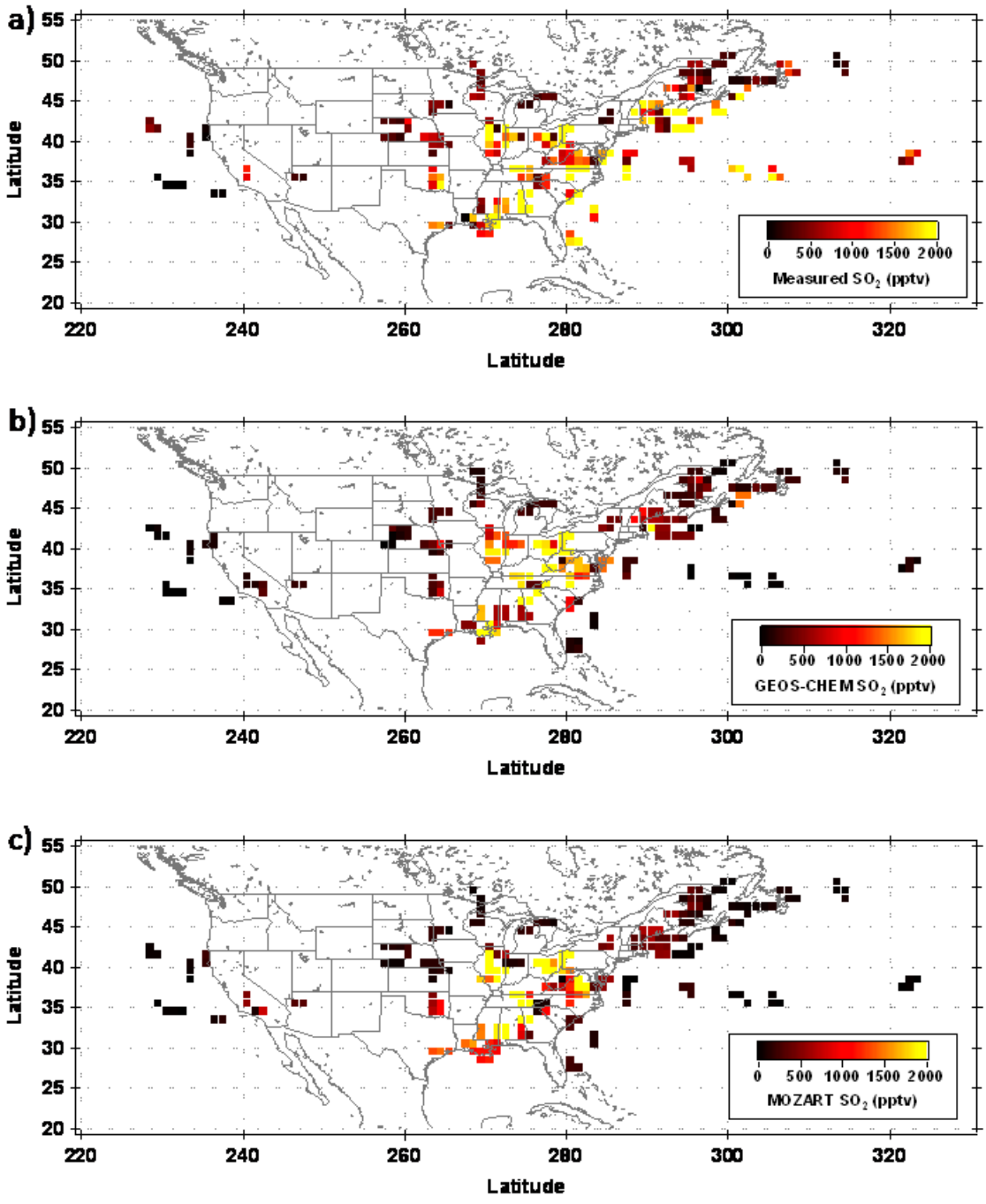

Figure 5.16 Distributions of SO_2 in the boundary layer of a) measurements, b) GEOS-CHEM, and c) MOZART during INTEX-NA.

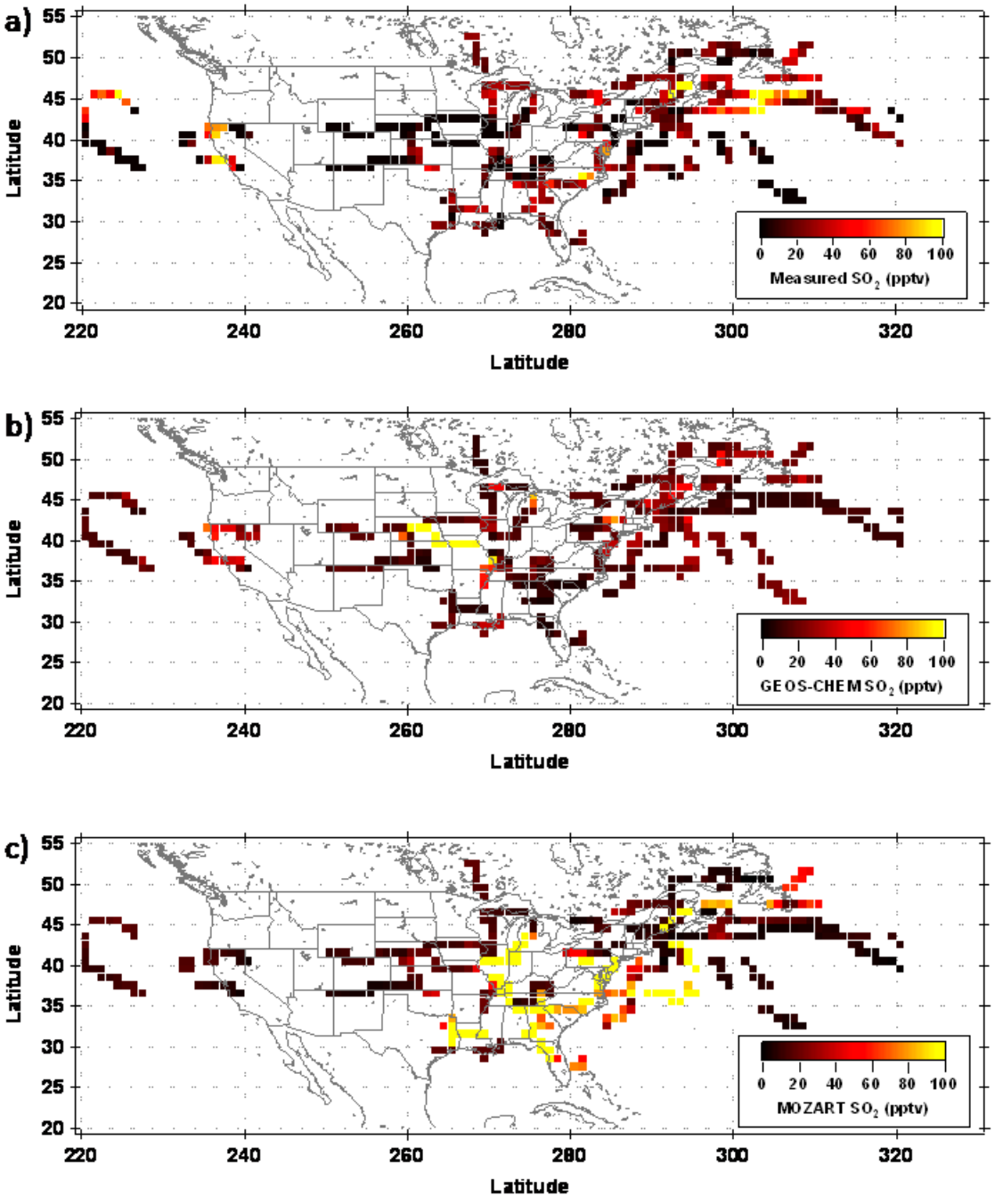

Figure 5.17 Distributions of SO_2 in the upper troposphere of a) measurements, b) GEOS-CHEM, and c) MOZART during INTEX-NA.

5.2.3.2 INTEX-B Phase 1

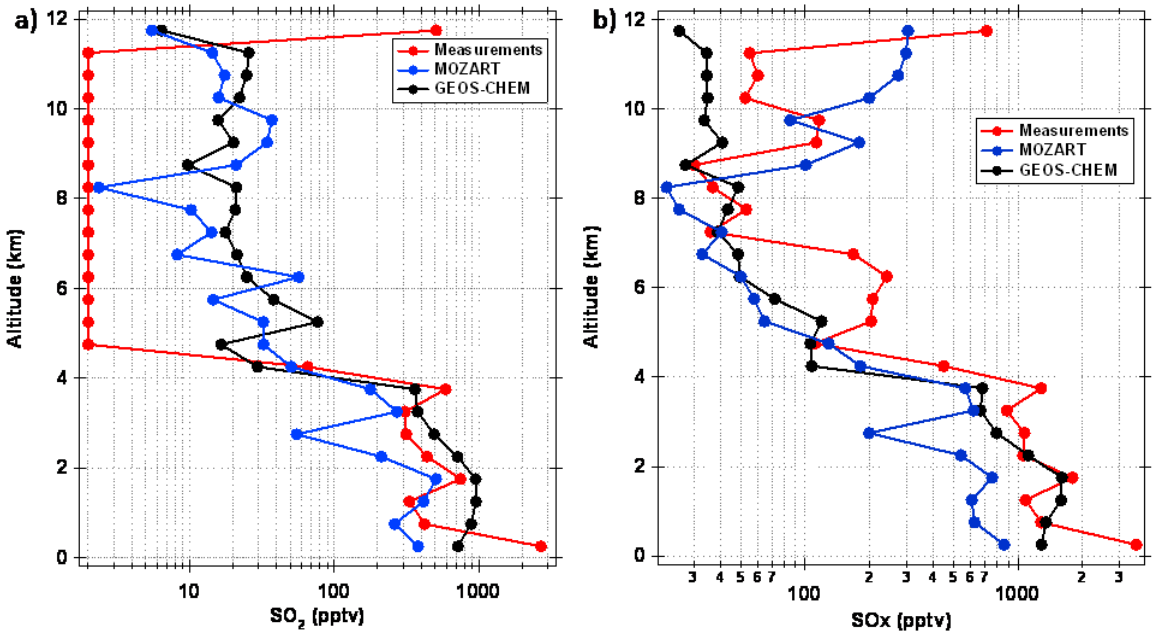

Figure 5.18 Profiles of a) SO_2 and b) SO_x (=SO_2 + SO_4^{2-}) from measurements (Red) and two model products (GEOS-CHEM: Black and MOZART: Blue) over the Gulf of Mexico during INTEX-B Phase I.

Figures 5.18 a) and b) illustrate median profiles of both measured and modeled a) SO_2 and b) SO_x in the Gulf of Mexico during INTEX-B Phase I. Both models predict significant levels of SO_2 (10 – 100 pptv) in the free troposphere (z > 4 km) over the Gulf of Mexico even though SO_2 observations were mostly measured below detection limit. However, GEOS-CHEM underestimates SO_x in the free troposphere and MOZART underestimates SO_x in the mid troposphere.

In addition, although results from both models and measurements reasonably correlate in the altitude of 0 km – 4 km, at the very bottom of the profile models significantly underestimate both measured SO_2 and SO_x. Indeed, as indicated in Figure

5.19, which presents SO_2 distributions of model products and measurements in the boundary layer during the field campaign, models significantly underestimate boundary layer SO_2 especially in the Gulf of Mexico. On the other hand, distributions of SO_2 in the upper troposphere indicate overestimates by models as shown in Figure 5.20.

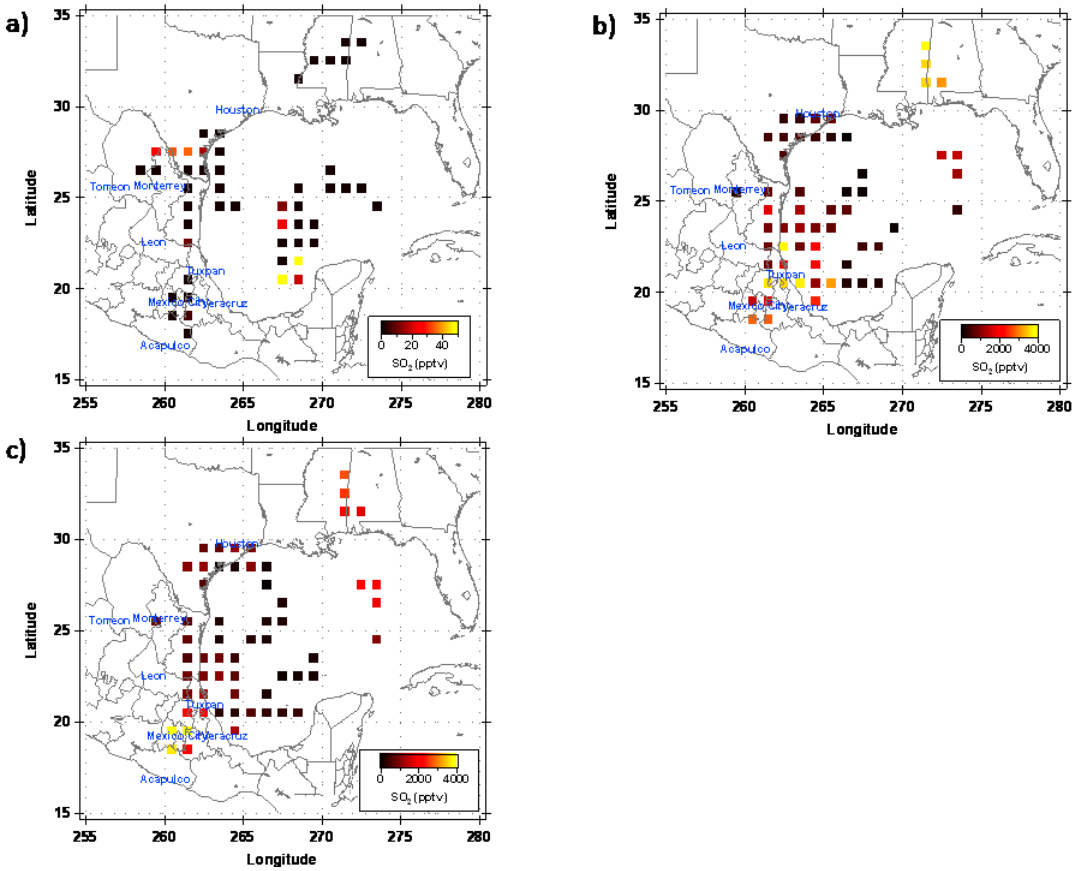

Figure 5.19 Distributions of SO_2 in the boundary layer of a) measurements, b) GEOS-CHEM, and c) MOZART during INTEX-B Phase I.

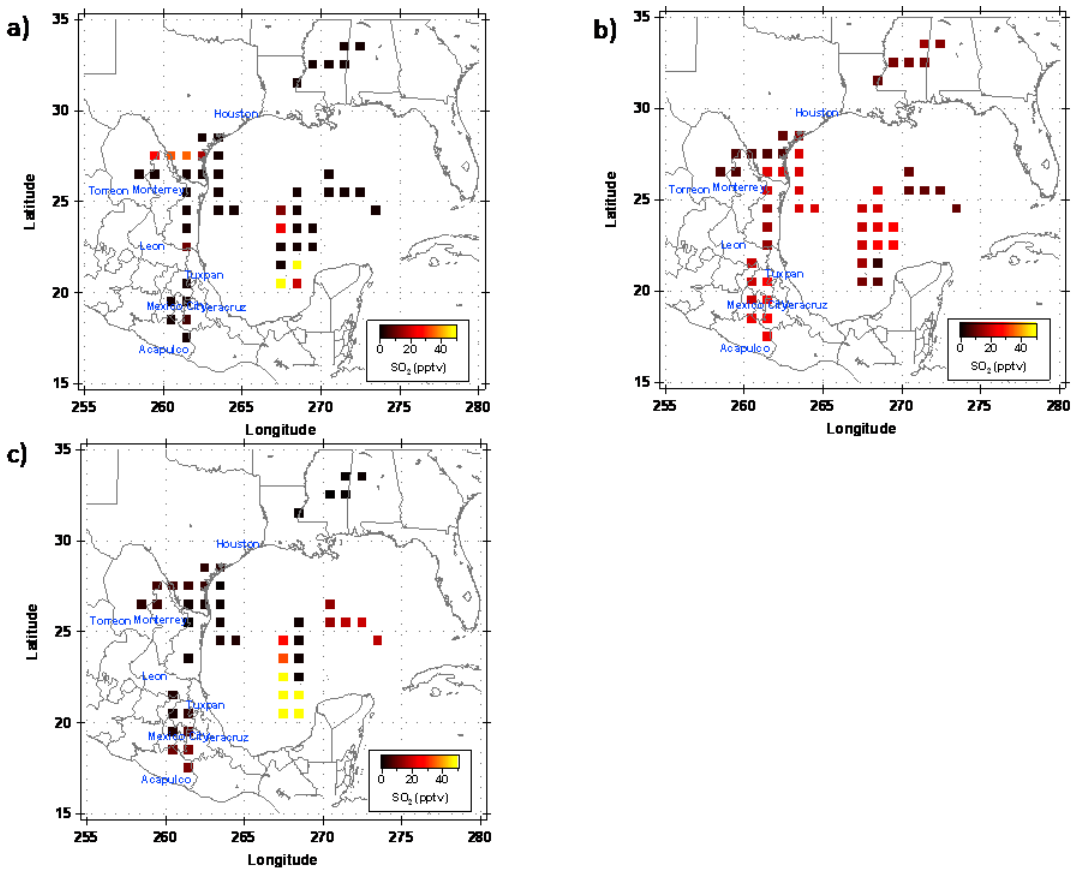

Figure 5.20 Distribution of SO_2 in the upper troposphere of a) observations b) GEOS-CHEM and c) MOZART during INTEX-B Phase I.

5.2.3.3 INTEX-B Phase II

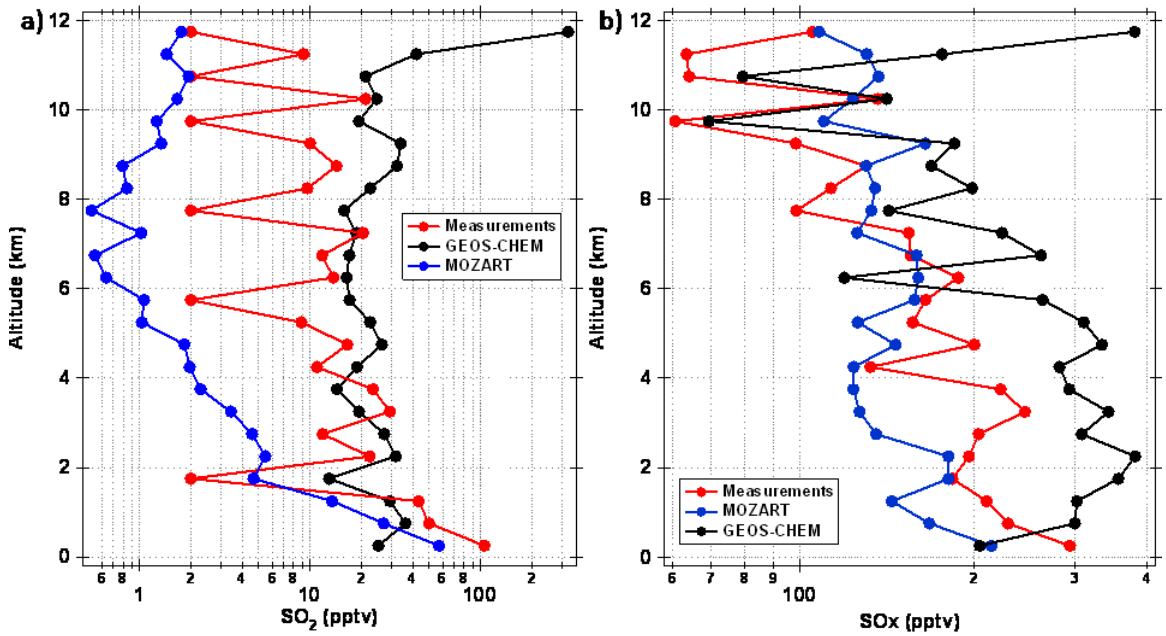

Figure 5.21 Profiles of a) SO_2 and b) SO_x (=SO_2 + SO_4^{2-}) from measurements (Red) and two model products (GEOS-CHEM: Black and MOZART: Blue) over the north Pacific during INTEX-B Phase II.

Figures 5.21 a) and b) present profiles of median SO_2 and SO_x of measurements and both models over the north Pacific. The measured SO_2 profile depicts many enhanced SO_2 layers in the free troposphere. On the other hand, both models simulate very different profiles of SO_2. GEOS-CHEM depicts consistent enhancements of SO_2 all over the free troposphere. Conversely, MOZART predicts very low levels of SO_2 in the free troposphere. However, the SO_x profile, simulated by MOZART is close to the measured profile, indicating that total sulfur levels are better described than the partitioning.

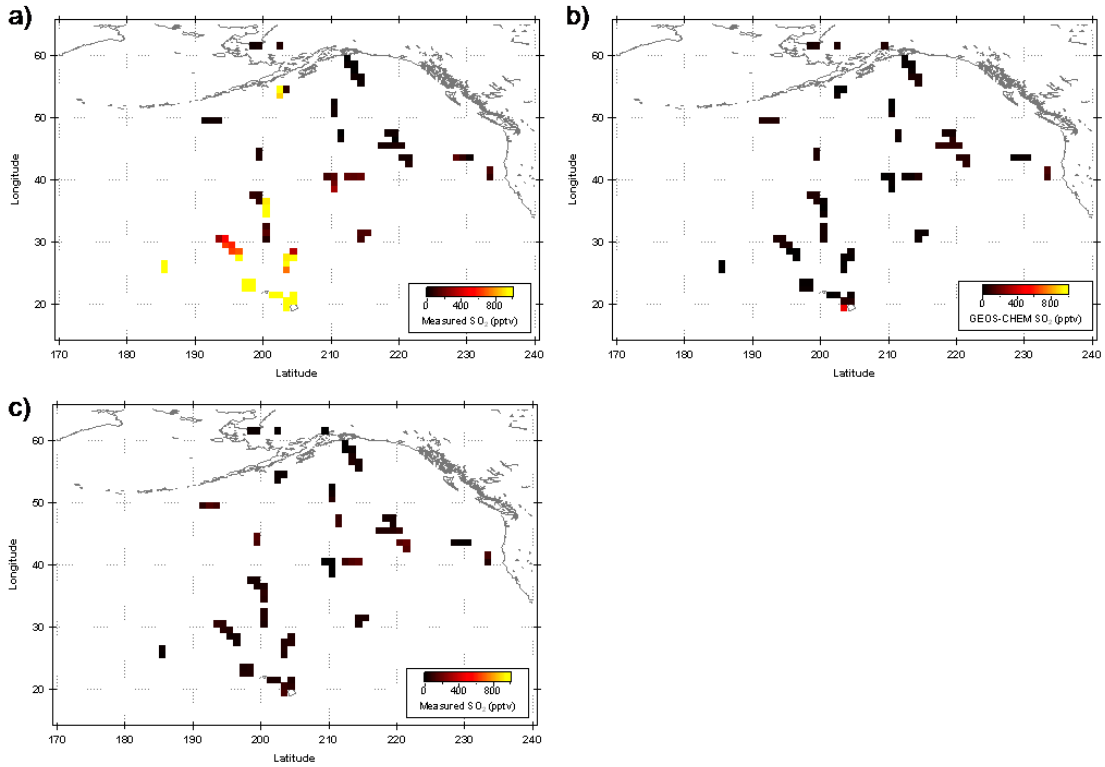

Figure 5.22 Distributions of SO_2 in the boundary layer a) observations b) GEOS-CHEM, and c) MOZART during INTEX-B Phase II.

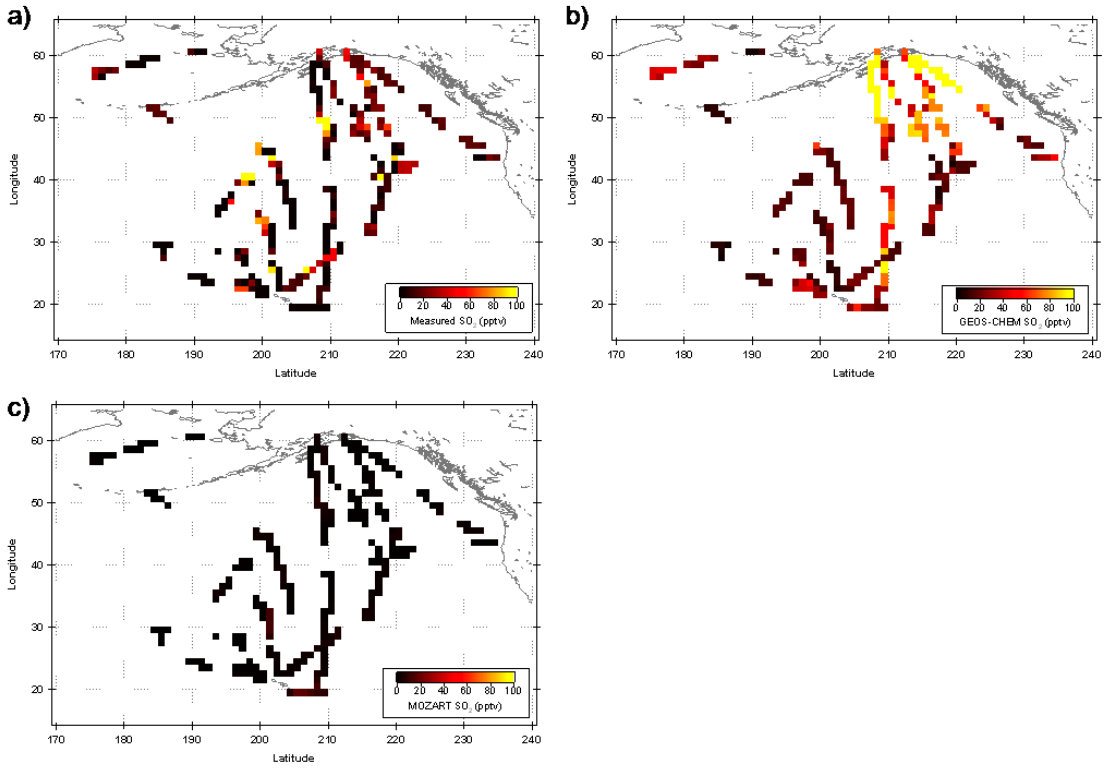

Figure 5.23 Distributions of SO_2 in the boundary layer a) observations, b) GEOS-CHEM, and c) MOZART during INTEX-B Phase II.

Figure 5.22 shows horizontal distributions of SO_2 in the boundary layer from observations and both models. Both models could not capture high SO_2 in the MBL. Upper tropospheric SO_2 distributions, predicted by GEOS-CHEM are significantly higher than measurements (Figure 5.23). Conversely, MOZART predicts very low concentrations of SO_2 in the upper troposphere over the entire north Pacific region.

5.2.4. SO_2 and DMS Correlation in the Clean MBL

For the investigation of SO_2 in the remote MBL, this section presents the MBL samplings dataset during a local flight of the Anchorage deployment (May 4, 2006). The flight track of the MBL sampling during the science flight presents in Figure 5.24. Conditions of the MBL during the flight were generally clean (O_3-45 ppbv, HCHO-150 pptv, NO_x < 50 pptv) with very little variability of chemical and physical conditions.

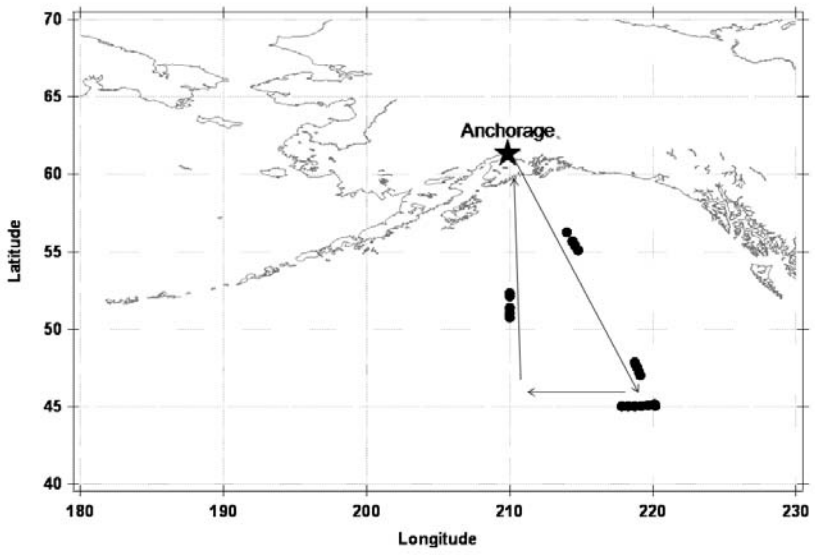

Figure 5.24 The flight track of the case study to examine DMS contributions to SO_2 distributions in the clean MBL. The dotted data points along the flight track indicate MBL sampling points.

Figure 5.25 shows temporal variations of measured and model (MOZART) predicted DMS and SO_2 during four MBL legs of the flight. In general, observed SO_2 levels were between 20 and 40 pptv even though DMS levels were observed to be consistently very low (< 50 pptv). In contrast, model predictions of DMS were consistently above 150 pptv. Although the model did predict SO_2 levels reasonably well.

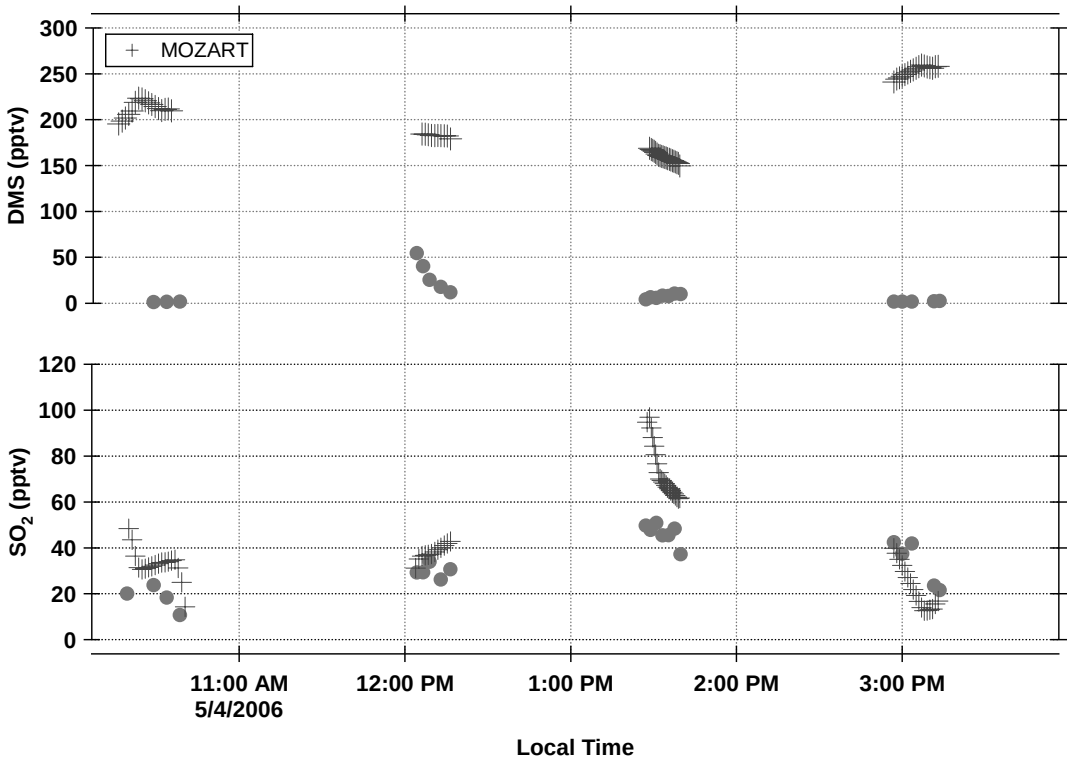

Figure 5.25 Temporal variations of SO_2 (the lower panel) and DMS (the upper panel) from both measurements (circle) and MOZART model products (cross) over the north Pacific MBL.

In MOZART, DMS distributions over the MBL are estimated by a global-coupled ocean-atmosphere method, introduced in Kloster et al. [2006]. The estimated DMS is the main source of SO_2 from oxidation by OH and NO_3. Therefore, the predicted SO_2 concentration with over-estimated DMS should be much higher than observed if the model accurately captures the oxidation chemistry.

For a more detailed investigation, the rate of DMS destruction is calculated to determine if it can explain the observed levels of SO_2 in the MBL. The major loss pathway of DMS in the MBL during the daytime is the OH oxidation, which has two different reaction pathways- the addition and the abstraction reaction. Through those reaction channels, 72 % (± 22 %) of DMS was expected to be oxidized to SO_2 in the clean MBL [Davis et al., 1999]. Loss pathways of SO_2 in the MBL can be divided into two categories. The first one includes dry deposition, aerosol and sea-salt scavenging, estimated as a constant loss rate at 1.1×10^{-5} sec^{-1} [Davis et al. 1999]. The second is the gas phase oxidation by OH. For the estimation of the oxidation rate, measured OH concentrations and rate constants from Sander et al. [2006] are used. The calculation results with the above scheme show that median destruction rates of DMS and SO_2 are estimated as 4.89 pptv day^{-1} and 69.0 pptv day^{-1}, respectively. Although a significant fraction of DMS oxidation products are converted to SO_2, the DMS destruction rate is too small to explain the measured level of SO_2. In addition, the median sulfate ratio in the MBL during the flight was 0.80, indicating relatively aged air rather than fresh SO_2 from DMS oxidation. Therefore, the trace level of SO_2 in the MBL in this case study appears to come from transport rather than DMS oxidation.

5.2.5 SO_2 in the Lower Stratosphere

During the Anchorage deployment of INTEX-B, the DC-8 sampled air masses in the lower stratosphere as well as air masses in the upper troposphere with significant stratospheric influence. Even though stratospheric SO_2 has been implicated as an important source of stratospheric sulfate aerosols, primarily modeling approaches, due to a lack of simultaneous measurements of SO_2 and OCS, have been used to asses the role of SO_2 in the stratosphere. The only reported simultaneous measurements of stratospheric SO_2 and OCS are Singh et al. [1997] in the latitude range of 37 – 57 ^{o}N, consistent with this study. The reported medians of stratospheric SO_2 and OCS are 54 pptv and 427 pptv, respectively. The median value of stratospheric OCS, observed in this work is 423 pptv is consistent with the previous study. However, the median value of stratospheric SO_2 in this study, 19.6 pptv, is much lower than the previous study.

The correlation of SO_2 with CO for stratospheric data is presented in Figure 5.26. Except for a few points, SO_2 concentrations show no variation over the dynamic range of the observed CO (~60 ppbv). Figure 5.27 presents the correlation of SO_2 with O_3 for stratospheric data. SO_2 concentrations are relatively constant over the O_3 concentration range of 200 – 600 ppbv. However, above 600 ppbv of O_3, SO_2 concentrations are below the detection limit.

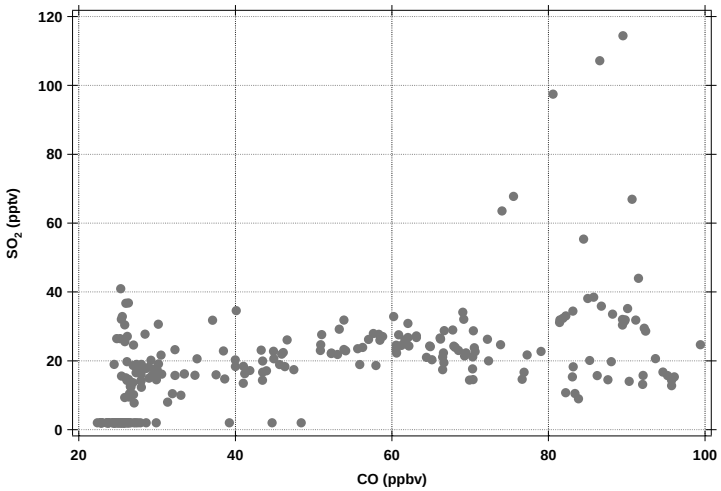

Figure 5.26 The correlation plot of SO_2 with CO of the stratospheric dataset from INTEX-B Phase II.

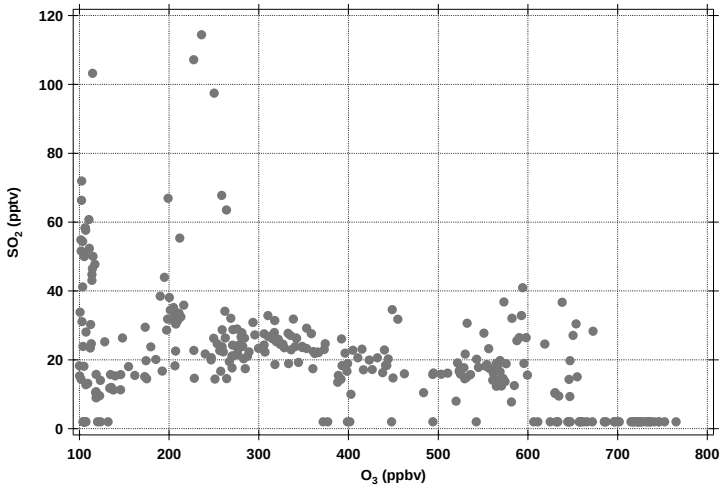

Figure 5.27 Correlation plot of SO_2 with O_3 of the stratospheric dataset from INTEX-B Phase II

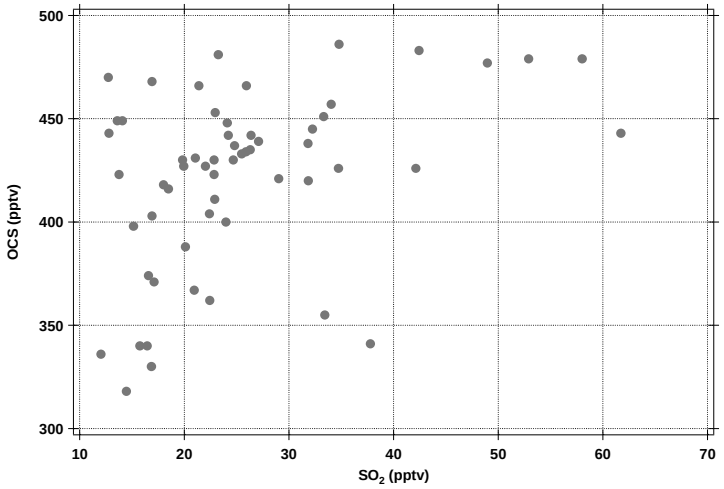

Figure 5.28 Correlation plot of SO_2 with OCS for the stratospheric dataset from INTEX-B Phase II

The analysis of the stratospheric data by Singh et al. [1997] demonstrated a correspondence between a decrease in the OCS mixing ratio (30 pptv) and the same increase in the SO_2 mixing ratio. They claimed that this correspondence indicated that OCS is a major source of SO_2 in the stratosphere. However, in this mission the negative correlation between OCS and SO_2 cannot be found (Figure 5.28) even with the higher dynamic range of OCS (~100 pptv).

To further investigate this issue, simple calculations of OCS removal rates by photolysis and SO_2 removal rates by OH are conducted. The OCS photolysis rate in the lower stratosphere is too low to be accurately measured. Therefore, this study adapts the average lifetime of OCS in the stratosphere, reported as 71 years by Engel and Schmidt [1994], to deduce an OCS photolysis rate as 4.5×10^{-10} sec^{-1}. SO_2 removal rates by OH are calculated from measured OH concentrations and the rate constant from Sander et al. [2006]. The calculations indicate that the median of OCS removal rates in the stratosphere is 0.16 pptv day^{-1}, which is significantly lower than the median SO_2 removal rate of 2.55 pptv day^{-1}. The results suggest that OCS photolysis is not the major source of SO_2 in the lower stratosphere. This indicates that the stratospheric SO_2 observed in this study may be due to transport from the troposphere. This assumption is supported by the fact that SO_2 was not detected at high O_3 levels (more than 600 ppbv).

5.3 References

Aydin, M. O., De Bruyn, W. J., and Saltzman, E. S.: Preindustrial atmospheric carbonyl sulfide (OCS) from an Antartctic ice core, Geophysical Research Letters, 29, 1359,doi:1310.1029/2002GL014796, 2002.

Bandy, A. R., Thornton, D. C., and Driedger, A. R.: Airborne measurements of sulfur dioxide, dimethyl sulfide, carbon disulfide, and carbonyl sulfide by isotope dilution gas chromatobraphy/mass spectrometry, Journal of Geophysical Research, 98, 23422-23442, 1993.

Barnes, I., Bastian, V., Becker, K. H., and Martin, D.: Fourier-Transform IR studies of the reactions of dimethyl-sulfoxide with OH, NO_3, and Cl radicals, ACS symposium Series, 393, 476, 1989.

Barone, S. B., Turnipseed, A. A., and Ravishankara, A. R.: Reaction of OH with dimethyl sulfide(DMS). 1. Equilibrium for OH+DMS reaction and the kinetics of the OH-DMS+O_2 reaction, Journal of Physical Chemistry, 100, 14694-14702, 1996.

Barth, M. C., and Church, A. T.: Regional and global distributions and lifetimes of sulfate aerosols from Mexico City and southeast China, Journal of Geophysical Research, 104, 30231-30239, 1999.

Barth, M. C., Rasch, P. J., Kiehl, J. T., Benkovitz, C. M., and Schwartz, S. E.: Sulfur chemistry in the National Center for Atmospheric Research Community Climate Model: Description, evaluation, features, and sensitivity to aqueous chemistry, Journal of Geophysical Research, 105, 1387-1415, 2000.

Berresheim, H., Wine, P. H., and Davis, D. D.: Sulfur in the atmosphere, in: Composition, Chemistry, and Climate of the Atmosphere, edited by: Singh, H. B., Van Nostrand Reinhold, New York, 1995.

Bertram, T. H., Perring, A. E., Wooldridge, P. J., Crounse, J. D., Kwan, A. J., Wennnberg, P. O., Scheuer, E., Dibb, J., Avery, M., Sachse, G., Vay, S., Crawford, J. H., McNaughton, C. S., Clarke, A., Pickering, K. E., Fuelberg, H., Huey, G., Blake, D. R., Singh, H. B., Hall, S. R., Shetter, R. E., Fried, A., Heikes, B. G., and Cohen, R. C.: Direct measurements of the convective recycling of the upper troposphere, Science, 315, 816 - 820, 2007.

Bey, I., Jacob, D. J., Yantosca, M., Logan, J. A., Field, B. D., Fiore, A. M., Li, Q., Liu, H. Y., Mickley, L. J., and Schultz, G.: Global modeling of tropospheric chemistry with assimilated meteorology: Model description and evaluation, Journal of Geophysical Reserach, 106, 23073-23095, 2001.

Brasseur, G., Orlando, J. J., and Tyndall, G. S.: Atmospheric Chemistry and Global Change, 1st ed., Topics in Environmental Chemistry, edited by: Birks, J. W., Oxford University Press, New York, 1999.

Butkovskaya, N. I., and Lebras, G.: Mechanism of the NO_3+DMS reaction by discharge flow mass-spectrometry, Journal of Physical Chemistry, 98, 2582-2591, 1994.

Charlson, R. J., Schwartz, S. E., Hales, J. M., Cess, R. D., Coakley, J. A. J., Hansen, J. E., and Hofmann, D. J.: Climate forcing by anthropogenic aerosols, Science, 255, 423-430, 1992.

Chin, M., and Davis, D.: A reanalysis of carbonyl sulfide as a source of stratospheric background sulfur aerosols, Journal of Geophysical Research, 100, 8993-9005, 1995.

Chin, M., Jacob, D. J., Gardner, g. M., Foreman-Fowler, M. S., Spiro, P. A., and Savoie, D. L.: A global three-dimensional model of tropospheric sulfate, Journal of Geophysical Research, 101, 18667-18690, 1996.

Chin, M., Rood, R. B., Lin, S.-J., Muller, J.-F., and Thompson, A. M.: Atmospheric sulfur cycle simulated in the global model GOCART: Model description and global properties, Journal of Geophysical Research, 105, 24671-24687, 2000.

Crutzen, P. J.: The possible importance of OCS for the sulfate layer of the stratosphere, Geophysical Research Letters, 3, 73-76, 1976.

Davis, D., Chen, G., Bandy, A., Thornton, D., Eisele, F., Mauldin, L., Tanner, D., Lenschow, D., Fuelberg, H., Huebert, B., Heath, J., Clarke, A., and Blake, D.: Dimethyl sulfide oxidation in the equatorial Pacific: Comparison of model simulations with field observations for DMS, SO_2, H_2SO_4(g), MSA(g), MS, and NSS, Journal of Geophysical Research, 104, 5765-5784, 1999.

Engel, A., and Schmidt, U.: Vertical profile measurements of Carbonylsulfide in the stratosphere, Geophysical Research Letters, 21, 2219-2222, 1994.

Eyring, V., Stevenson, D. S., Lauer, A., Dentener, F. J., Butler, T., Colins, W. J., Ellingsen, K., Gauss, M., Hauglustaine, D. A., Isaksen, I. S. A., Lawrence, M. G., Richter, A., Rodriguez, J. M., Sanderson, M., Strahan, S. E., Sudo, K., van Noije, T. P. C., and Wild, O.: Multi-model simulations of the impact of international shipping on Atmospheric Chemistry and Climate in 2000 and 2030, Atmospheric Chemistry and Physics, 7, 757-780, 2007.

Forster, P., Ramaswamy, V., Artaxo, P., Berntsen, T., Betts, R., Fahey, D. W., Haywood, J., Lean, J., Lowe, D. C., Myhre, G., Nganga, J., Prinn, R., Raga, G., Schulz, M., and Van Dorland, R.: Changes in atmospheric constituents and in radiative forcing, in: Climate Change 2007: The Physical Science Basis, edited by: Solomon, S., Qin, D., Manning, M., Chen, Z., Marquis, M., Averyt, K. B., Tignor, M., and Miller, H. L., Cambridge University Press, Cambridge, U.K. and New York, U.S., 2007.

Fuelberg, H. E., Porter, M. J., Kiley, C. M., Holland, J. J., and Morse, D.: Meteorological conditions and anomalies during the Intercontinental Chemical Transport

Experiment-North America, Journal of Geophysical Reserach, 112, doir:10.1029/2006JD007734, 2007.

Haywood, J., and Boucher, O.: Estimates of the direct and indirect radiative forcing due to tropospheric aerosols: a review, Reviews of Geophysics, 38, 513-543, 2000.

Hegg, D. A.: The importance of liquid-phase oxidation of SO_2 in the troposphere, Journal of Geophysical Research, 20, 3773-3779, 1985.

Hynes, A. J., and Wine, P. H.: OH-initiated oxidation of biogenic sulfur compounds-kinetics and mechanisms under atmospheric conditions, ACS symposium Series, 393, 1989.

Jacob, D. J., and Hoffmann, M. R.: A dynamic model for the production of H^+, NO_3^-, and SO_4^{2-}, Journal of Geophysical Research, 88C, 6611-6621, 1983.

Junge, C. E., Chagnon, C. W., and Manson, J. E.: A world-wide stratospheric aerosol layer, Science, 133, 1478-1479, 1961.

Kazil, J., Lovejoy, E. R., Jensen, E. J., and Hanson, D. R.: Is aerosol formation in cirrus clouds possible?, Atmospheric Chemistry and Physics, 7, 1407-1413, 2007.

Kloster, S., Feichter, J., Maier-Reimer, E., Six, K. D., Stier, P., and Wetzel, P.: DMS cycle in the marine ocean-stmosphere system - a global model study, Biogeosciences, 3, 29-51, 2006.

Lovelock, J. E., Maggs, R. J., and Rasmussen, R. A.: Atmospeheric dimethyl sulphide and the natural sulfur cycle, Nature, 237, 462-463, 1972.

Molina, L. T., Kolb, C. E., de Foy, B., Lamb, B. K., Brune, W. H., Jimenez, J. L., Ramos-Villegas, R., Sarmiento, J., Paramo-Figueroa, V. H., Cardenas, B., Gutierrez-Avedoy, V., and Molina, M. J.: Air quality in North America's most populous city-overview of the MCMA-2003 campaign, Atmospheric Chemistry and Physics, 7, 2447-2473, 2007.

Ohara, T., Akimoto, H., Kurokawa, J., Horii, N., Yamaji, K., Yan, X., and Hayasaka, T.: An Asian emission inventory of anthropogenic emission sources for the period 1980-2020, Atmospheric Chemistry and Physics, 7, 4419-4444, 2007.

Park, R. J., Jacob, D. J., Field, B. D., Yantosca, R. M., and Chin, M.: Natural and transboundary pollution influences on sulfate-nitrate-ammonium aerosols in the United Sates: Impications for policy, Journal of Geophysical Research, 109, doi:10.1029/2003JD004473, 2004.

Park, R. J., Jacob, D. J., Palmer, P. I., Clarke, A. D., Weber, R. J., Zondlo, M. A., Eisele, F. L., Bandy, A. R., thornton, D. C., Sachse, G. W., and Bond, T. C.: Export efficiency of black carbon aerosol in continental outflow: Global implications, Journal of Geophysical Research, 110, doi:10.1029/2004JD005435, 2005.

Patroescu, I. V., Barnes, I., Becker, K. H., and Mihalopoulos, N.: FT-IR product study of the OH-initiate oxidation of DMS in the presence of NO_x, Atmospheric Environment, 33, 3083-3084, 1999.

Pitari, G., Manicini, E., Rizi, V., and Shindell, D. T.: Impact of future climate and emission changes on stratospheric aerosols and ozone, Journal of Atmospheric Sciences, 59, 414-440, 2002.

Raes, F., Van Dingenen, R., Vignati, E., Wilson, J., Putaud, J.-P., Seinfeld, J. H., and Adams, P.: Formation of cycling of aerosols in the global troposphere, Atmospheric Environment, 34, 4215-4240, 2000.

Sander, S. P., Friedl, R. R., Ravishankara, A. R., Golden, D. M., Kolb, C. E., Kurylo, M. J., Molina, M. J., Moortgat, G. K., Keller-Rdek, H., Finlayson-Pitts, B. J., Wine, P. H., Huie, R. E., and Orkin, V. L.: Chemical kinetics and photochemical data for use in atomspheric studies, Evaluation Number 15, JPL Publication 06-02, 2006.

Shon, Z.-H., Davis, D., Chen, G., Grodzinsky, G., Bandy, A., Thornton, D., Sandholm, S., Bradshaw, J., Stickel, R., Chameides, W., Kok, G., Russell, L., Mauldin, L., Tanner, D., and Eisele, F.: Evaluation of the DMS flux and its conversion to SO_2 over the southern ocean, Atmospheric Environment, 35, 159-172, 2001.

Singh, H. B., Brune, W. H., Crawford, J., and Jacob, D.: Overview of the summer 2004 Intercontinental Chemical Transport Experiment-North America (INTEX-A), Journal of Geophysical Reserach, 111, doi:10.1029/2006JD007905, 2006.

Singh, H. B., Chen, Y., Gregory, G. L., Sachse, G. W., Talbot, R., Blake, D. R., Kondo, Y., Bradshaw, J. D., Heikes, B., and Thornton, D.: Trace chemical measurements from the northern midlatitude lowermost stratosphere in early spring: Distribution, correlaiton, and fate, Geophysical Research Letters, 24, 127-130, 1997.

Sorensen, S., FalbeHansen, H., Mangoni, M., Hjorth, J., and Jensen, N. R.: Observation of DMSO and $CH_3S(O)OH$ from the gas phase reaction between DMS and OH, Journal of Atmospheric Chemistry, 24, 299-315, 1996.

Stern, D. I.: Global sulfur emissions from 1850 to 2000, Chemosphere, 58, 163-175, 2005.

Stockwell, W. R., and Calvert, J. G.: The mechanism of the OH-SO_2 reaction, Atmospheric Environment, 17, 2231-2235, 1983.

Streets, D. G., Bond, T. C., Carmichael, G. R., Fernandes, S. D., Fu, Q., He, D., Klimont, Z., Nelson, S. M., Tsai, N. Y., Wang, M. Q., Woo, J.-H., and Yarber, K. F.: An inventory of gaseous and primary aerosol emissions in Asia in the year 200, Journal of Geophysical Research, 108, 8809,doi:8810.1029/2002JD003093, 2003.

Streets, D. G., Wu, Y., and Chin, M.: Two-decaldal aerosol trends as a likely explanation

of the global dimming/brightening transition, Geophysical Research Letters, 33, doi:10.1029/2006GL026471, 2006.

Thornton, D., Bandy, A. R., Tu, F. H., Bloomquist, B. W., Mitchell, G. M., Nadler, W., and Lenschow, D. H.: Fast airborne sulfur measurements by Atmospheric Pressure Ionization Mass Spectrometer (APIMS), Journal of Geophysical Research, 107, 4632,doi:4610.1029/2002JD002289, 2002.

Thornton, D. C., Bandy, A. R., Bloomquist, B. W., Bradshaw, J. D., and Blake, D. R.: Vertical Transportation of sulfur dioxide and dimethyl sulfide in equatorial convection and its role in new particle formation, Journal of Geophysical Research, 102, 28501-28509, 1997a.

Thornton, D. C., Bandy, A. R., Bloomquist, B. W., Bradshaw, J. D., Davis, D. D., and Talbot, R. W.: Sulfur dioxide as a source as a source of condensation nuclei in the upper troposphere of the Pacific Ocean, Journal of Geophysical Research, 101, 1883-1890, 1996.

Thornton, D. C., Bandy, A. R., Bloomquist, B. W., Driedger, A. R., and Wade, T. B.: Sulfur dioxide over the Pacific Ocean 1991-1996, Journal of Geophysical Research, 104, 5845-5854, 1999.

Thornton, D. C., Bandy, A. R., Bloomquist, B. W., Talbot, R. W., and Dibb, J. E.: The transport of sulfur dioxide from the Asian Pacific rim to the North Pacific troposphere, Journal of Geophysical Research, 102, 28489-28499, 1997b.

Timmreck, C.: Three-dimensional simulation of stratospheric background Journal of Geophysical Research, 106, 28313-28332, 2001.

Tu, F. H.: Dynamics and transport of sulfur dioxide in the North Pacific Troposphere, Ph. D., Department of Chemistry, Drexel University, Philadelphia, 101 pp., 2004.

Tu, F. H., Thornton, D. C., Bandy, A. R., Carmichael, G. R., Tang, Y., Thornhill, K. L., Sachse, G. W., and Blake, D. R.: Long-range transport of sulfur dioxide in the central Pacific, Journal of Geophysical Research, 109, doi:10.1029/2003JD004309, 2004.

Tu, F. H., Thornton, D. C., Bandy, A. R., Kim, M.-S., Carmichael, G., Tang, Y., Thornhill, L., and Sachse, G.: Dynamics and transport of sulfur dioxide over the Yellow Sea during TRACE-P, Journal of Geophysical Research, 108, 8790:8710.1029/2002JD003227, 2003.

Turnipseed, A. A., Barone, S. B., and Ravishankara, A. R.: Reaction of OH with dimethyl sulfide 2. Products and mechanisms, Journal of Physical Chemistry, 100, 14703-14713, 1996.

Vijay, S., Molina, L. T., and Molina, M. J.: Estimating air pollution emissions from fossil fuel use in the electricity sector in Mexico, Integrated Program on Air Pollution,

21, 2004.

Wine, P. H., Thompson, R. J., Ravishankara, A. R., Semmes, D. H., Gump, C. A., Torabi, A., and Nicovich, J. M.: Kinetics of the reaction OH + SO_2 + M → $HOSO_3$ + M, Temperature and pressure dependence in the fall-off region, Journal of Physical Chemistry, 88, 2095-2104, 1984.

CHAPTER 6

SUMMARY AND CONCLUSIONS

This study uses chemical ionization mass spectrometry with SF_6^- as a reagent ion to simultaneously measure HO_2NO_2, HCl, and SO_2 from the boundary layer to the lower stratosphere. This allows an examination of our understanding of HO_x-NO_x and chlorine chemistry in the troposphere. In addition, we can test the ability of models to handle sulfur emissions and chemistry. These topics are important as they are critical to understanding distributions of tropospheric ozone and sulfate aerosols, important radivative forcing agents.

The first direct measurements of HO_2NO_2 in the free troposphere were performed from the NASA DC-8 during summer 2004. Comparisons with calculations and models demonstrate that our understanding of pernitric acid below 8 km, where thermal decomposition dominates its lifetime, is very good. However, above 8 km our observations of pernitric acid are incompatible with measured HO_x but in good accord with photochemical theory. In addition, in this high NO_x environment, due to active convection, the measured HO_x levels are much larger than expected from photochemical theory. These results indicate that either our ability to measure HO_x in the upper troposphere is flawed or that the agreement between our HO_2NO_2 observations and photochemical models is fortuitous. If the latter situation is correct then there is much lower pernitric acid than we expect in the upper troposphere given the HO_x observations. This indicates that either pernitric acid production is slower or its loss is faster than expected. This also implies that ozone production in the convectively active upper

troposphere is much greater than represented in models. Clearly this discrepancy needs further investigation.

This work provides the first definitive vertical profile of HCl from the marine boundary layer to the lower stratosphere. In particular, we demonstrate that background levels of HCl in the mid and upper troposphere are very low and that the primary source of HCl in these regions is stratospheric transport. This is in accord with recent work by Marcy et al.,[2004] on stratospheric mixing and utility of HCl as a tracer for this process. Our observations are not in accord with much of the work on HCl measurements reviewed by Keene et al [1999] and indicate a lower burden and less active chlorine chemsistry than previously suggested. We also find little evidence for activated chlorine chemistry in polluted marine air in contradiction to a series of recent studies [Finley and Saltzman, 2006; Tanaka et al, 2003; Chang et al., 2002; Spicer et al., 1998].Although it should be noted that our observations are over a limited geographical extent and should be extended to investigate this issue. Finally, the use of HCl as both a stratospheric tracer and a marker for tropospheric chlorine chemistry is demonstrated in this work.

SO_2 observations in this work allow us to test our understanding of sulfur emissions and chemistry. In general, we find that chemical transport models (MOZART and GEOS-CHEM) do a reasonable job of capturing the gross features of the SO_2 vertical distribution observed during the INTEX campaign. The models do a better job of reproducing the SO_x (= SO_2 + SO_4^{-2}) vertical distribution; suggesting that emissions are handled better in models than the conversion chemistry. This is also supported by the models doing a good job of representing the horizontal distribution of sulfur in source regions. However, there are several areas where model performance is clearly not as

good. For example, models do a poor job representing the spatial distribution of SO_2 in the upper troposphere suggesting that convection schemes may be problematic. In addition, the DMS emission and oxidation scheme of the MOZART model is clearly not in agreement with our observations over the northern Pacific Ocean.

6.1 References

Chang, S., E. C. McDonald-Buller, Y. Kimura, G. Yarwood, J. D. Neece, M. Russell, P. Tanaka, and D. Allen: Sensitivity of urban ozone formation to chlorine emission estimates, Atmospheric Environment, 36, 4991-5003,2002.

Finley, B., and E. Saltzman: Measurement of Cl_2 in coastal urban air, Geophysical Research Letters, 33, L11809,doi:11810.11029/12006GL025799,2006.

Keene, W. C., M. Aslam, K. Khalil, D. J. Erickson, A. McCulloch, T. E. Graedel, J. M. Lobert, M. L. Aucott, S. L. Gong, D. B. Harper, G. Kleiman, P. Midgley, R. M. Moore, C. Seuzaret, W. T. Sturges, C. M. Benkovitz, V. Koropalov, L. A. Barrie, and Y. F. Li: Composite global emissions of reactive chlorine from anthropogenic and natural resorces; Reactive Chlorine Emissions Inventory, Journal of Geophysical Research, 104(D7), 8429-8440,1999.

Marcy, T. P., D. W. Fahey, R. S. Gao, P. J. Popp, E. C. Richard, T. L. Thompson, K. H. Rossenlof, E. A. Ray, R. J. Salawitch, C. S. Atherton, D. J. Bergmann, B. A. Ridley, A. J. Weinheimer, M. Loewenstein, E. M. Weinstock, and M. J. Mahoney: Quantifying stratospheric ozone in the upper troposphere with in situ measurements of HCl, Science, 304(5668), 261-265,2004.

Spicer, C. W., E. G. Chapman, B. J. Finlayson-Pitts, R. A. Plastridege, J. M. Hubbe, and J. D. Fast: Unexpected high concentrations of molecular chlorine in coastal air, Nature, 394, 353-356,1998.

Tanaka, P. L., D. D. Riemer, S. Chang, G. Yarwood, E. C. McDonald-Buller, E. C. Apel, J. J. Orlando, P. J. Silva, J. L. Jimenez, M. R. Canagaratna, J. D. Neece, C. B. Mullins, and D. T. Allen: Direct evidence for chlorine-enhanced urban ozone formation in Houston, Texas, Atmospheric Environment, 37, 1393-1400,2003.

APPENDIX A

AN IGOR PROCEDURE FOR THE STEADY STATE HO_2NO_2 CALCULATION

(FOR DETAILED DESCRIPTIONS ON CALCULATIONS, SEE 2.3.1 SEADY STATE CALCULATIONS IN CHAPTER 2)

```
#pragma rtGlobals=1                // Use modern global access method.
function Get_Steady_State(OH_calc, HO2_calc, NO2_calc, j_HO2NO2, Pressure, Temperature,
Altp, Name)

Wave OH_calc, HO2_calc, NO2_calc, j_HO2NO2, Pressure, Temperature, Altp
// declarations of input parameters, needed to calculate steady-state HO2NO2
String Name
// the string to be a name of output wave (steady state HO2NO2)

variable n = numpnts(pressure), i


//a process, which calculate third body number density (M molecules/cm3) using the ideal gas law

duplicate pressure M
M = NaN
M = Pressure/1013.25*10^-3/(0.0821 * Temperature) * 6.02 *10^23


//the porcess, which calculate rate constants from JPL ver 15 Sander et al, 2006
//a unit of cm3 molecules-1 s-1
//k1 HO2 + NO2 + M -> HO2NO2
//k2 HO2NO2 + heat -> HO2 + NO2
//k3 HO2NO2 + OH -> products

duplicate temperature k_1_0 k_1_00 k_1 k_3 k_2
k_1_0  = NaN  // the low pressure limiting rate constant
k_1_00 = NaN // the high pressure limiting rate constant
k_1 = NaN
k_2 = NaN
k_3 = NaN

k_1_0  = 2.0 *10^-31 * ( Temperature/300)^-3.4
k_1_00 = 2.9 * 10^-12 * (Temperature/300)^-1.1

k_1 = (k_1_0 * M/(1+k_1_0*M/k_1_00)) * 0.6^((1+(log(k_1_0*M/k_1_00))^2)^-1) //effectiver
second rate constant
k_2 = k_1/(2.1*10^-27*exp(10900/Temperature))
k_3 =1.3*10^-12*exp(380/Temperature)
```

```
//Calculate steady_state_HO2NO2
duplicate/o pressure dummy
dummy = NaN
dummy = k_1 * HO2_calc * NO2_filter * M * 10^-12 / (k_2 + k_3 * OH_calc * 10^-12 * m +
J_ho2no2)

for(i = 0; i<n; i+=1)
//loop for eliminating any calculated number under the altitude of 4km
//I did this b.c. most of measured data were only available over 4km
//if lower altitude data are avaialble for specific applications, you can block this loop.
        if(altp[i]<4)
                dummy[i] = NaN
        endif
endfor

rename dummy $Name


//Lifte time calculation
duplicate pressure LT_OH LT_Thermal LT_Photo LT_Overall
LT_OH = 1/(k_3*OH_calc*M*10^-12)
LT_Thermal = 1/k_2
LT_photo = 1/J_ho2no2
LT_overall = 1/ (k_2 + k_3 * OH_calc * 10^-12 * m + J_ho2no2)


end
```

APPENDIX B

A METLAB CODE FOR TIME DEPENDENT CALCULATIONS OF HO_2NO_2

B-1 The Matlab Code

An Igor procedure for the time dependent HO_2NO_2 calculation (For detailed descriptions on calculations, see 2.3.2 Time Dependent Model in Chapter 2)

```
%HO2NO2 including 0-D box model based on a reaction list, followed


% Module for reading initial condition from a array [HO2NO2, HNO3, NO, NO2, PAN,
% NO3, N2O5]. All mixing ratios in the unit of pptv

   no_2i = initial(1,4) * 10^-3;
   noi   = initial(1,3) * 10^-3;
   n_2o_5i = initial(1,7) * 10^-3;
   no_3i = initial(1,6) * 10^-3;
   ho_2no_2i = initial(1,1) * 10^-3;
   hno_3i = initial(1,2) * 10^-3;
   pani = initial(1,5) * 10^-3;

% Change model duration and start_hour (24 hours unit) in here

   Model_Duration  = 24;
   start_hour = 0;

% Constranined conditions in ppbv, seconds, K, and atm

   co   = 107
   o_3  = 65
   ch_4 = 1779
   hcho = .312
   h_2o_2 = .328
   ch_3ooh = .150
   ch_3coch_3 = 2.0
   del_t = 2
   temp  = 238.76
   press = .3

% Loop size determination

   n = (Model_Duration * 60 * 60)/del_t;
```

```
% Determination of number density of M

   m = press * .001/(.0821*temp)*6.02*10^23;


%Water vapor mixing ratio (put appropriate number in ppmv)

   h2o = 468.041*10^-6*m;


   %Bi-molecular rate constant (From JPL Evaluation # 15 Sander et sl 2006)

   k_3 = 3.0*10^-12*exp(-1500*1/temp);%O3 + NO -> NO2 + NO
   k_5 = .2*3.3*10^-11*exp(55*1/temp) + .8*2.15*10^-11*exp(110*1/temp);
  %O(1D)+  (0.2 O2 + 0.8 N2)-> O +M
   k_6 = 1.63*10^-10*exp(60/temp); %O(1D)+H2O -> 2OH
   k_11  = 2.4*10^-14*exp(460/temp)+6.5*10^-34*exp(1335/temp)*m/(1+6.5*10^-
     34*exp(1335/temp)*m/(2.7*10^-17*exp(2199/temp)));
   %HNO3+OH -> H2O + NO3
   k_15 = 1.3*10^-12*exp(380/temp); % HO2NO2 + OH -> H2O + O2 + NO2
   k_17 = 4.8*10^-11*exp(250/temp); % OH + HO2 -> H2O + O2
   k_18 = 1.7*10^-12*exp(-940/temp); %O3+ OH -> HO2 + O2
   k_19 = 3.5*10^-13*exp(430/temp) + 1.77*10^-33 * m * exp(1000/temp);
   %HO2 + HO2 -> H2O2 + O2
   k_20 = 1.0*10^-14*exp(-490/temp);%HO2 + O3 -> OH + 2O2
   k_21 = 3.5*10^-12*exp(250/temp); %HO2 + NO -> NO2 + NO
   k_24 = 1.8 *10^-12; %H2O2 + OH -> H2O + HO2
   k_25 = 2.45*10^-12*exp(-1775/temp); %CH4 + OH -> CH3 + H2O
   k_27 = 2.8*10^-12*exp(300/temp); %CH3O2 + NO -> CH3O + NO2
   k_28 = 3.9*10^-14*exp(-900/temp); %CH3O + O2 -> HCHO + HO2
   k_30 = 5.2*10^-12; %HCO + O2 -> CO + HO2
   k_31 = 5.5*10^-12 * exp(125/temp); % HCHO + OH -> H2O + HCO
   k_34 = 8.1*10^-12*exp(270/temp); % CH3CO3 + NO -> CH3O2 + CO2
   k_38 = 3.0*10^-14; % PAN + OH -> 1/2 NO2 + products (upper limt)
   k_39 = 1.2*10^-13*exp(-2450/temp); % NO2 + O3 -> NO3 + O2
   k_42 = 2.0 *10^-21; % N2O5 + H2O -> 2HNO3 (upper liimt)
   k_10 = 0.3*3.141592*(2.53*10^-
5)^2*25754*0.24/(1+3*0.3*(1+0.47*12.81)/(4*12.81*(1+12.81)));
   % HNO3 heterogeneous Rxn (Equation from Brasseur et al., 1999)
   k_44 = 0.1*3.141592*(2.53*10^-
5)^2*25754*0.24/(1+3*0.1*(1+0.47*12.81)/(4*12.81*(1+12.81)));
   % HO2NO2 heterogeneous Rxn (Equation from Brasseur et al., 1999)
   k_45 = 4.3*10^-13*exp(1040/temp); % HO2 + CH3COO2 -> Product

   %termolecular rate constant

   k_7_1_0= 5.9*10^-33*(temp/300)^-1.4; k_7_1_00=1.1*10^-12*(temp/300)^1.3;
   %CO+ OH + M -> COOH + M (will be immediately decomposed into H + CO2 in the
   %presence of oxygen)
   k_7_1 = (k_7_1_0*m/(1+k_7_1_0*m/(k_7_1_00)))*.6^((1+(log10(k_7_1_0*m/k_7_1_00))^2)^-
1);
   k_7_2_0=1.5*10^-13*(temp/300)^0.6 ; k_7_2_00=2.1*10^9*(temp/300)^6.1 ;
   %CO+ OH + M -> CO+H+M
   k_7_2 = (k_7_2_0/(1+k_7_2_0/(k_7_2_00/m)))*.6^((1+(log10(k_7_2_0/(k_7_2_00/m)))^2)^-1);
   k_7 = k_7_1 + k_7_2; % overall CO + OH -> HO2 + CO2
```

```
k_12_0=2.0*10^-31*(temp/300)^-3.4; k_12_00=2.9*10^-12*(temp/300)^-1.1 ;
%OH+ NO2 + M -> HO2NO2 + M
k_12 = (k_12_0*m/(1+k_12_0*m/(k_12_00)))*.6^((1+(log10(k_12_0*m/k_12_00))^2)^-1)    ;

k_14 = k_12/(2.1*10^-27*exp(10900/temp)); % HO2NO2 -> HO2 + NO2


k_8_0= 1.8*10^-30*(temp/300)^-3; k_8_00=2.8*10^-11;
%OH+ NO2 + M -> HNO3 + M
k_8 = (k_8_0*m/(1+k_8_0*m/(k_8_00)))*.6^((1+(log10(k_8_0*m/k_8_00))^2)^-1);

k_26_0=4.0*10^-31*(temp/300)^-3.6; k_26_00=1.2*10^-12*(temp/300)^-1.1 ;
%CH3 + O2 + M -> CH3O2 + M
k_26 = (k_26_0*m/(1+k_26_0*m/(k_26_00)))*.6^((1+(log10(k_26_0*m/k_26_00))^2)^-1);

k_35_0 = 9.7*10^-29*(temp/300)^-5.6; k_35_00 = 9.3*10^-12*(temp/300)^-1.5;
%CH3CO3 + NO2 + M -> PAN + M
k_35 = (k_35_0*m/(1+k_35_0*m/(k_35_00)))*.6^((1+(log10(k_35_0*m/k_35_00))^2)^-1);
k_37 = k_35/(9.0*10^-29*exp(14000/temp)); PAN -> NO2 + CH3CO3

k_41_0=2.0*10^-30*(temp/300)^-4.4; k_41_00=1.4*10^-12*(temp/300)^-0.7 ;
%NO3+ NO2 + M -> N2O5 + M
k_41 = (k_41_0*m/(1+k_41_0*m/(k_41_00)))*.6^((1+(log10(k_41_0*m/k_41_00))^2)^-1)    ;
k_43 = k_41/(2.7*10^-27*exp(11000/temp)); % N2O5 -> NO2 + NO3

% array building for each species


hco = 0
o_1d = 0
ch_3 = 0
ch_3o_2= 0
ch_3o = 0
ch_3co_3 =0



no(1) = noi*10^-9*m;
no_2(1) = no_2i*10^-9*m    ;
hno_3(1) = hno_3i *10^-9*m;
ho_2no_2(1) = ho_2no_2i*10^-9*m;
pan(1) = pani*10^-9*m;
oh(1) = 0;
ho_2(1) =0;
no_3(1) = no_3i *m*10^-9;
n_2o_5(1) = n_2o_5i *m*10^-9;
ho_2no_2_ss(1) = 0;
% This array will contain the steady state HO2NO2 from time dependent calculated
%NO2, HO2, and OH

h_2o_2=h_2o_2*10^-9*m    ;
o_3 = o_3*10^-9*m;
ch_4=ch_4 * 10^-9*m;
hcho = hcho *10^-9*m;
co = co* 10^-9*m;
```

```
    ch_3ooh= ch_3ooh * 10^-9*m;
    ch_3coch_3 = ch_3coch_3*10^-9*m;

    % calculation for each species in each time step - Euler method
    % to save model calculation time, an embedded inner loop for an hour calculation is
    % applied

for i = 1:Model_Duration

    no_h(1) = no(1+(i-1)*60*60/2);
    no_2_h(1) = no_2(1+(i-1)*60*60/2);
    hno_3_h(1) = hno_3(1+(i-1)*60*60/2);
    ho_2no_2_h(1) = ho_2no_2(1+(i-1)*60*60/2);
    pan_h(1) = pan(1+(i-1)*60*60/2);
    no_3_h(1) = no_3(1+(i-1)*60*60/2);
    n_2o_5_h(1) = n_2o_5(1+(i-1)*60*60/2);
    oh_h(1) = oh(1+(i-1)*60*60/2);
    ho_2_h(1) = ho_2(1+(i-1)*60*60/2);
    ho_2no_2_ss_h(1)=ho_2no_2_ss(1+(i-1)*60*60/2);

    for j = 2:1800
    sec = (start_hour+(i-1))*60*60 + (j-1)*del_t;
    s = fix(sec/900);

    %j calculation loop
    % You need J value arrays, containing the daily variation in every 15 minutes

    j_1    = jno2(s+1); %NO2 + hv -> NO + O
    j_9    = jhno3(s+1); % HNO3 + hv -> NO2 + OH
    j_4_b    = jo3b(s+1); %O3 + hv -> o2 + O(1P)
    j_4_a  = jo3a(s+1); % O3 + hv -> O2 + O(1D)
    j_4 = j_4_a + j_4_b; %O3 + hv -> product
    j_22   = jh2o2(s+1);% H2O2 + hv -> 2OH
    j_29_a = jch2oa(s+1); % HCHO + hv -> HO2 + HCO
    j_29_b = jch2ob(s+1); % HCHO + hv -> H2 + CO
    j_29   = j_29_a + j_29_b ;
    j_13   = jho2no2(s+1) + 10^(-5); %HO2NO2 + hv -> HO2 + NO2
    j_32   = jch3ooh(s+1); % CH3OOH + hv -> CH3O + OH
    j_33   = jch3coch3(s+1); % CH3COCH3 + hv -> CH3O2 + CH3CO3
    j_36    = jpan(s+1); % PAN + hv -> CH3CO3 + NO2
    j_46    = jno3(s+1); % NO3 + hv -> NO2 + O(3P)
    j_47    = jn2o5(s+1); % N2O5 + hv -> NO3 + NO2

    %the species for Euler calculation


      no_2_h(j) = no_2_h(j-1) + (-j_1*no_2_h(j-1)+k_3*no_h(j-1)*o_3+k_21*ho_2_h(j-1)*no_h(j-1) -
                  k_8*oh_h(j-1)*no_2_h(j-1)+j_9*hno_3_h(j-1)+k_27*no_h(j-1)*ch_3o_2-
                  k_12*ho_2_h(j-1)*no_2_h(j-1)+j_13*ho_2no_2_h(j-1)+k_14*ho_2no_2_h(j-
                  1)+k_15*ho_2no_2_h(j-1)*oh_h(j-1)-k_35*ch_3co_3*no_2_h(j-
                  1)+j_36*pan_h(1)+k_37*pan_h(j1)+k_38*0.5*pan_h(j-1)*oh_h(j-1)-k_39*no_2_h(j-
                  1)*o_3-k_41*no_2_h(j-1)*no_3_h(j-1)+k_43*n_2o_5_h(j-1)+j_46*no_3_h(j-
                  1)+j_47*n_2o_5_h(j-1))*del_t;
```

```
   no_h(j) = no_h(j-1) + (j_1*no_2_h(j-1)-k_3*o_3*no_h(j-1)-k_21*ho_2_h(j-1)*no_h(j-1)...
                    -k_27*ch_3o_2*no_h(j-1)-k_34*no_h(j-1)*ch_3co_3)*del_t;


   hno_3_h(j) = hno_3_h(j-1) + (k_8*oh_h(j-1)*no_2_h(j-1) - j_9*hno_3_h(j-1)- k_11*hno_3_h(j-
                    1)*oh_h(j-1)+2*k_42*n_2o_5_h(j-1)*h2o)*del_t;

   no_3_h(j)  = no_3_h(j-1) + (k_39*no_2_h(j-1)*o_3 - k_41*no_2_h(j-1)*no_3_h(j-1)+
                    k_43*n_2o_5_h(j-1)-  j_46*no_3_h(j-1)+j_47*n_2o_5_h(j-1))*del_t;

  n_2o_5_h(j) = n_2o_5_h(j-1) + (k_41*no_2_h(j-1)*no_3_h(j-1) - k_43*n_2o_5_h(j-1)-
                    k_42*n_2o_5_h(j-1)*h2o - j_47*n_2o_5_h(j-1)) * del_t;

 ho_2no_2_h(j) = ho_2no_2_h(j-1) +(k_12*ho_2_h(j-1)*no_2_h(j-1)-j_13*ho_2no_2_h(j-1)-
                      k_14*ho_2no_2_h(j-1)-k_15*ho_2no_2_h(j-1)*oh_h(j-1))*del_t;

   pan_h(j) = pan_h(j-1) + (k_35*ch_3co_3*no_2_h(j-1) - k_37*pan_h(j-1) - j_36*pan_h(j-1)-
                  k_38*pan_h(j-1)*oh_h(j-1))*del_t;



   no2_s=no_2_h(j) ; no_s=no_h(j) ; pan_s=pan_h(j) ; hno3_s=hno_3_h(j);
   ho2no2_s=ho_2no_2_h(j);

%the species for steady state calculation all based on the simple steady-state calculations
%except HOx, see text more details

    o_1d = j_4_a*o_3/(k_5*m + k_6*h2o);

       %partitioning of hox species
       r =(k_7 * co+k_25*ch_4+k_18*o_3)/(k_21*no_s+k_20*o_3);
      % r=[HO2]/[OH]

       %calculations to get steady state of HOx
       p_hox=2*k_6*o_1d*h2o+2*j_22*h_2o_2 + j_32*ch_3ooh + 2*j_29_a*hcho;
       l1 = 1/(1+r)*k_8*no2_s +1/(1+r)* k_11*hno3_s + r/(r+1)*k_12*no2_s +
              1/(1+r)*k_15*ho2no2_s;
       l2 = r/(r+1)*r/(r+1)*k_19 + r/(r+1)*1/(r+1)*k_17;
       hox = (-l1 + sqrt(l1*l1 +4*l2*p_hox))/(2*l2);



    oh_h(j) = hox/(1+r);
    ho_2_h(j) =(hox-oh_h(j));
    oh_s = oh_h(j);
    ho2_s = ho_2_h(j);
    ho_2no_2_ss_h(j)=(k_12*ho2_s*no_2_h(j))/(k_14+k_15*oh_s+j_13);
    ch_3 = k_25*ch_4*oh_s/(k_26*.2*m);
    ch_3co_3 =
                    (j_36*pan_s+j_33*ch_3coch_3+k_37*pan_s)/(k_35*no2_s+k_34*no_s+k_45*ho2_s
                    );
    ch_3o_2 = (k_26*ch_3*.2*m+j_33*ch_3coch_3+k_34*no_s*ch_3co_3)/(k_27*no_s);
end

    no_2 =  [no_2, no_2_h];
```

```
    no   =  [ no, no_h];
    hno_3 = [hno_3, hno_3_h];
    no_3 = [no_3, no_3_h];
    n_2o_5 = [n_2o_5, n_2o_5_h];
    ho_2no_2 = [ho_2no_2, ho_2no_2_h];
    oh = [oh,oh_h];
    ho_2 = [ho_2, ho_2_h];
    pan = [pan, pan_h];
    ho_2no_2_ss=[ho_2no_2_ss,ho_2no_2_ss_h];
   clear no_2_h no_h hno_3_h no_3_h n_2o_5_h ho_2no_2_h oh_h ho_2_h pan_h
         ho_2no_2_ss_h

end


% Building a time array and unit change to pptv

t=[0:1:n]

ho_2no_2_ppt = ho_2no_2/m*10^12;
hno_3_ppt = hno_3/m*10^12;
oh_ppt = oh/m*10^12;
ho_2_ppt = ho_2/m*10^12;
no_ppt = no/m*10^12;
no_2_ppt = no_2/m*10^12;
pan_ppt = pan/m*10^12;
no_3_ppt = no_3/m*10^12;
n_2o_5_ppt = n_2o_5/m*10^12;
ho_2no_2_ss_ppt=ho_2no_2_ss/m*10^12;
```

B-2 A Reaction List for Time Dependent Model

O_3-NO_2 Chemistry

$NO_2 + hv \rightarrow NO + O$	J_1
$O_2 + O + M \rightarrow O_3 + M$	k_2
$O_3 + NO \rightarrow NO_2 + NO$	k_3

O_3 Photolysis

$O_3 + hv \rightarrow O(^1D) + O_2$	J_{4_a}
$\rightarrow O + O_2$	J_{4_b}
Overall $J_4 = J_{4\_a} + J4\_b$	

$O(^1D)$ Chemistry

$O(^1D) + M \rightarrow O + M$	k_5
$O(^1D) + H_2O \rightarrow 2OH$	k_6

CO Chemistry

$CO + OH + M \rightarrow HOCO + M$	k_{7_a}
$CO + OH + M \rightarrow H + CO_2$	k_{7_b}

HNO_3 Chemistry

$OH + NO_2 + M \rightarrow HNO_3 + M$	k_8
$HNO_3 + hv \rightarrow NO_2 + OH$	J_9
$HNO_3 \rightarrow$ heterogeneous uptake	k_{10}
$HNO_3 + OH \rightarrow H_2O + NO_3$	k_{11}

HO_2NO_2 Chemistry

$HO_2 + NO_2 + M \rightarrow HO_2NO_2 + M$	k_{12}
$HO_2NO_2 + hv \rightarrow HO_2 + NO_2$	J_{13}
$HO2NO2 + Heat \rightarrow HO2 + NO2$	k_{14}
$HO_2NO_2 + OH \rightarrow H_2O + O_2 + NO_2$	k_{15}
$HO_2NO_2 \rightarrow$ heterogeneous uptake	k_{44}

PAN Chemistry

$CH_3CO_3 + NO_2 + M \rightarrow PAN$	k_{35}
$PAN + hv \rightarrow CH_3CO_3 + NO_2$	J_{36}
$PAN + heat \rightarrow CH_3CO_3 + NO_2$	k_{37}
$PAN + OH \rightarrow ½\ NO_2 + Products$	k_{38}
$CH_3CO_3 + HO_2 \rightarrow$ products	k_{45}

HO_x regenerations

$O_3 + OH \rightarrow HO_2 + O_2$	k_{18}
$HO_2 + O_3 \rightarrow OH + 2O_2$	k_{20}
$HO_2 + NO \rightarrow NO_2 + OH$	k_{21}
$H_2O_2 + OH \rightarrow H_2O + HO_2$	k_{24}

HO_x self destructions

$HO_2 + HO_2 + M \rightarrow H_2O_2 + O_2$	k_{19}
$OH + HO_2 \rightarrow H_2O + O_2$	k_{17}

CH_4 chemistry

$CH_4 + OH \rightarrow CH_3 + H_2O$	k_{25}
$CH_3 + O_2 + M \rightarrow CH_3O_2 + M$	k_{26}
$CH_3O_2 + NO \rightarrow CH_3O + NO_2$	k_{27}
$CH_3O + O_2 \rightarrow HCHO + HO2$	k_{28}

HCHO chemistry

$HCHO + hv \rightarrow HO2 + HCO$	J_{29a}
$\rightarrow H2 + CO$	J_{29_b}
$HCO + O2 \rightarrow HO2 + CO$	k_{30}
$HCHO + OH \rightarrow HCO + H2O$	k_{31}

H_2O_2 photolysis

$H_2O_2 + hv \rightarrow 2OH$	J_{22}

CH_3OOH photolysis

$CH_3OOH + hv \rightarrow CH_3O + OH$	J_{32}

Acetone Chemistry

$CH_3OCH_3 + hv \rightarrow CH_3O_2 + CH_3CO_3$	J_{33}
$CH_3CO_3 + NO \rightarrow CH_3CO_2 + NO_2$	k_{34}

NO_3-N_2O_5 Chemistry

$NO_2 + O_3 \rightarrow NO_3 + O_2$	k_{39}
$NO_3 + hv \rightarrow NO_2 + O$	J_{46}
$NO_2 + NO_3 \rightarrow N_2O_5$	k_{41}
$N_2O_5 \rightarrow NO_2 + NO_3$	k_{43}
$N_2O_5 + H_2O \rightarrow 2HNO_3$	k_{42}
$N_2O_5 + hv \rightarrow NO_2 + NO_3$	J_{47}